AN INVESTIGATION OF A SUPERSONIC CHEMICAL REACTOR.

BY

RORY LOIVEIG CHRISTIAN FLEMMER.

Submitted in partial fulfilment of the requirements for the degree of Doctor of Philosophy in the Department of Chemical Engineering, University of Natal.

Durban,

December 1977.

ABSTRACT

The development of a supersonic chemical reactor is examined. The central concept of such a reactor is that gases can be expanded to supersonic speed which will result in a decrease in their static temperature to the extent that no reaction will occur when the gases are mixed together. After mixing has occurred the mixture can then be passed through a standing shock to raise this temperature very rapidly, thus controlling the product spectrum.

The main areas of interest for such a reactor, namely the establishment of a shock and the mixing of two gases at supersonic speed are examined.

ACKNOWLEDGEMENTS.

The author would like to express his thanks and appreciation to Professor E.T. Woodburn and Dr. R.C. Everson for their encouragement and advice during the course of this work. Thanks are also due to Mr W.T. Mandersloot of the C.S.I.R. and Mr D. Hurlin of the South African Inventions Development Corporation.

Except where otherwise indicated, this dissertation is entirely the work of the author.

ADDENDUM

1. ROBERTS' TIME-TEMPERATURE PROFILE

The time-temperature profile produced by Roberts and referred to on page 7 is represented below.

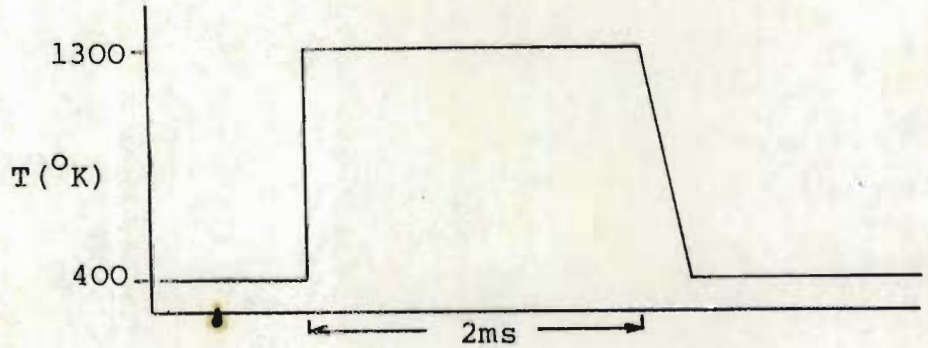

2. SUPERSONIC WIND TUNNEL LITERATURE

The literature on shock production in the second throat of a wind tunnel is inapplicable because shock-boundary layer interaction precludes a normal shock at high Mach numbers.

3. FRICTION FACTOR IN MIXING DUCT

It is of interest to consider the friction factor to be expected for the flow in the mixing duct of Chapter 6.

The concept of an average Mach number at any cross-section cannot be applied as it normally is (see Shapiro, p167), because of the highly non-uniform nature of the flow. Never-the-less a computation was performed using the centre-line Mach number at each of the six stations at which measurements were taken. The mean value obtained was $f = 0{,}0044$.

LIST OF SYMBOLS

A	Area	m^2
a	Velocity of sound	m/s
C	Mass fraction	
M	Mach number	
P	Pressure	Pa
r	Radius	m
T	Temperature	K
v	Transverse velocity	m/s
u	Axial velocity	m/s
ρ	Density	Kg/m^3
γ	Specific Heat Ratio - C_p/C_v	

Subscripts and Superscripts

*	Conditions at the throat of a de Laval nozzle
0	Reservoir conditions
1	Conditions before the shock
2	Conditions after the shock

TABLE OF CONTENTS

CHAPTER ONE

INTRODUCTION

The thesis which is proposed is that it is possible to build and run a supersonic chemical reactor and that this reactor can be designed and controlled to provide a specific time-temperature profile. The purpose of the reactor is to provide very rapid heating of a gaseous mixture and it is envisaged that heating rates of 10^9 K/s, or higher, can be obtained.

In principle the reactor, depicted in Figure 1.1, will consist of four stages. Firstly, the reactant gases will be separately heated, at high pressure. They will then be expanded to supersonic velocity. This will cause a decrease in static temperature, the magnitude of this decrease being controlled

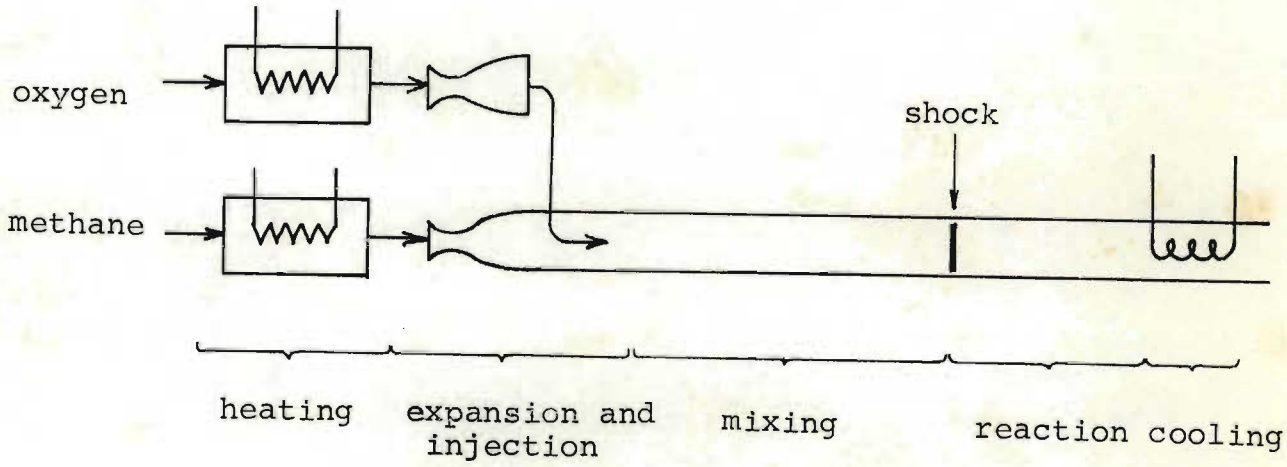

FIGURE 1.1

by the Mach number to which they are expanded.

In the second stage of the reactor, the two (or more) gases will be mixed together is such a way as to avoid the formation of shocks and stagnation heating. By virtue of their low static temperature, the gases will mix without any significant chemical reaction occurring. Also, the very high speed will imply a very short residence time in the mixing zone. Mixing will continue until the composition is sufficiently uniform, whereupon the mixture will enter the third stage.

In the third stage, the mixture will pass through a standing normal shock which will compress the gas very rapidly. Associated with this compression will be an increase in temperature back to approximately the initial stagnation temperature. The mixture will be allowed to remain at this temperature for a controlled period of time until, in the fourth stage, it is quenched to a lower temperature or, alternatively, heat is removed in a heat-exchanger.

The reactor will have particular relevance to free radical reactions where it will be possible to control reaction products by heating the mixture very rapidly through the temperatures at which intermediate reactions would take place. By avoiding the branching which would then occur, it is possible to obtain different reaction products.

This aspect has been investigated by Roberts (1970) who studied the partial oxidation of methane in a batch shock tube. His experimental scheme provided a static mixture of

methane and oxygen in a tube, at room temperature. By rupturing a diaphragm separating this gas from an inert gas at high pressure, a compressive shock was caused to travel down the length of the tube, thus heating the methane-oxygen mixture very rapidly. It was possible to control conditions such that a rarefaction wave passed over the mixture after a short time interval (of the order of milliseconds), quenching the reaction products. He found that, by controlling the strength of the shock and thus the reaction temperature, he was able to obtain conversions of methane to ethylene. The conversion of methane to ethylene is attractive because in coal gasification, particularly low temperature gasification, substantial quantities of methane are obtained as a by-product, and upgrading it to ethylene would be economically very desirable. Other potential sources of methane are the natural gas deposits often associated with mineral oil deposits and the methane available from anaerobic digestion of vegetable matter, which has the advantage of being a renewable resource. Of the order of 50% by weight of vegetable matter can be converted to methane using very simple technology.

A batch shock tube is not suitable for industrial application because of the very small amounts processed. It was proposed that it might be possible to establish a continuous process using a de Laval nozzle and this research has been to that end.

The advantages of such a continuous supersonic reactor would be:-

(1) Its throughput would be very high.

(2) Capital costs per kilogram of products would be very low.

(3) It would probably have many applications in free radical reactions.

(4) The reactor would have the unique advantage that reaction conditions would be uniform because diffusional processes would be absent. Mixing of the gases would be complete before the shock occurred and, because heating is as a result of a pressure increase, the heating throughout the mixture would be fairly uniform; as opposed to any other reactor, where temperature gradients exist.

There are, however, several areas in the design of such a reactor where difficulties might be expected. These are, firstly, the mixing of two gases under supersonic conditions and within a reasonable distance. Secondly, the establishment of a standing normal shock, perhaps at a high Mach number. Thirdly, the minimisation of overall pressure ratio across the reactor. Because the shock is not isentropic, it produces a large stagnation pressure loss. This implies a high running cost for the reactor and, in order to make it economically attractive, this must be kept to a reasonable level.

Fourthly, it will not be possible to quench the reactant products as sharply as could Roberts. However, it is argued, Woodburn (private communication), that the rate constants of the reaction are so high that, whether the reactant gases are quenched or cooled slowly, they will still remain in equilibrium.

This research will therefore consider the three crucial aspects of the reactor. They are:-

(1) The establishment of a normal shock and the best conditions for its establishment.
(2) The injection of the secondary gas into the primary gas stream so that the supersonic flow is not disrupted and so that sufficient mixing occurs.
(3) The nature of the flow in the diffusion section to establish the radial mixing mechanisms which will determine the length of the mixing zone.

CHAPTER TWO

GAS-DYNAMIC ANALYSIS

2.1. INTRODUCTION

It was necessary at the outset to examine the gas dynamic implications of duplicating the time-temperature profile used by Roberts (1970).

Working with a batch shock tube he established that a reaction temperature of about 1300^{o}K provided optimum conversion to ethylene. The temperature of the methane-oxygen mixture before the shock was ambient, but this was merely for experimental convenience. The limitation on this temperature is that no significant reaction should occur before the shock heating occurs. Because the residence time in the mixing section of the proposed reactor will be less that a millisecond, it was anticipated that fairly high static temperatures could be tolerated.

The optimum proportion of methane to oxygen is not known. Roberts studied molar concentrations of methane to oxygen of 11:5, 4:1 and 1:1 and found that of these, the 11:5 ratio gave the best ethylene yields. He suggested that a higher ratio might be better still.

In view of the fact that neither the maximum tolerable pre-shock temperature, nor the optimum methane to oxygen ratio was known, these aspects would need investigation in the continuous reactor. It was not even certain that the optimum conditions in the batch reactor would correspond to the best conditions in the continuous reactor. Before a methane-oxygen reaction could be considered, it was necessary to gain information of the gas-dynamic processes involved. It was the purpose of this research to establish, using inert gases, the gas-dynamic configuration which would be necessary for the reactor.

It was decided to use inert gases for two reasons. Firstly, it would be necessary to evaluate mixing of gases and, with reacting gases, this is more difficult than with inert gases. Secondly, it was preferable to avoid the necessity for taking the precautions associated with experimental work with hazardous gases.

Accordingly, the experimental program was planned, using nitrogen in place of methane and carbon dioxide in place of oxygen. The purpose of this chapter was to establish what was implied in terms of pressures, temperatures, velocities, mass flows and equipment requirements for a continuous reactor duplicating Roberts' time-temperature profile.

2.2 Conditions in the Proposed Reactor

Since the precise conditions required for optimum methane conversion to ethylene were not known, it was proposed to choose conditions of gas ratio and mixing temperature arbitrarily, but so that the information gained would be useful in designing a methane reactor.

It was proposed to design the experimental reactor for a maximum mixing temperature of 400°K. This temperature is almost certainly lower than that which will be used in an actual methane reactor. The rationale behind this choice is that it would be desirable to be able to establish a jump from 400°K to 1300°K, in which case any lesser jump could be confidently accomplished. As will be seen later, there is a strong economic incentive towards having as small a jump as possible.

A secondary injection rate of 9.3% w/w was chosen, although higher and lower injection rates were examined experimentally in order to asses the sensitivity of the reactor to secondary injection rate.

The scale of the reactor was chosen to be as small as possible without making the scale of probes technically difficult. It will be seen that this never-the-less implied large gas flow rates and power consumption.

For convenience the well known equations governing flow in supersonic nozzles are reproduced (Houghton and Boswell 1969):

For an isentropic stream tube;

$$\frac{T_o}{T} = 1 + \frac{\gamma-1}{2} M^2 \qquad (2.1)$$

$$\frac{P_o}{P} = \left[1 + \frac{\gamma-1}{2} M^2 \right]^{\gamma/\gamma-1} \qquad (2.2)$$

$$\frac{A}{A^*} = \frac{1}{M} \left[\frac{1+\frac{\gamma-1}{2} M^2}{\frac{\gamma+1}{2}} \right]^{\gamma+1/2(\gamma-1)} \qquad (2.3)$$

The Rankine-Hugoniot equations which apply across a normal shock;

$$\frac{T_2}{T_1} = \frac{2\gamma M^2 - \gamma + 1}{\gamma+1} \times \frac{2+(\gamma-1)M^2}{(\gamma+1)M^2} \qquad (2.4)$$

$$\frac{P_2}{P_1} = \frac{2\gamma M^2 - \gamma + 1}{\gamma+1} \qquad (2.5)$$

Rearrangement of (2.2) and (2.5) yields

$$\frac{P_0}{P_2} = \frac{\left[1 + \frac{\gamma-1}{2} M^2 \right]^{\gamma/\gamma-1}}{\left[\frac{2 M^2 - \gamma + 1}{\gamma+1} \right]} \qquad (2.6)$$

Inspection of equations (2.3) and (2.6) reveals that the Mach number at any point in the nozzle depends only on the area ratio, A/A^*, provided that the overall pressure ratio is sufficient to prevent the formation of a shock.

Specification of the pre-shock temperature and the post shock pressure and temperature will specify the Mach number before the shock and the reservoir conditions for a fixed value of γ, the specific heat ratio of the gas. For experimental convenience the post shock stagnation pressure was chosen as 101 kPa (atmospheric pressure). In order to optimise ethylene yield the post shock temperature must be about 1300°K.

For a fixed reservoir temperature, the post-shock stagnation temperature is relatively insensitive to the Mach number at which the shock occurs.

Rearrangement of equations (2.1) and (2.4) yields

$$\frac{T_0}{T_2} = \frac{1 + \frac{\gamma-1}{2} M_1^2}{\frac{2\gamma M_1^2 - \gamma + 1}{\gamma+1} \cdot \frac{2+(\gamma-1)M_1^2}{(\gamma+1)M_1^2}} \qquad (2.7)$$

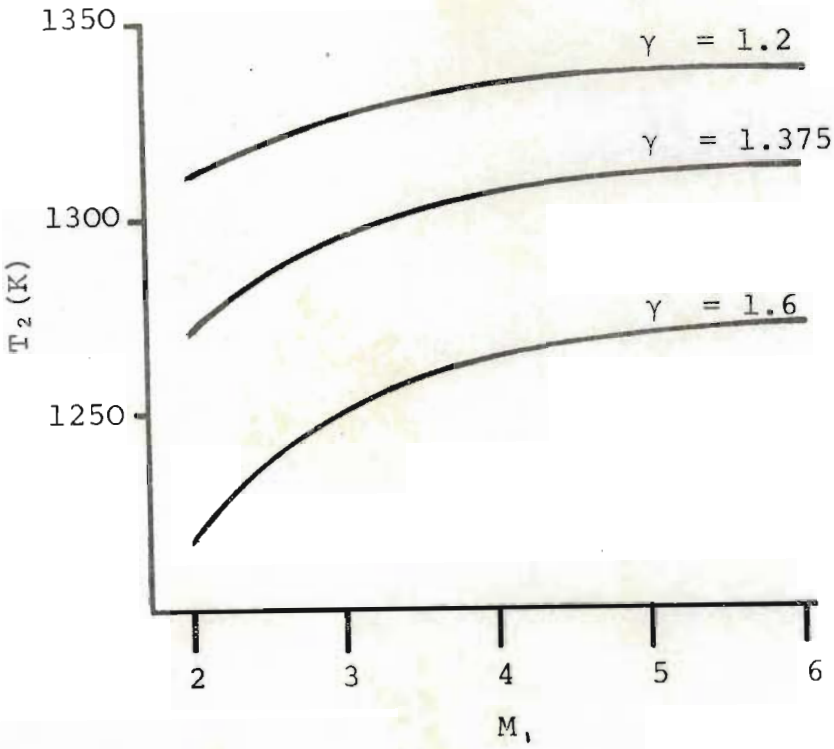

FIG 2.1. VARIATION OF POST SHOCK TEMPERATURE WITH MACH NUMBER

Taking a reservoir temperature, T_0=1350K, the variation of the final temperature, T_2, is shown as a function of Mach number at shock and γ in figure 2.1.

The choice of Mach number at shock does, however, have a profound influence on the pressure ratio across the nozzle and this has important implications as far as running costs of the nozzle are concerned.

From equation (2.6) the variation of pressure ratio across the nozzle with Mach number at shock and γ is plotted in Figure 2.2.

The Mach number at shock is specified by the pre-shock temperature as shown by equation (2.1). The variation of Mach number is plotted in Figure 2.3, in terms of T_1, the pre-shock temperature, and γ. The reservoir temperature was taken to be 1350^{o}K.

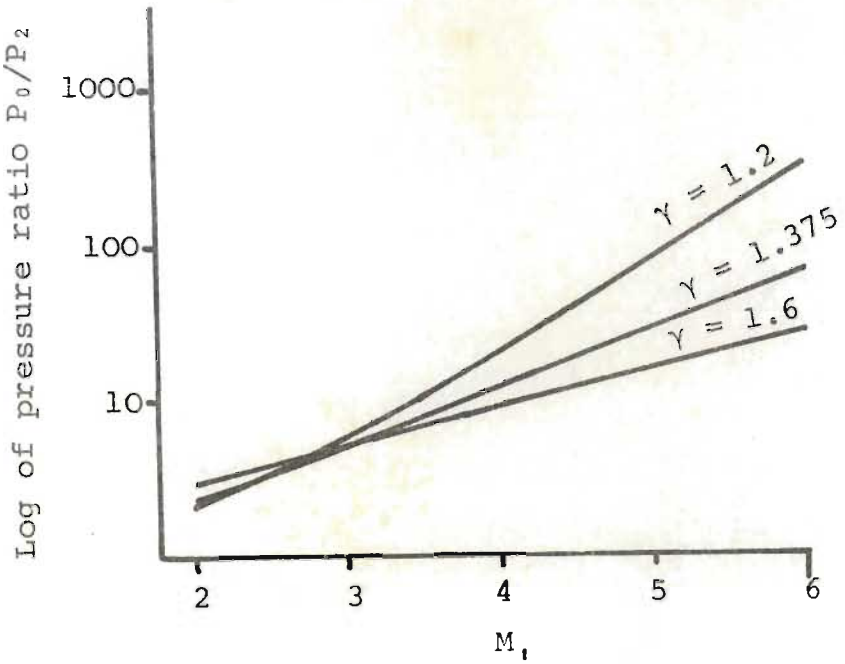

FIG 2.2 VARIATION OF PRESSURE RATIO ACROSS NOZZLE

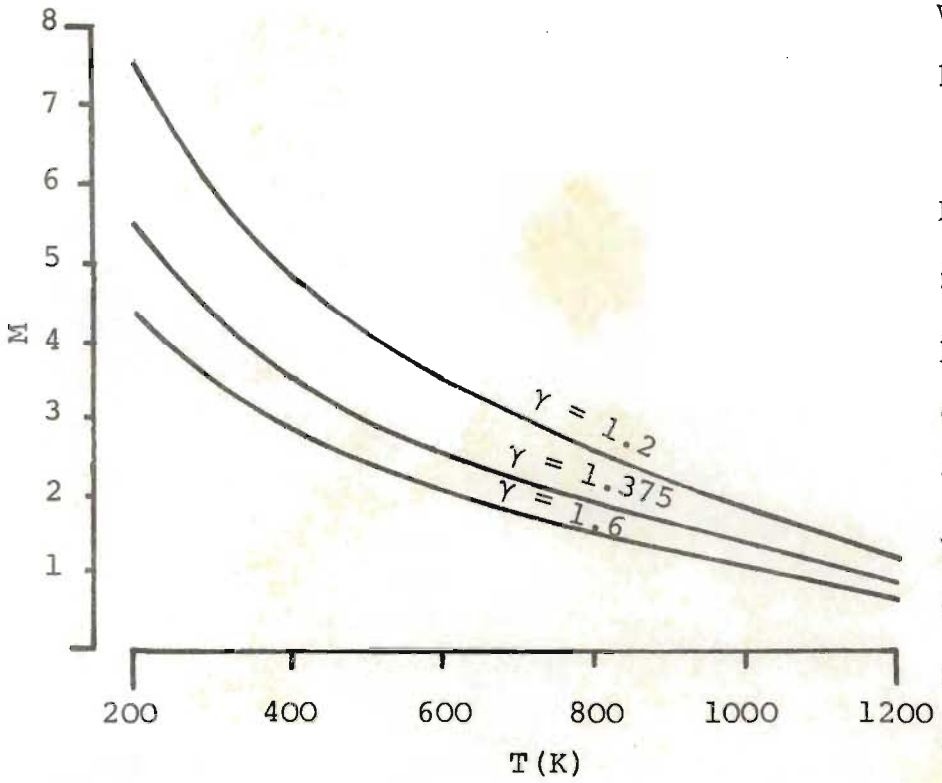

FIG 2.3 MACH NUMBER REQUIRED TO PRODUCE A PRE-SHOCK TEMPERATURE

Examination of Figures 2.1, 2.2 and 2.3 shows that it is desirable to choose as high a pre-shock temperature as possible and that a severe penalty is paid in running costs for a low pre-shock temperature. It may also be seen that a similar penalty is paid for using a gas with a low specific heat ratio, γ.

For a choice of nitrogen as the primary gas and carbon dioxide as the secondary gas, with a mixing temperature of 400°K, a reaction temperature of 1300°K and a final pressure of approximately 101 kPa

(atmospheric), it is possible to calculate the conditions required for the experimental reactor.

The configuration envisaged is shown in Figure 2.4.

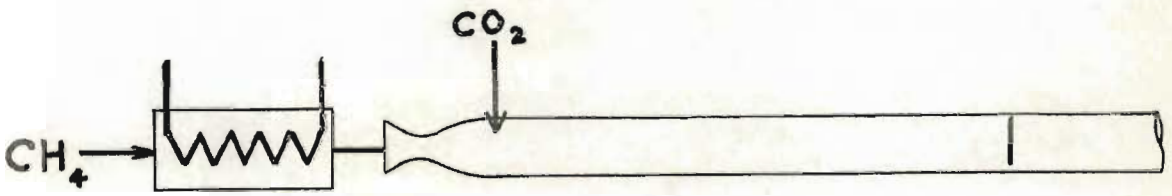

FIG 2.4

Because of the small proportion of secondary injection, it was proposed to inject the carbon dioxide at relatively low speed and stagnation temperature. This was experimentally attractive.

It was necessary to calculate the speed of nitrogen flow necessary to produce a static temperature of about 400°K in the mixing zone. On the basis of the one-dimensional equation (2.1), of perfect mixing and inviscid flow, the nitrogen Mach number at the injection point was calculated in Appendix 2.1 to be 3,74. It was anticipated that the momentum loss to the walls of the mixing duct would be significant, but it was difficult to set a realistic figure to it, partly because the length of the required mixing duct was not known. It was expected therefore that the temperature

in the mixing zone would rise above 400°K but with the information gained from these experiments it will be possible to tailor the conditions in a prototype reactor more closely.

In Appendix 2.2, the reservoir pressure upstream of a de Laval nozzle running at Mach 3,74 was calculated, assuming that the pressure after the shock was 101 kPa. The pressure obtained was 892 kPa. It was anticipated that this figure would be too low because no allowance was made for frictional losses in the mixing tube.

In Appendix 2.3, the mass flow of nitrogen per unit area of throat was calculated at this pressure. The specific heating load was also estimated. The specific mass flow rate was found to be 852,3 Kg/m^2s and the specific heating load was found to be 1031 MW/m^2.

In view of these large numbers, it was decided to use a de Laval nozzle of 10mm throat diameter. This implied a nitrogen flow of 66,8 g/s and a heating load of 80,8 kW. Although these figures are not very high, it was anticipated that a capacity of double this might be necessary and this was felt to be sufficiently large for a laboratory investigation.

After some preliminary work with a 10mm throat it was decided that the experimental program would be much easier with a nozzle half this size and a half-scale nozzle was used

thereafter. At this stage the heater and power supply had already been constructed.

CHAPTER THREE

REVIEW OF THE LITERATURE

3.1. INTRODUCTION

The proposed investigation dealt essentially with three different aspects, namely, the feasibility of a supersonic chemical reactor, the establishment of a standing shock at high Mach number and the problem of supersonic mixing in a duct. These three aspects are covered in the literature to varying degrees and are dealt with separately below.

3.2. SHOCK WAVE REACTORS

Research into batch shock tubes is very well documented (see for instance Bershader and Griffith, 1973). However, the batch shock tube is essentially a laboratory instrument and cannot handle the large throughput necessary for commercial use.

The literature on the application of shock heating to a reactor which would have even moderate throughputs is very limited. Presumeably, this is for proprietary reasons. The information which has been found has come largely from a search of the international patent literature.

In Dutch patent 6 604 520 of April 1966, a patent was granted to the Sun Oil Company for an extension of the basic principle

of a batch shock tube to a quasi-continuous process. The device consisted of a series of tubes arranged in a circle. A high pressure was applied cyclically to the quiescent reaction gas in the tubes. This resulted in the passage of a shock over the gas mixture with consequent heating. There were purging and recharging phases in the cycle to transport the reaction constituents and products.

Information as to the capacity of the system or its effectiveness is not provided, but in the eleven years since the patent was granted no further mention was found in the literature. Presumably this implies that the device was not commercially significant.

In October 1967, United States patent number 3 348 814 was granted to the Macrosonic Process Corporation of Delaware for a device which could produce shocks (termed macrosonics) in a chemical mixture. The primary purpose of the shocks was to enhance mixing of the reacting substances. In particular, it provided for the guttation of two immiscible fluids, producing an emulsion in a very short space of time. The device consisted of a means of producing shocks in a column of gas and these shocks were introduced to a "guttation chamber" where they passed over an essentially static mixture.

In September 1975, West German patent number 2 510 080, was granted to the Institut de Rechérches de la Siderurgie Francaise for the invention of D.S. Borgnat and B.M. Eyglunent. This

invention provided for the gasification of heavy hydrocarbons to carbon monoxide and hydrogen in a continuous process. Their apparatus is sketched in Figure 3.1. Details of pressure ratios and Mach numbers were not provided in the patent specification but it is possible to infer certain information from Figure 3.1.

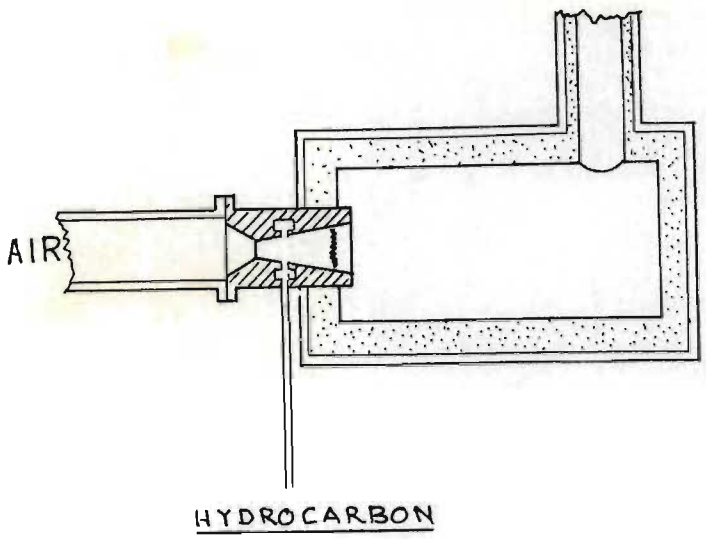

FIG. 3.1 REACTOR OF BORGNAT AND EYGLUNENT

Firstly, the fact that a shock is shown as occuring in the nozzle implies that the Mach number at the shock was low - below about 1,5. Secondly, the secondary gas was injected normal to the primary flow, and this implies that there was a bow shock ahead of the injection point. It seems therefore, and it is stated in the specification, that the device primarily provided rapid heating and mixing of the gases. It does not seem that smooth mixing of the gases was established at a static temperature low enough to prevent a chemical reaction, and the mixture

then passed through a shock.

Diesner and Schugerl (1974) discussed a supersonic reactor in which the reaction between methane and fluorine was carried out. The rationale for the use of the supersonic reactor was to protect the walls of the reaction vessel from the highly corrosive and hot reaction products. The scheme employed a central stream of fluorine around which flowed a stream of methane and around the methane stream flowed yet another stream. The outer concentric stream was of an inert gas whose function was to protect the walls of the reaction vessel. The streams expanded freely once they had emerged from their orifices. Thereafter a reaction occurred when the mixture passed through a set of retardation shocks. The advantage of this system was that the reaction occurred away from any surface. No attempt was made to tailor the mixing in any way once the gases were admitted to the nozzles at room temperature. The nozzles were not contoured, consisting simply of a central tube, surrounded by annular slits.

A type of reactor which is similar to the concept put forward is the plasma jet reactor. (For a survey of plasma reactors, see Baddow and Timmins, 1967). In this scheme, a gas is ionised and heated by electrical arc. This heated jet can then be mixed (at subsonic speeds) with secondary gases. It is possible by this method to have short reaction times at potentially very high temperatures. A limitation of the process

is that mixing is not uniform and diffusion effects tend to control the reaction.

Ibberson and Sen (1976), discuss a plasma jet reactor in which they investigate the conversion of methane to acetylene and ethylene. Argon was ionised in a DC arc to produce a plasma jet at high temperature. Methane was then fed into the periphery of the jet. The result was a highly non-uniform reaction zone with an annulus of cooler methane around a very hot argon core. Samples of the reaction products were then quenched by being drawn off in a water cooled probe of small bore. Yields of up to 82% acetylene (on a carbon basis) were obtained. With other hydrocarbon feed stocks, yields of up to 27% ethylene (again on a carbon basis) were obtained.

Although this gaseous reactor scheme employs rapid heating rates, it does not have the feature of shock heating the reactant gases.

3.3. The Establishment of a Standing Shock in a Duct

Although standard texts (Liepman and Roshko, 1957, inter alia) discuss the flow through a de Laval nozzle and the fact that deceleration should occur through a normal shock, in practice, this is not the case at high Mach numbers. Schlieren photo-

graphs are reported (op cit) which show the phenomenon for low Mach numbers.

Seddon (1960), demonstrated the upper limit at which a normal shock can occur in a duct. He studied the interaction between the duct boundary layer and a standing shock wave at a flow of Mach 1,47. At this flow rate, the shock was considerably distorted.

It is possible for the sharp pressure rise associated with a normal shock to exist away from the boudary because the high pressure cannot be communicated upstream to the supersonic flow. However, in the presence of a wall, there exists a boundary layer, a portion of which is subsonic. The pressure behind a shock wave intersecting this boundary layer is transmitted upstream and causes a thickening of the boundary layer ahead of the shock. This produces an oblique shock or series of oblique shocks corresponding to the behaviour of supersonic flow at a concave corner. (Green, 1970). This phenomenon gives rise to what is termed a lamda shock, because of its shape. If the Mach number in the duct rises further, the effect becomes so severe as to disrupt the flow and produce a complex pattern of weak shocks.

The formation of shocks is encountered in several areas of high speed gas flow.

In the field of high speed turbine flow, the problem is considered, but the emphasis is on avoiding the formation of shocks.

In high speed propulsive devices for aircraft, it is necessary to decelerate the incident supersonic flow ahead of the device to a subsonic speed in order to permit economical compression. The problem of shock wave-boundary layer interaction is also considered in this context. One solution to the problem of deceleration is to establish a standing shock at the mouth of the diffuser because this can be made to have a relatively small cross-sectional area. This is discussed by Hill & Peterson (1967), but the situation in a duct is different from that in an infinite flow field.

In the design of rocket exhausts, the phenomenon of shocks is again encountered. (Hill and Peterson, 1967). The formation of shocks in a rocket exhaust carries efficiency penalties and is avoided.

It therefore seems that the proposed supersonic chemical reactor provides the first stimulus for establishing a normal shock in a duct at high Mach number.

3.4. Supersonic Mixing

Although no reference was found in the literature to super-

sonic mixing in long ducts, there are extensive reports of investigation into enclosed mixing in the near field and to mixing in free jets.

Squire and Trouncer (1944), presented the classic treatment of an incompressible jet in a moving ambient. Since then this has been refined by subsequent authors * and good mathematical models are available for incompressible mixing.

Supersonic shear layers have been studied in relation to film cooling (Freedman, Radbill and Kay, 1963), thrust vectoring (Hawk and Amick, 1967) and to supersonic combustion ramjets (SCRAMJETS). The investigation into film cooling has little value for this investigation because it is concerned with heat and momentum transfer to a wall from an infinite flow. Thrust vectoring uses normal or oblique injection, and because this produces a bow shock ahead of the injection point (Hsia, 1966), it is unsuited to the present investigation.

Scramjets ingest air at supersonic speed, compress it by varying the duct area, inject hydrogen or suitable fuel which is ignited and burns supersonically in an exhaust nozzle, thus producing thrust. Such a device is capable of operating at speeds up to the Earth's escape velocity.

*Corrsin and Uberoi (1952), Forstall and Shapiro (1949), Abramovich (1963) and Schligting (1968).

One of the difficulties of the concept is the injection and mixing, at supersonic speeds, of the fuel because only a limited mixing length is available.

A considerable amount of research has gone into this aspect. The most relevant work is listed below *. No adequate predictive technique has emerged and unfortunately the empirical correlations developed are of little use for this application because generally, only mixing in the near field is considered and because the scale of injection is

---

* Abramovich (1963)
Alpinieri (1964)
Bauer (1966)
Bluston (1966)
Channapragada (1963)
Channapragada & Woolly (1965)
Cookson, Flanagan & Penny (1968)
Crane (1957)
Donaldson & Gray (1966)
Ferri & Fox (1968)
Grabitz (1976)
Kleinstein (1963)
Libby (1961)
Libby & Schetz (1963)
Lorber & Schetz (1975)
Maydew & Reed (1963)
Morganthaler (1965)
Newton & Dowdy (1963)
Osgerby (1965)
Schetz & Favin (1966)
Schetz & Gilreath (1967)
Schetz & Gilreath + Lubard (1969)
Shivamoggi (1976)
Switchenbank & Chigier (1968)
Thayer & Corlet (1972)
Visich & Libby (1960)
Zakkey & Krause (1963)
Zakkey, Krause & Woo (1964)
Zukoski & Spaid (1964)

such that the effect of the walls is minimised and it cannot be regarded as mixing in a long duct.

The techniques used for the analytical treatment of free mixing are not applicable to the treatment of ducted mixing because although the conservation equations can be written in the same form, the boundary conditions are different. In free mixing, all the properties on the axis of the jet decay to those of the free stream at an infinite distance from the jet. Thus if unit Prandtl and Lewis numbers are assumed, the simplification results that the profiles of species concentration, velocity and temperature become similar. Then the main difficulty is the description of the variation of eddy viscosity. It is customary to employ some form of the Prandtl mixing length hypothesis to describe the variation of eddy viscosity, often assumed constant at any axial station. This will be enlarged upon in Chapter 7.

For supersonic ducted flows, the boundary conditions are more difficult. The temperature at the wall will depend upon internal radiation as well as external heat transfer and axial heat conduction by the wall. The condition of no mass transfer through the wall is convenient but, for momentum, an estimate must be made of wall friction. For these reasons the analysis of free jets has little value for the analysis of mixing in a long duct.

No reference was found to any investigation of supersonic mixing in a long duct.

CHAPTER FOUR

EXPERIMENTAL

4.1. INTRODUCTION

This chapter deals with the design and development of equipment and techniques which were used to:

(1) Provide nitrogen at a controlled high pressure and temperature.
(2) Expand this nitrogen to supersonic speed.
(3) Measure pressures, temperatures and gas concentrations in the supersonic flow.

Particularly, in the design and development of the nitrogen heater, but also in the choice of the material of construction of the nozzle, a large number of failures were recorded. These are not discussed and the final working design is presented.

4.2. Design and Construction of the de Laval Nozzle

The aim of the nozzle design was to produce an expansion to Mach 3,74. It was thought desirable that the gas leaving the nozzle should be reasonably uniform and parallel. This would simplify any analytical treatment of the mixing problem.

The technique which is traditionally used, the method of characteristics by Prandtl and Busemann (1929), requires modification when applied to axi-symmetric flow. This makes the technique tedious.

Several techniques for nozzle design are presented in the literature *. These techniques were developed for wind tunnels where it is important that the supersonic flow be uniform. For this application, the requirements were not as stringent and so an older but simpler technique (Foelsch, 1949) was used, together with a boundary-layer correction by Tucker (1951). The profile developed is shown, full size in Figure 4.1.

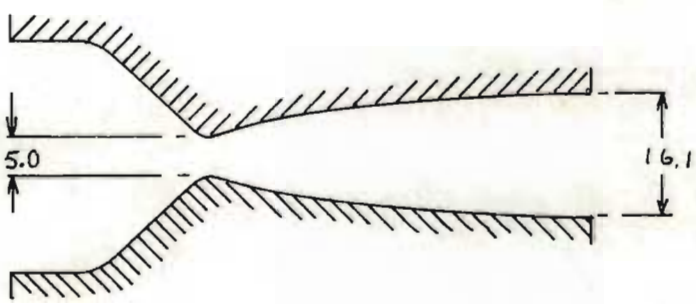

FIG 4.1 PROFILE OF NOZZLE

It was established experimentally that the radial temperature and velocity profiles of the supersonic flow at exit from the nozzle did not vary by more than 3%, except in the boundary layer.

*Conlan and Trytten (1964), Glowacki (1965), Dumitrescu (1975)

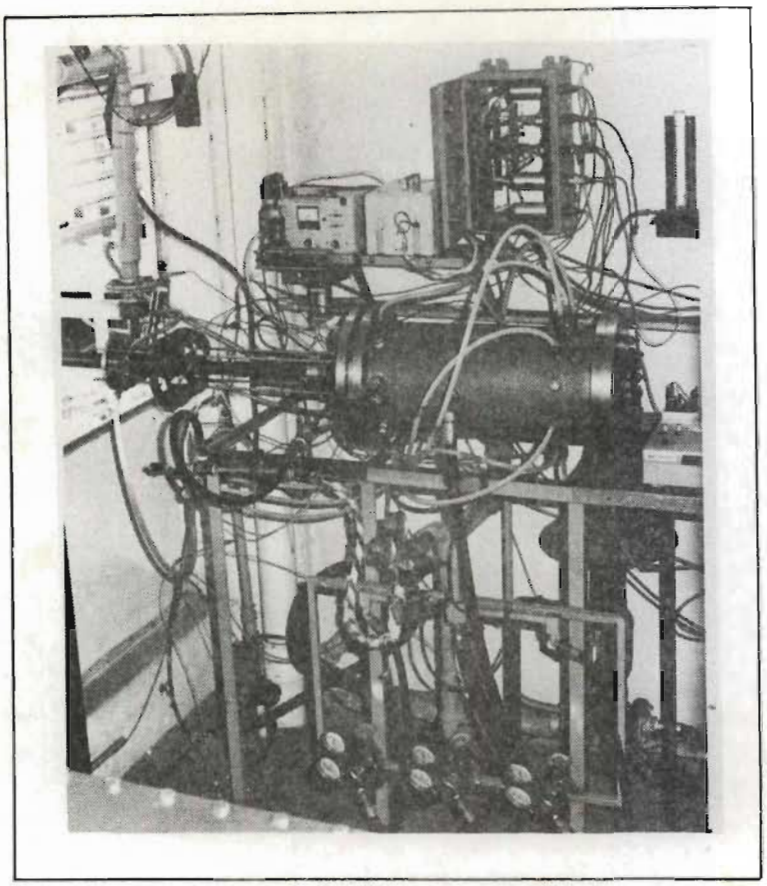

FIG. 4.2 Heater mounted on test bed.

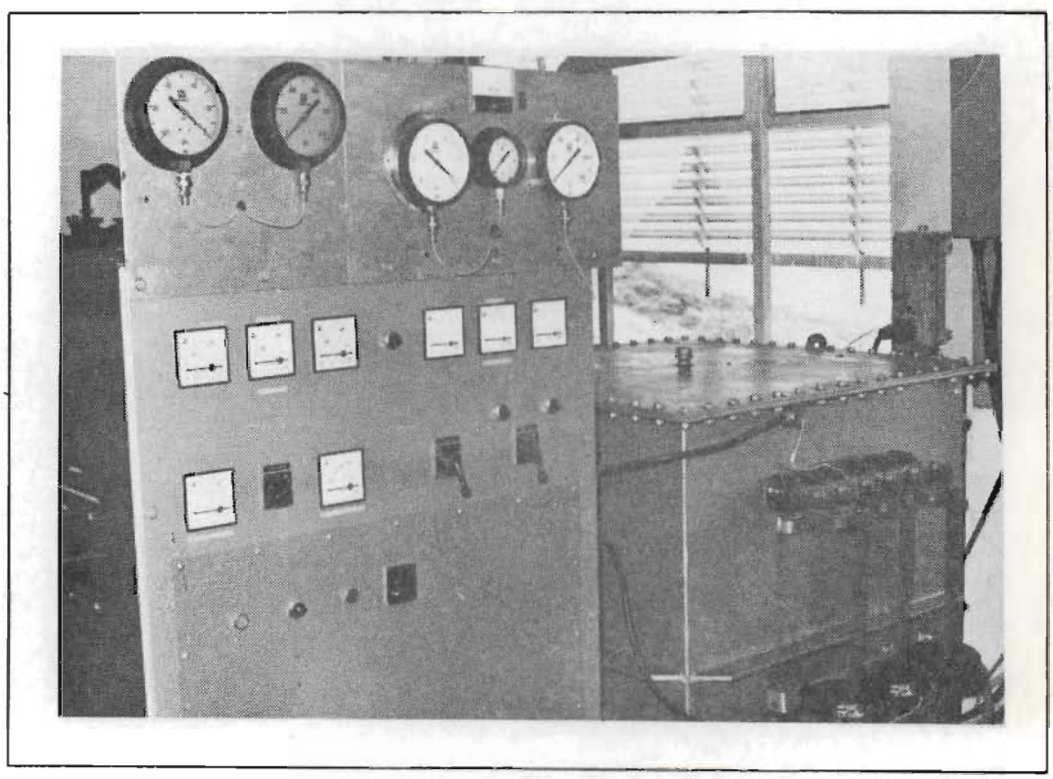

FIG. 4.3 Power Supply

After several trials it was found that 316 stainless steel was suitable for the construction of the nozzle.

4.3. Heating of the Gas

As discussed in Appendix (4.1), an electric resistance heater was developed which would operate continuously, providing nitrogen at a temperature of up to 2000^{o}K, and at a pressure of up to 2MPa. The resistance elements were of graphite. The heater ran on a three phase power supply and had a capacity of 250kVa. Figure 4.2 shows the gas heater mounted on the test bed.

The power supply, also discussed in Appendix (4.1), provided up to 2500 amps per phase at a phase voltage of 60V and this could be continuously varied from zero up to its maximum value. Control of the power was either manual or by means of an SC 1700 on-line computer. Figure 4.3 shows the power supply.

Nitrogen was provided from a trolley of 10 high pressure bottles from where it was led, to three Harris regulators, connected in parallel. Between the regulators and the heater was a pneumatic needle valve which could be controlled either manually or by computer. This system allowed pressure control either by setting the regulators or, at a fixed regulator setting by variation of the needle valve, under computer control.

4.4. Measurement Techniques Used

4.4.1. Pressure Measurement

Both static and stagnation pressures were measured during the course of the experimental work. Static pressures were measured by means of wall tappings. A hole 0.35mm in diameter was drilled orthogonally through the surface at which the pressure was to be measured and connected to this tapping was a 3mm OD metal tube which conveyed the pressure signal to a pressure transducer. Stagnation pressures were recorded using 1,5mm stainless tubing, with a hemispherical tip. This pressure was also transmitted to pressure transducers. In some cases, the pressure signal was also taken to a Bourdon gauge in order to provide a visual display.

In all, ten transducers were used, comprising two types, namely "Hottinger, Baldwin, & Messtechnik" and "Kyowa". All the transducers worked on the wire strain gauge principle and provided a full scale signal of the order of 10mV when excited by a stabilized excitation voltage of 5V. The outputs from the transducers were fed into the Analogue-to-Digital converter of a Control Data SC 1700 computer, which was used in real time mode. The A to D converter had a resolution of 25μV so that a resolution of 0,25% of full scale pressure was available.

In an attempt to improve this resolution, DC amplifiers were built but their stability was not satisfactory. The vendor-quoted accuracy of the transducers was 0,5% or better. Transducers of several different pressure ranges were used to ensure that readings were well up in the available measuring range.

The measurement of the low pressures occuring in the mixing tube presented a problem. Pressures of less than 10kPa, absolute were expected. If the transducers were used in the normal mode i.e. to register a gauge pressure, the reading would have been approximately -91kPa. A 1% error in this reading would have produced a 10% error in the absolute pressure reading. In order to overcome this problem, differential pressure transducers were used. This allowed two pressures to be fed to the transducer - one on each side of its diaphragm. It registered the difference between the two pressures. For the scheme employed, the pressure acting on the back of the diaphragm, instead of being atmospheric, was the pressure of a large evacuated vessel. This pressure was read on a Torricellian manometer and transmitted to the computer at the start of each run. The measurement recorded by the computer was then the difference between the pressure to be measured and that in the evacuated vessel - which remained accurately constant. Thus, effectively, an absolute pressure was measured without the inaccuracies implied by taking the difference between relatively large numbers.

4.4.2. Probe Advancement

In order to measure stagnation pressures in the mixing tube, it was desirable to be able to advance a pitot probe across a diameter of the mixing tube. It will be seen that the diameter of the mixing tube which was used was approximately 18mm. Thus it was desirable to be able to advance the probe by increments of about 500 microns, preferably on instructions from the computer in order to minimise the time taken to scan a diameter. A device was designed and built which used an electric solenoid to accomplish this. It is shown in Figure 4.4.

4.4.3. Temperature Measurement

Temperatures were measured with Platinum/Platinum-14% Rhodium thermocouples, reading into the computer. The measurement of temperature in high speed flow requires a special probe. The probe used is drawn below. The probe was made from a thermocouple sheathed by a 1,5mm OD inconel sheath. This implied that the pitot probes and the temperature probe fitted interchangeably into the probe advancement apparatus. In supersonic flow, a detached bow shock will

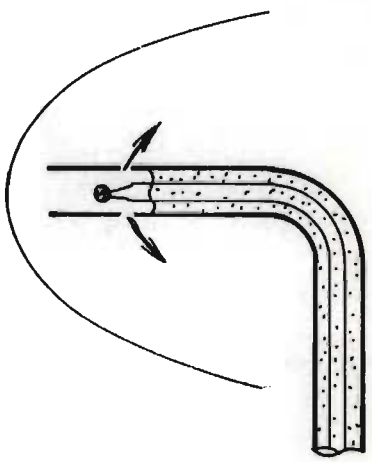

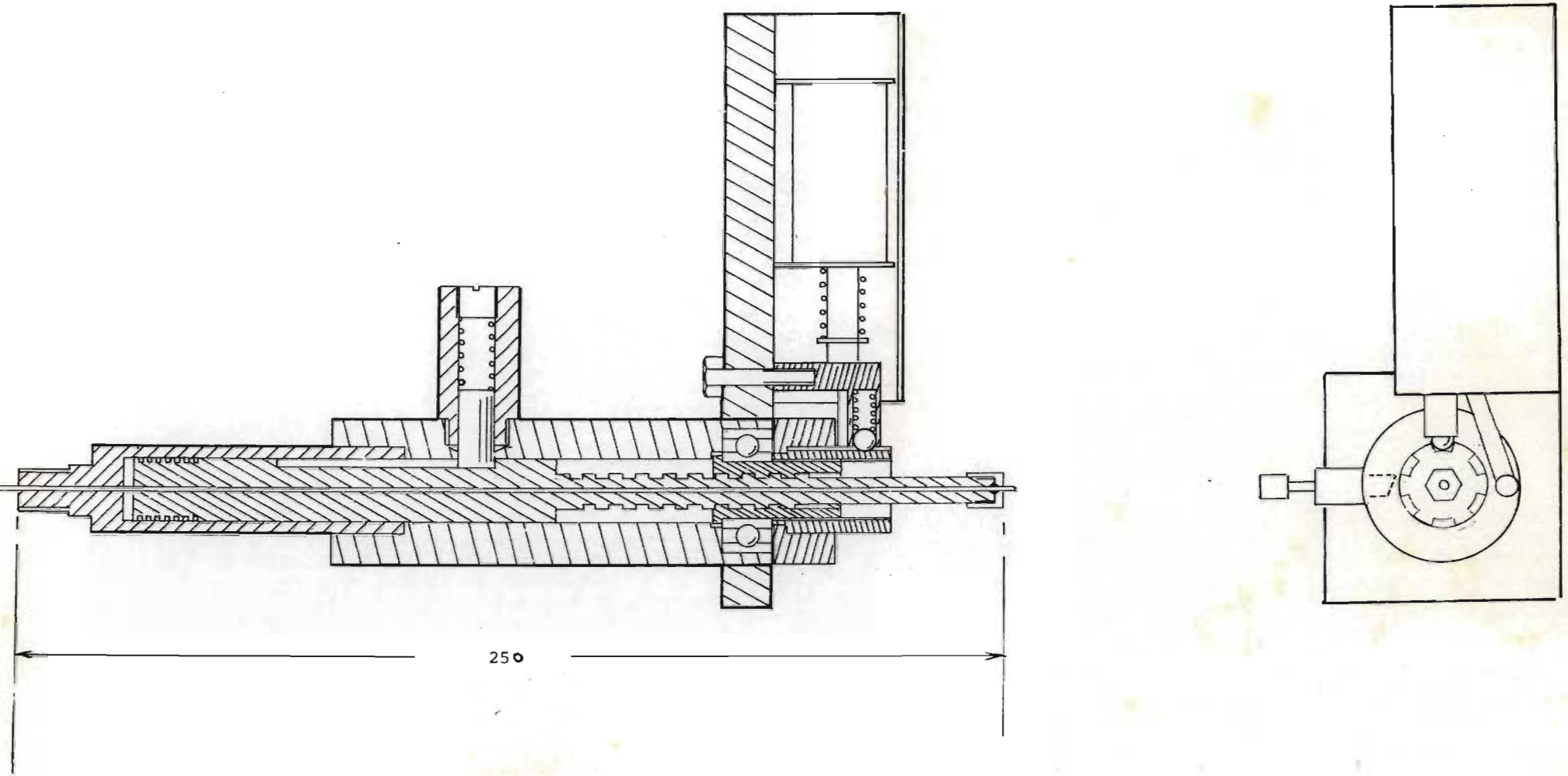

FIG. 4.4 PROBE ADVANCEMENT APPARATUS

form ahead of such a probe. This will imply that the gas is decellerated to subsonic flow through a normal shock. Thereafter, it is necessary for the gas to be retarded isentropically to stagnate on the thermocouple junction. The junction was shielded to some extent from radiation losses by the inconel sheath but it was desirable to maintain a small flow past the probe in order to make up any heat losses. For this reason two 0.35mm diameter holes were drilled behind the junction to enable a small bleed of gas. Clearly the recovery factor of such a probe is less than unity. Liepman and Roshko (1957) state that it can be expected to be greater than 0,95 but it should nevertheless be determined by calibration. The probe used was run under known conditions and its recovery factor was found to be unity. This was probably due to error in the manufacturer's data on the performance of the junction.

4.4.4. Concentration Measurement

It was proposed to use a pitot tube in conjunction with the probe advancement mechanism described above to withdraw samples from the mixing tube. It was judged to be necessary to take at least ten measurements on a radius of the mixing tube, at any station. Therefore, either ten evacuated ampoules with solenoid valves could have been used for later analysis, or else a short-period on-line technique was necessary so that the probe could be advanced to a point, the gas sampled and analysed, and the probe then moved on

to the next point.

Because of the high running costs of the nozzle, it was necessary that any sampling and analysis technique should take less than say 15 seconds per sample. A further complication was that although the sampling probe would be exposed to the stagnation pressure of the flow, it was anticipated that, particularly near the walls, the pressure on the probe would be less than atmospheric pressure and could be expected to vary by a factor of four. The scheme developed is described in Appendix 4.2. It provided analyses to approximately 0,1% accuracy, taking approximately 10 seconds to analyse each sample.

4.4.5. Experimental Control and Data Handling

Because of the extreme conditions of the experiments and because of the financial incentive to keep the experimental runs as short as possible, all the experiments were run under computer control.

Using a program which compared a set point with a measurement of the gas temperature and applied P.I.D. control, it was possible to raise the gas temperature to circa 1350^{o}K in 20 seconds. This could then be maintained within about 1% of this value, despite changes in the gas discharge of the

nozzle resulting from changes to reservoir pressure.

The safety of the experiment was monitored and, in the event of the readings available to the computer indicating a dangerous or undesirable situation, the run was aborted and gas and power supplies terminated by the computer.

All the instruments were read each second and the data was stored on magnetic disc for later processing. 21 measurements were taken each second.

At the end of each run, the experimental results were processed and the secondary results of the tests were printed out for retention. The files on the discs were then overwritten in subsequent runs. It is estimated that during the course of the experimental work, more than 500 000 experimental measurements were taken.

CHAPTER FIVE

ESTABLISHMENT OF A NORMAL SHOCK

5.1. INTRODUCTION

In an attempt to avoid a shock-boundary layer interaction the flow configuration depicted in Figure 5.1 was employed.

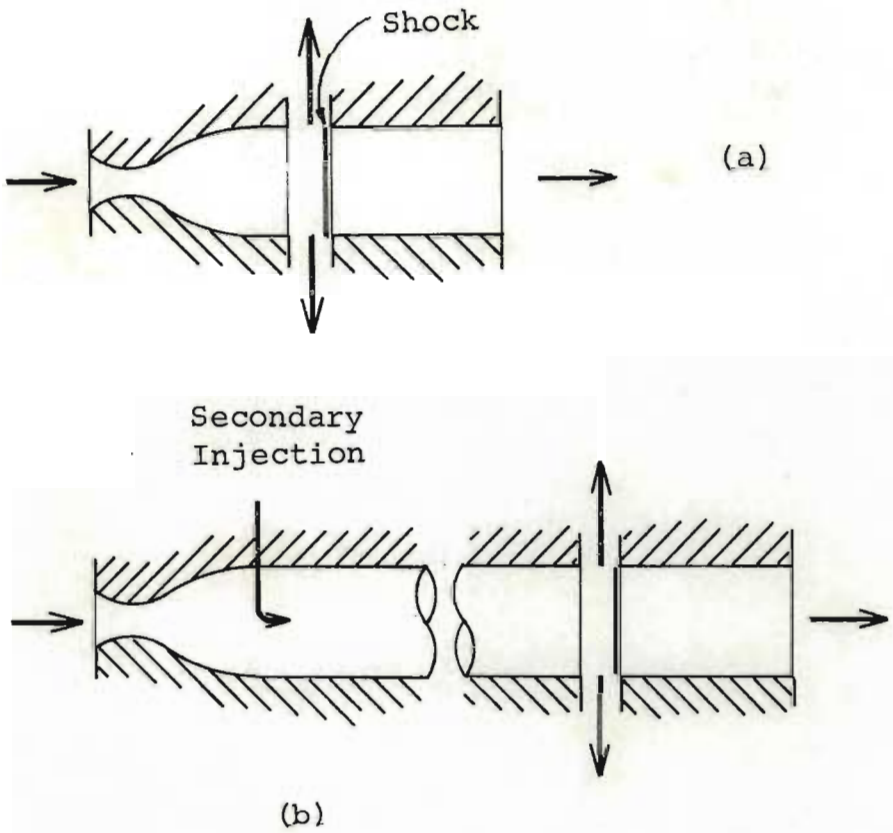

FIG.5.1. BOUNDARY LAYER REMOVAL.

The techniques which are reported in the literature* are inadequate for the mathematical prediction of the position at which a shock could be expected to occur. The work which has been reported deals with the prediction of the position and shape of the detached bow shock ahead of a bluff body or a supersonic diffuser in an infinite supersonic stream. For the more complex flow schemes depicted in Figure 5.1, it seemed that a mathematical prediction would be very difficult

* Berman (1965), Korkan (1966), Aungier (1970), Schulte (1974) Korkan and Gregorek (1977).

(Curle and Davis, 1971, p 130) and the problem was handled empirically.

The experimental treatment was divided into a preliminary investigation of the establishment of a shock at the end of a nozzle as shown in Figure 1a and the consideration of the establishment of a shock after the secondary gas had been injected and mixed as shown in Figure 1b. A further factor in electing not to attempt a mathematical prediction of the formation of the shock for the simple case was that it was unlikely that such a technique could be extended to the case where a non-uniform, mixed gas stream approached the shock. This would be the situation after the secondary injection had been accomplished.

The flow configuration of Figure 5.1 can be likened to the operation of the diffuser of the supersonic air intake of a jet engine. This behaviour has been discussed using a one dimensional analysis (Hill and Peterson, 1967) and from this analysis, the concept of a detached shock "spilling" air past the diffuser is useful. It can be argued that if the diffuser cannot ingest all the air which it would capture if the flow were not deflected, the flow in the diffuser becomes subsonic. The pressure in the diffuser builds up until it compels a detached bow shock to form ahead of the diffuser. By virtue of its curvature, the bow shock deflects some of the incident air stream and the flow through the

diffuser is regulated by diffuser pressure.

It was anticipated that similar phenomena would be observed in the present case with the added complication that the amount of spillage would be limited by the capacity of the vacuum system. If the vacuum system became overloaded, the flow would probably degenerate to a diamond pattern of shocks.

5.2. Establishment of a Shock Directly after Expansion

5.2.1. Experimental

A housing as shown in Figure 5.2 was constructed from stainless steel. It presented a diffuser symmetrically to the supersonic flow as it emerged from the nozzle. It also allowed the gap between the nozzle and the diffuser to be varied.

The volume available for removal of the evacuated gas was so contoured as to provide uniform suction all around the diffuser gap and to provide some pressure recovery if the spilled flow should be supersonic.

The housing also incorporated two ports which permitted shadow graphs to be taken through the diffuser gap. The ports were water-cooled to protect the tempered glass.

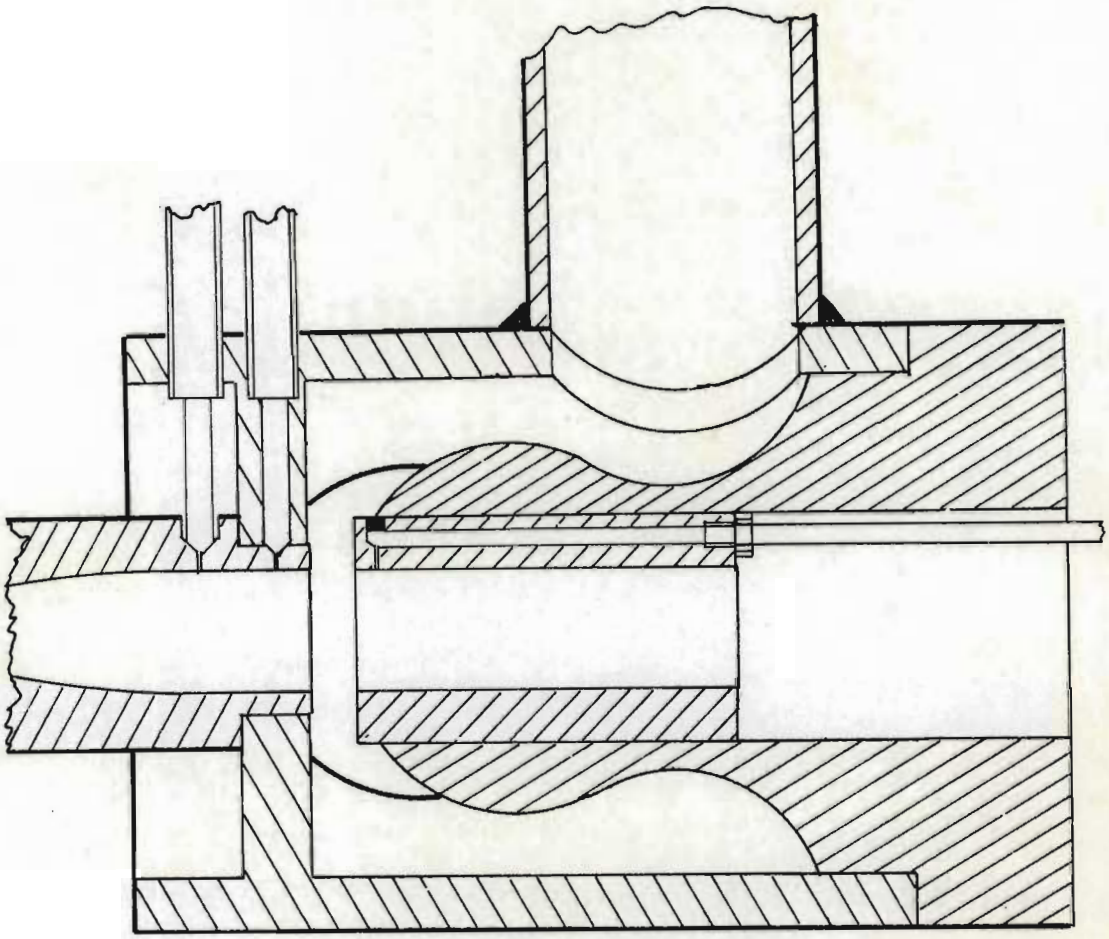

FIG. 5.2 VACUUM HOUSING

The vacuum system was composed of two liquid ring pumps - an FBM P520 and an FBM P624. These pumps consumed about 30kW of electrical power and between them drew a maximum of

approximately 1225m^3/h of air at a vacuum up to 740 mm Hg. The steel vacuum line, of 38mm diameter was water cooled and contained a gate valve which enabled the variation of the amount of gas to be drawn off. The pumps were run with water as the sealing liquid although mono-ethylene glycol was tried in an unsuccessful attempt to improve the vacuum.

Four different diffuser shapes were tested. They are shown below in Figure 5.3.

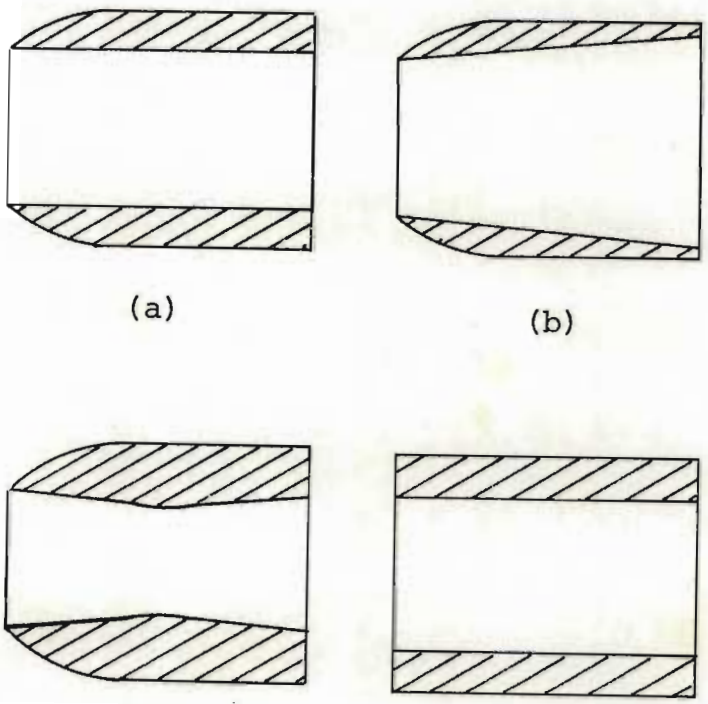

FIG 5.3

Diffusers of each shape were tested with the inlet diameters larger than, the same size, and smaller than the exit diameter of the nozzle.

Static pressure measurements were made by means of wall tappings, in the diffusers. Generally two measurements were made - one about 3mm from the lip and the other 10mm further back. The tappings were connected to stainless steel tubing which carried

the signal down the exhaust duct and to pressure transducers remotely situated.

For each shape, tests were run with the gap between diffuser and nozzle being varied from zero to a distance of 12mm. At each setting the reservoir pressure of the nitrogen was continuously varied up to a value of approximately 1,3MPa. This was approximately twice the anticipated value required to produce a shock, as determined from the one-dimensional theory. Reservoir temperature was maintained constant at 1350^{o}K.

In an attempt to photograph the shock, a shadowgraph technique was used, employing a collimated electronic flash and a 35mm camera with a focal plane shutter.

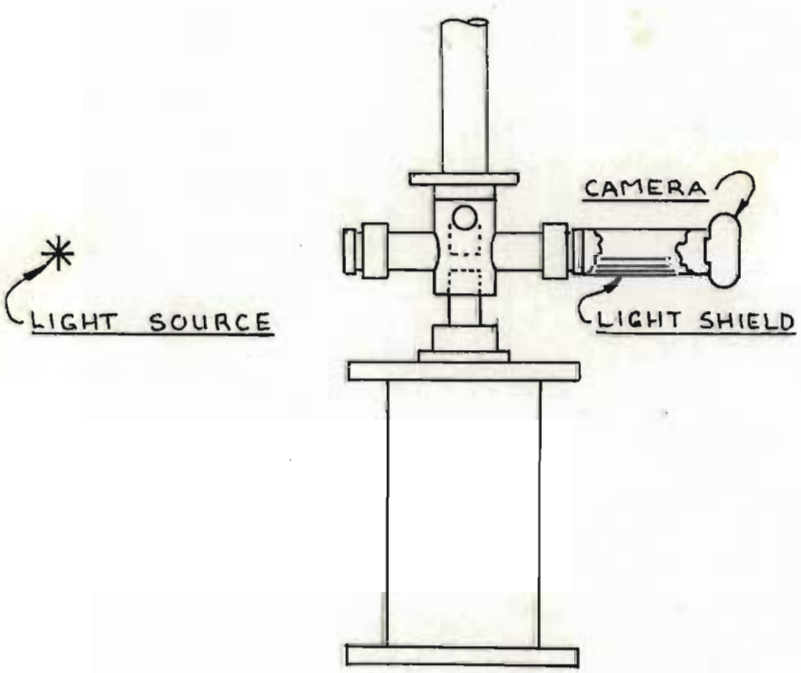

FIG 5.4 SHADOWGRAPH ARRANGEMENT

The arrangement is shown in Figure 5.4.

It was not anticipated that a good picture would be obtained, but an indication was

required as to whether or not the shock was occuring as a detached shock in the diffuser gap.

5.2.2. Results and Discussion

It was found that only the last shape in Figure 5.3, namely the bluff diffuser, produced a shock. In the other cases, it was possible to establish supersonic flow for a fairly narrow range of diffuser gaps but the flow then recompressed back to subsonic flow over an appreciable distance in the diffuser - presumeably indicating a diamond pattern of shocks. The diffuser gap spacing which permitted supersonic flow depended upon the ratio of nozzle exit diameter to the inlet diameter of the diffuser in order to permit supersonic flow in the mixing tube. Diffusers with an inlet diameter smaller than the nozzle exit diameter had to be closer to the nozzle than those with larger diameters.

Approximately 100 sets of pressures were measured for each diffuser gap setting. The readings shown in Table 5.1 were selected from these readings in increments of approximately 50kPa of the reservoir pressure to show the development of the shock profile.

The downstream end of the diffuser was connected to a short water-cooled exhaust system. Thus the downstream end of the diffuser was effectively exposed to atmospheric pressure.

It is postulated that there are two basic reasons why a shock could not be obtained with any of the other diffuser shapes tested. Firstly the incident flow is sensitive to diffuser behaviour. Because the vacuum system was limited (though fairly large), it is possible that the correct flow regime could not be reached before the pressure around the diffuser gap became too high and the whole flow degenerated. Secondly, the incident velocity profile was not uniform as it would be in an infinite flow field. Around the edges of the nozzle there was a boundary layer which might have affected the performance of the diffuser.

From Table 5.1 may be seen the way in which the shock develops. Considering the set of readings at a diffuser gap of 4,8mm, it can be seen that for a reservoir pressure of 714kPa the pressure at the nozzle exit is very much higher than it would be if the flow were supersonic (approximately $P_{reservoir}/114$ = 6,3kPa). Presumably there is a set of diamond shocks in the nozzle and diffuser, which explains why the static pressure gradually increases in the direction of flow.

This trend continues for the next set of readings except that the flow has become faster. This may be inferred from the fact that, although the reservoir pressure is higher, the pressures in the nozzle and diffuser are slightly lower.

At the next reading the shock has become established at the

TABLE 5.1

RESULTS OF VARYING DIFFUSER GAP AND RESERVOIR PRESSURE

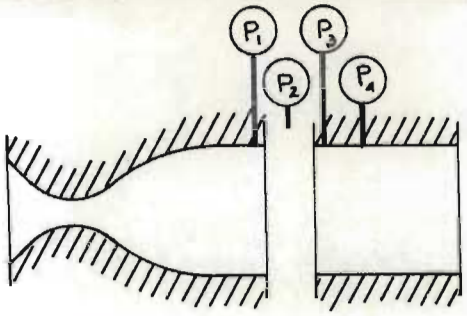

Diffuser gap (mm)	Reservoir	Pressures (kPa) P_1	P_2	P_3	P_4
1,5	804	56	58	58	64
	855	36	10	46	59
	906	31	9	41	53
	958	30	9	40	50
	996	28	9	37	47
	1047	20	7	36	43
	1086	12	4	34	40
3,2	753	56	57	41	69
	804	22	13	41	53
	855	21	11	38	51
	906	15	8	40	53
	958	9	4	45	54
	983	10	4	43	50
4,8	714	59	60	64	72
	804	53	55	59	68
	855	9	5	70	89
	906	9	5	66	79
	958	10	5	52	62
6,5	701	60	61	66	74
	753	54	57	64	72
	804	51	55	60	69
	855	9	7	85	98
	906	10	5	75	92
8,0	714	15	14	40	54
	753	12	11	52	65
	804	9	9	92	93
	855	10	7	90	98
10,0	727	11	11	47	71
	753	9	10	61	84
	804	8	8	82	95
	855	9	7	90	97
	868	9	6	91	97
12,0	727	13	15	39	51
	753	12	13	37	50
	817	9	9	43	64
	855	9	6	66	94
	894	8	6	71	95

diffuser mouth. While running the experiment, it was possible to hear, very distinctly, the instant at which a shock became established. Experimental runs were so noisy that it was necessary to wear ear protection but when the shock was formed the noise diminished sharply. An explanation for this effect is that before the formation of the normal shock, highly turbulent gas was issuing from the exhaust

whereas after the shock, a slower, more uniform gas stream was emerging.

With a further increase in reservoir pressure, the pressure at the end of the nozzle increases slightly as a consequence of the fixed maximum pressure ratio.

Table 5.1 shows that the least reservoir pressure required to produce a shock depends upon the diffuser gap. In order to assess the best diffuser gap setting, it is helpful to define a shock efficiency, η , as the ratio between the static pressure measured immediately after the shock and that predicted from the reservoir pressure on the basis of one-dimensional theory. For the gas-dynamic configuration proposed, namely an isentropic expansion to Mach 3,74 followed by a standing normal shock, an overall pressure ratio of reservoir pressure to post-shock pressure of 7,05 is implied.

Figure 5.5 shows a plot of shock efficiency against diffuser gap.

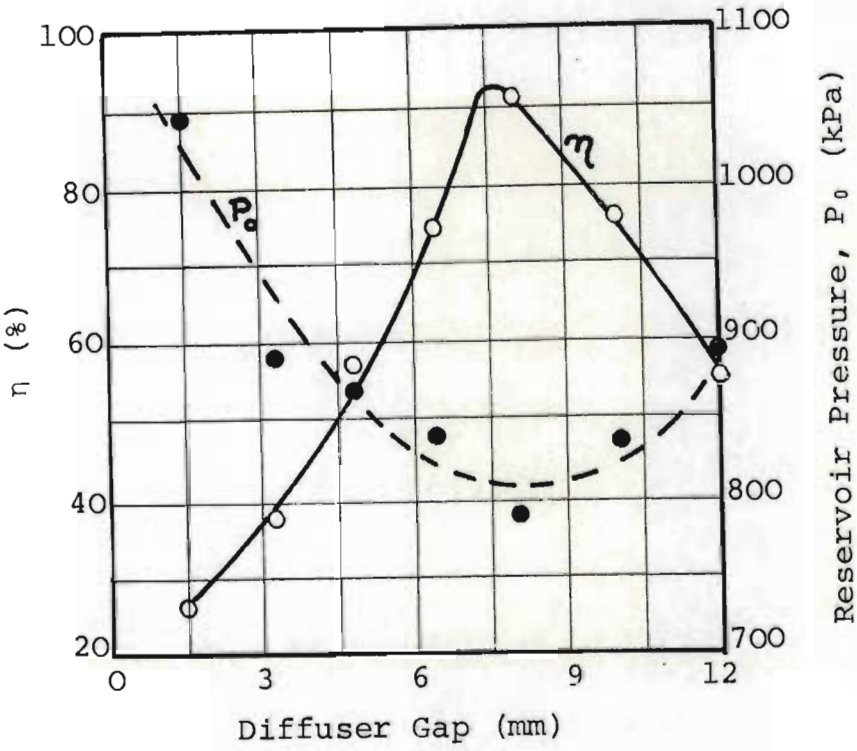

FIG 5.5

In calculating the optimum efficiency for each diffuser setting, the best set of readings was not necessarily one of those tabulated in Table 5.1.

Superimposed on Figure 5.5 is the reservoir pressure which produced the sharpest pressure profile at each diffuser gap setting.

The pressures recorded in the diffuser were derived from wall tappings and are an indication of the pressure in the boundary layer of the diffuser. It is probable that static pressures inside the diffuser are not constant over the cross-sections just behind the shock. (This aspect was investigated in more detail for the case of the shock at the end of the mixing tube - where a non-uniform pressure profile behind the shock was found). It is postulated that the pressure at the wall

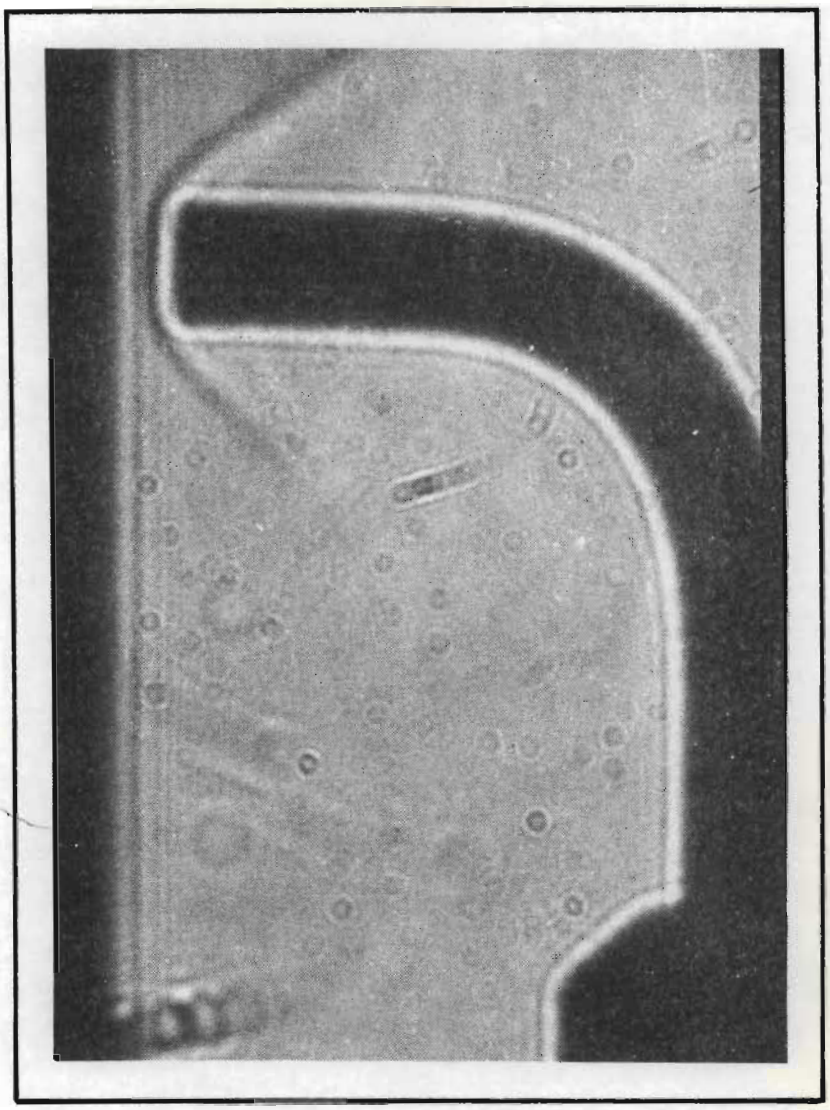

FIG. 5.6 Shadowgraph taken through diffuser gap. The shadow at left is the end of the nozzle. The probe was 1,5mm. in diameter.

is below the theoretical value because some of the slower-moving boundary layer finds its way into the diffuser. Because it has a lower Mach number, the pressure after the shock is correspondingly lower. The pressure equalises rapidly behind the shock as may be seen from pressures P_3 and P_4, tabulated in Table 5.1. Again, this phenomenon was investigated in greater detail in Section 5.3. Depending upon the diffuser gap and the vacuum around the gap, either more or less of this slow moving gas is removed. Thus the efficiency of the shock improves in Figure 5.5 until, at a diffuser gap of about 8mm, the optimum is reached whereafter the vacuum system becomes overloaded and efficiency drops again.

No photograph of a detached shock was recorded in the diffuser gap. Figure 5.6 demonstrates the effectiveness of the photographic technique.

It shows the detached bow shock produced by a probe inserted into the supersonic flow. The quality of the photograph is poor because it is an axi-symmetrical shock, because of the turbulence and heat gradients in the tubes of the observation ports and because of severe astigmatisms in the heat-treated glass of the ports. However, the shock is seen quite distinctly and, had a detached bow shock formed in front of the diffuser, it would have been observed. Thus it must either have been so close to the diffuser as to be indistinguishable from the edge of the diffuser

shadow or else have been inside the diffuser.

5.2.3. Conclusion

It is concluded that:

(1) A standing shock can be established using a bluff diffuser.

(2) The reservoir pressure required to produce the shock depends upon the diffuser gap and the vacuum around this gap. This is interpreted in terms of a boundary layer phenomenon.

(3) The reservoir pressure required to produce the shock was higher than a one-dimensional prediction based on overall pressure ratio.

(4) The shock conditions could not be gradually approached. At some instant the shock formed, it did not form over a period of time.

(5) It is probable that for a larger nozzle, the boundary layer would be less significant and a streamlined diffuser might produce a standing shock.

5.3. The Establishment of a Standing Shock at the End of the Mixing Duct

5.3.1. Introduction

It was necessary to investigate how a standing shock might be established at the end of a tube in which two gases were mixed supersonically and the gas-dynamic configuration which would produce the best shock. On the basis of the investigation for the simple case, a bluff diffuser was used but factors such as the diffuser gap, the mixing scheme and the reservoir pressure ahead of the nozzle would bear on the behaviour of the shock and would need to be examined for this case.

A supersonic reactor was built which allowed controlled injection of the secondary gas with a tube of variable length available for mixing of the two gases. A device for producing the shock could be situated at the end of this mixing tube and the behaviour of the shock examined.

Nitrogen was used as the primary gas, and CO_2 was injected. A decision had to be taken on the mode of injection. Two modes were possible. It has been shown (Hsia,1966) that radial injection of a secondary gas into a supersonic flow produces a bow shock ahead of the injectant stream. This was undesirable and it was decided to inject the secondary

gas co-axially. The choice then remained of whether to inject the secondary gas at the centre as in Figure 5.7(a) or at the periphery, as shown in Figure 5.7(b).

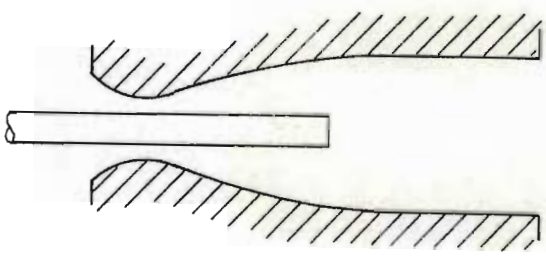

(a)

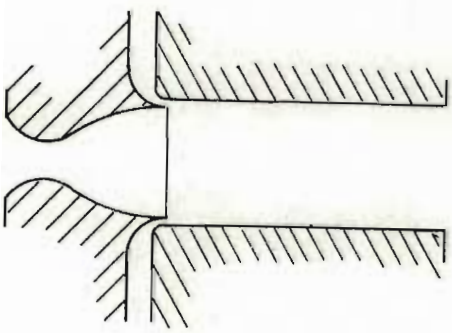

(b)

FIG 5.7.

Because the experiment had to be conducted on a relatively small scale, it was decided not to inject at the centre because the annulus between the injector stem and the nozzle throat would have been very small. This would have made dimensional stability of the arrangement important and, because of the high temperatures invisaged, very difficult. A second factor which opposed central injection was that an extra boundary layer would have developed - that on the injector.

Accordingly peripheral injection was chosen. This had the advantage that the area of interface between the two gas streams was very much larger than for central injection. Secondly, it could be expected that the mixing tube would run cooler with peripheral injection. (Freedman, Radbill and Kaye, 1963). Thirdly, fabrication would be easier.

The literature could provide useable information on the probable performance of neither scheme.

5.3.2. Basic Apparatus

The injection manifold is drawn in Figure 5.8. It was fabricated from 316 stainless steel. The manifold was designed to produce axial flow at the point of injection and to obtain uniform injection all the way around the periphery. The purpose of the annular throat was to provide a pressure drop between the outer torus and the inner

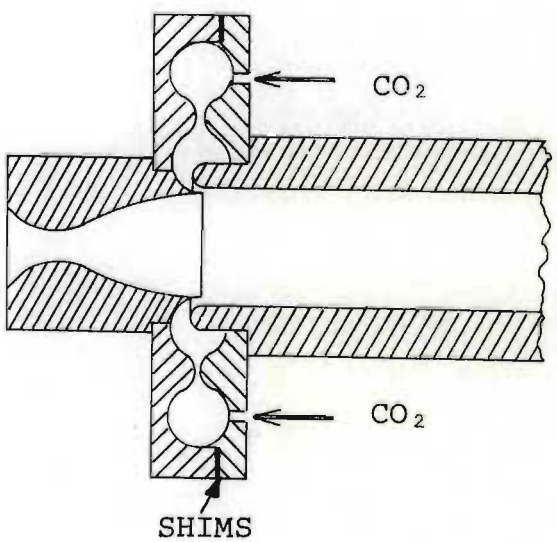

FIG 5.8 INJECTION MANIFOLD

torus, which communicated with the nitrogen flow. By changing the number of shimming washers at the mating face around the outside edge, it was possible to vary the gap between the potentially osculating faces of the annular throat. This ensured that the pressure in the outer torus would equalise fairly well and thus provide a uniform flow through the annular throat which would, in turn, ensure uniform injection around the central nitrogen flow. The material which served as a splitter ring between the two streams was turned to a knife edge in order to reduce the formation of a wake.

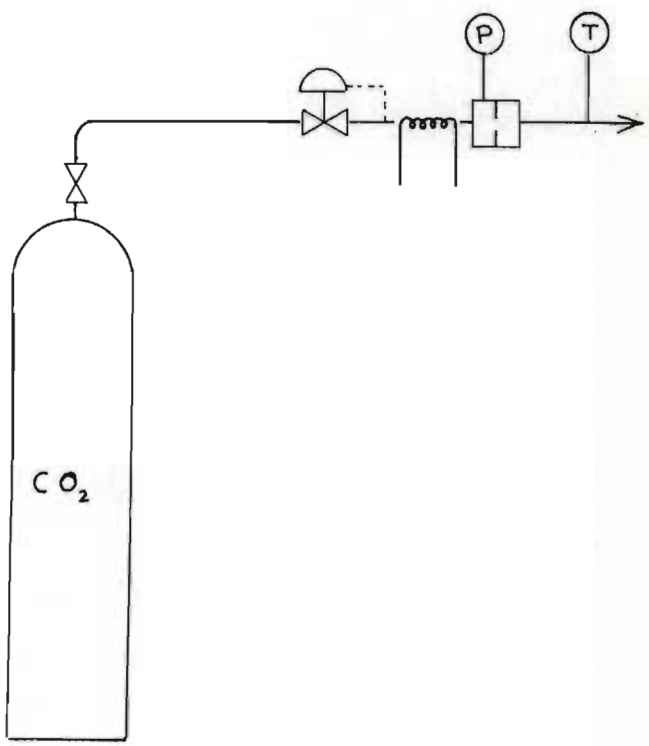

FIG 5.9 SECONDARY GAS CIRCUIT

The secondary gas circuit is shown in Figure 5.9. The injection rate was controlled by a regulator which adjusted the pressure before a super-critical orifice plate. The orifice plate was designed to run super-critically so that its flow could be calculated

from only one pressure measurement.

This pressure was recorded on a Bourdon guage to provide information for manual control of the pressure regulator. The pressure was simultaneously monitored by a pressure transducer and logged by computer to provide a record of the injection pressure at any time. A second Bourdon guage indicated the pressure in the outer torus of the injection manifold. This was necessary to enable the shims to be set so that a reasonable pressure drop occurred across the annular throat of the diffuser and also to ensure that the critical pressure ratio was always exceeded across the metering orifice. A 1mm diameter sharp-edged orifice was used and calibrated as described in Appendix 5.1.

The system enabled the pressure on the orifice plate to be set at a level calculated to provide the desired injection rate of secondary gas.

Electrical heating was employed on the carbon dioxide line to offset the Joule-Thompson cooling on expansion through the regulator.

The duct in which the gases were mixed was constructed from stackable sections as shown in Figure 5.10. The stainless steel sections were of such a length as to allow a mixing tube to be constructed up to 477mm long by increments of 53mm.

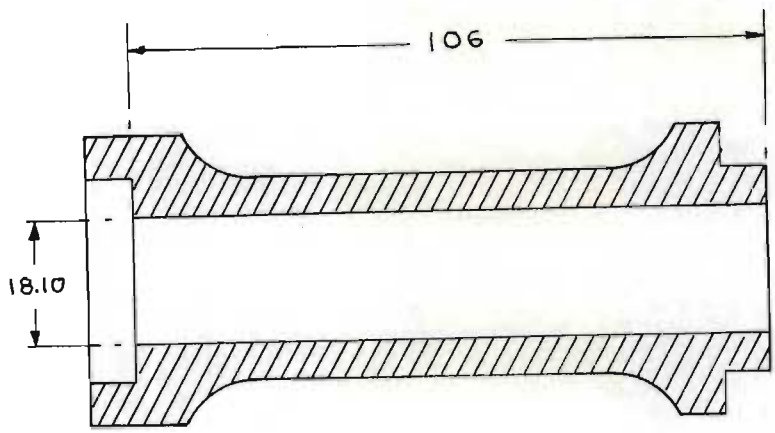

FIG 5.10 STACKABLE SECTION OF MIXING TUBE

The diameter of the tube was calculated to provide a secondary injection speed of Mach 0,95 when 2,4 g/s of CO_2 were injected.

Great care was taken with the internal surface finish and dimensions of the tubes. The outer diameters were extensively relieved to reduce their thermal masses.

The housing previously used for boundary layer withdrawal and diffuser gap adjustment was connected to the end of the mixing tube and the assembly, including an exhaust section, was secured by four tie rods as shown in Figure 5.11. The four rings were necessary to allow for thermal expansion of the mixing tube.

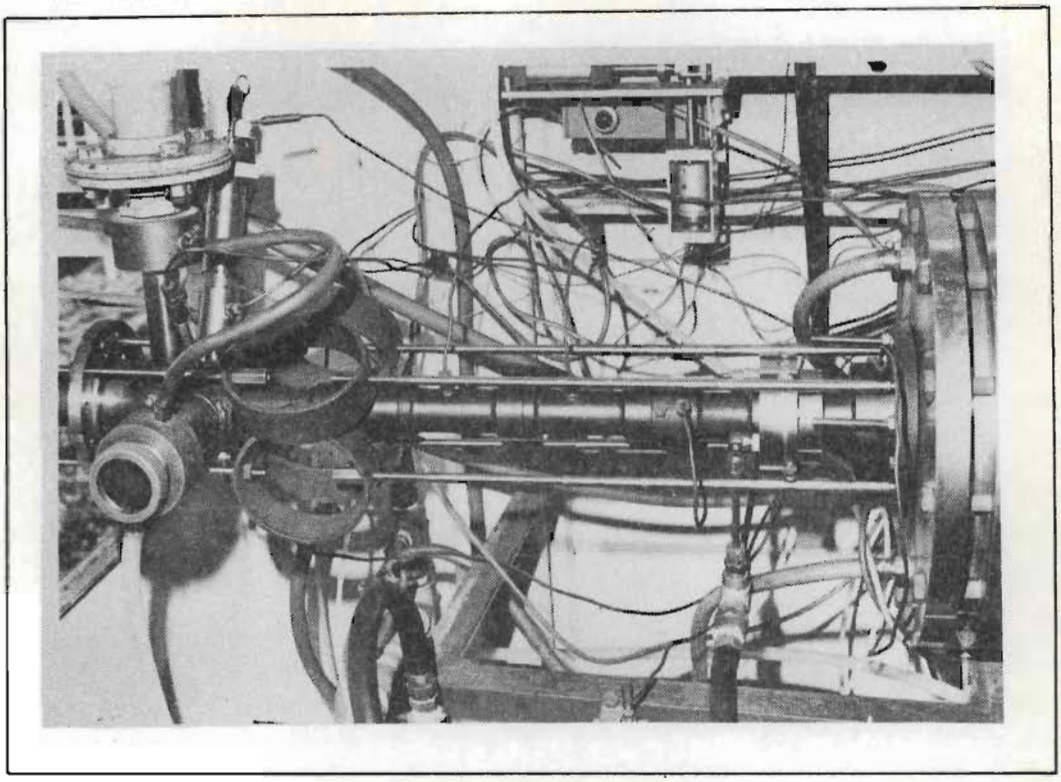

FIG. 5.11 Showing the heater at right leading into a stilling chamber, then the nozzle, mixing duct and diffuser housing. The vacuum take-off is at the top of the diffuser housing and the probe advancement apparatus is at rear right of the diffuser housing. The G.C. valve may be seen at top centre.

5.4. Instrumentation

As for the investigation into the formation of a shock under simple conditions, the static pressure was measured by means of wall tappings; at the end of the mixing tube, in the vacuum housing and at two points in the diffuser.

A shadowgraph photographic system was set up in case a detached shock formed in the diffuser gap.

In order more closely to investigate the shape of a possible shock, a device was designed and fabricated to allow an axial profile of stagnation pressure to be measured. The device used the probe advancement apparatus as described in Chapter 4 to advance a round-nosed 1,5mm Ø stainless steel tube up the axis of the diffuser, from the downstream side by increments of 500 microns, as shown in Figure 5.12.

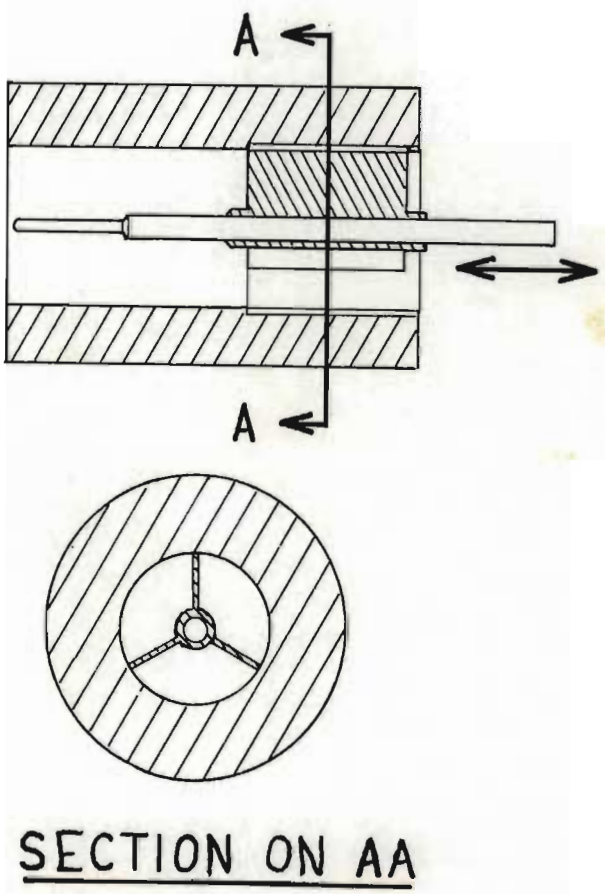

FIG. 5.12. AXIAL STAGNATION PRESSURE MEASUREMENT.

The stagnation pressure was transmitted to a remote pressure transducer and logged by computer against probe position and time. In order to determine the response of the probe, preliminary tests were performed in which the pressure was measured at intervals of 100 msecs and the probe was advanced every 5 seconds. It was found that the pressure as read at the computer changed exponentially with a time constant of approximately 1 second. Accordingly, during actual experiments, the probe pressure was read just before the next advancement and was advanced at intervals of 3 secs.

A pitot-static probe was not used because the effect of the probe ahead of the static pressure tapping would have been unpredictable in the vicinity of a strong shock.

5.5. Experimental Program

Two series of tests were condicted at a reservoir temperature of 1350^{o}K.

In the first series, static pressure readings were used to assess the influence of three factors on shock formation. Firstly, the influence of the diffuser gap was examined using a long (x/d=23,43) mixing tube. The reservoir pressure required to produce a shock for each of several spacings was determined and the pressure jump associated with the shock was measured. The mass injection rate of carbon

dioxide was controlled to provide an injection rate of 9,3% w/w at each reservoir pressure.

Secondly, the influence of injectant mass flow was examined. At a fixed diffuser gap of 6,5mm, and with a mixing tube 23,4 diameters long, static pressures were measured at the wall as well as axial stagnation profiles on the axis of the diffuser. Measurements were performed for secondary injections of 6%, 9,3% and 12% of the flow.

Thirdly, for a fixed injection rate of 9,3%, and a diffuser gap of 6,5m and a nitrogen reservoir pressure of 1163kPa, the effect of mixing tube length was examined. Static pressures were measured by wall tappings for mixing tube lengths of x/d=5,86, 11,71, 14,64, 17,57, 20,50, 23,43 and 26,35. In addition, axial stagnation pressure profiles were measured at mixing tube lengths of x/d=17,57 and 23,43. Measurements were made at intervals of 1mm along the axis of the diffuser.

For each set of conditions, a shadowgraph was taken through the diffuser gap.

5.6. Results and Discussion

At no stage was a detached shock seen on a shadowgraph This implies that the shock occurred either in the diffuser or so close to it as to be indistinguishable from its shadow.

The results are tabulated in Appendix 5.2 and discussed below.

5.6.1. Diffuser Gap Variation

The efficiency as previously defined for the assessment of the simple shock was not relevant to the complex case where momentum and heat had been lost to the walls of the mixing duct. Instead, the pressure ratio across the shock, P_2/P_1 is plotted for different diffuser gaps against nitrogen reservoir pressure in Figure 5.13.

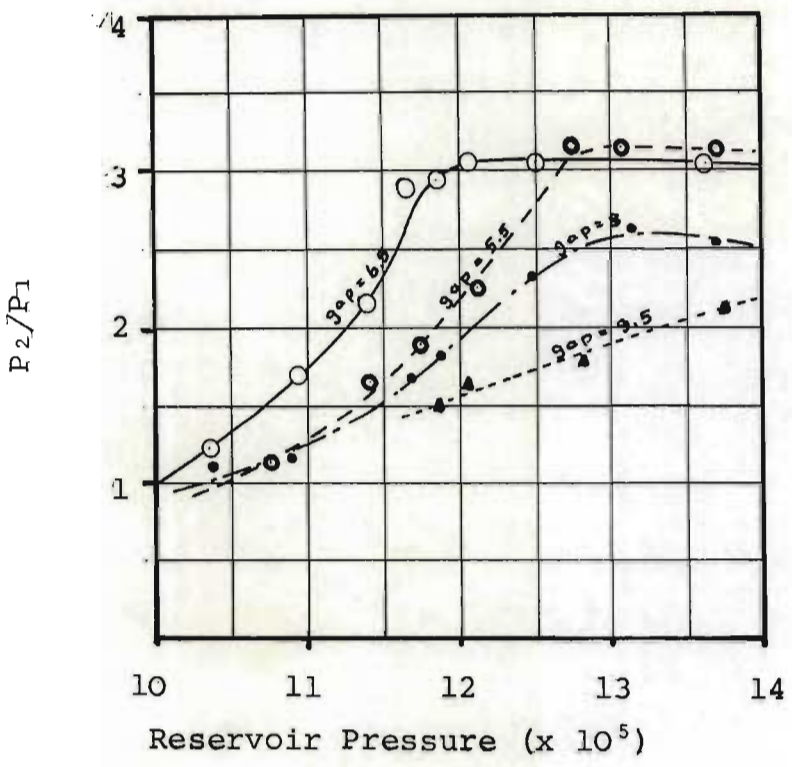

FIG. 5.13 EFFECT OF DIFFUSER GAP VARIATION

This figure demonstrates that the best

shock at the lowest overall pressure ratio occurs for a reservoir pressure of 1163kPa and a diffuser gap of 6, 5mm, or 0,36 diameters of the mixing tube. It must be born in mind that this is the pressure ratio as measured in the boundary layer. The pressure ratio in the core of the flow is likely to be higher.

The influence of the diffuser gap is interpreted as a boundary layer phenomenon. For gaps smaller than the optimum it can be argued that there is not enough length available for the flow to be diverted. Thus, slow-moving gas enters the periphery of the diffuser and wall pressure tappings indicate a lesser pressure ratio across the shock at the boundary. The central flow is not strongly affected as will be shown below when the results of the axial profiles are considered. The consequence is that there is a radial pressure gradient behind the shock.

For the case where the diffuser gap is too large, a slightly different phenomenon is postulated. Because the vacuum provided by the vacuum pump decreases with increased gas flow, the pressure around the diffuser gap increases. There is also mixing between the fast flow of the jet as it emerges from the mixing tube and the relatively still gas around the diffuser gap. Thus the shear layer extends further into the central flow with increased distance, slowing it down. If the vacuum capacity were large enough to suck off this slow-

moving material, a good pressure ratio across the shock would still be obtained. In fact, this would imply that the central flow had expanded to a higher Mach number.

5.6.2. Effect of Mixing Tube Length

The results of the static pressure measurements are plotted in Figure 5.14.

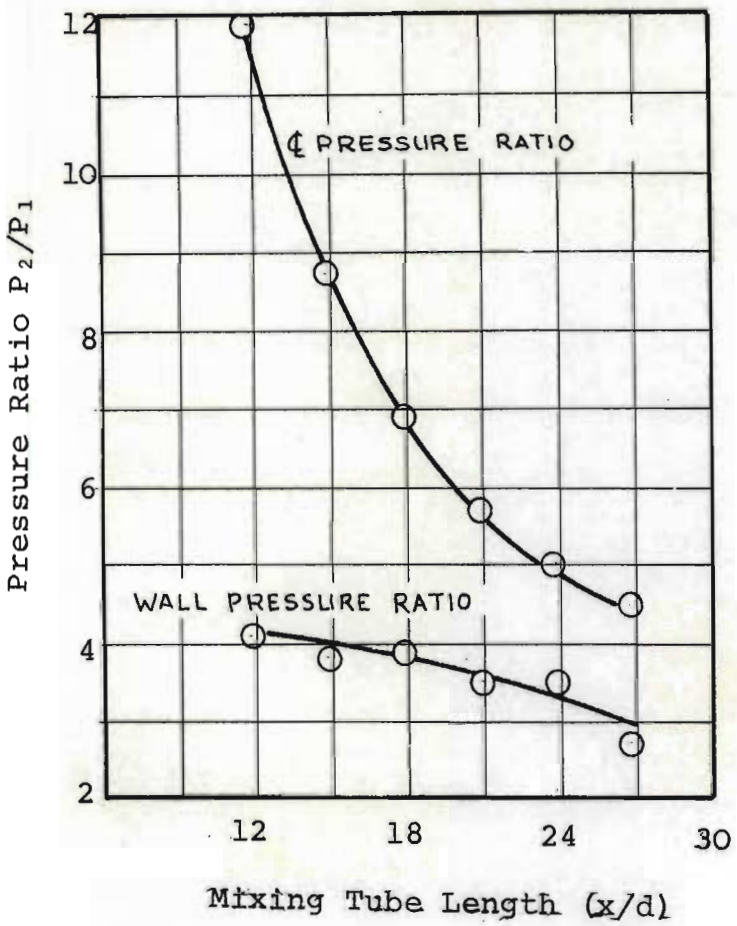

FIG. 5.14 EFFECT OF MIXING DUCT LENGTH ON SHOCK STRENGTH

They indicate that the wall pressure ratio across the shock decreases with increased mixing length. This is the result of momentum loss to the walls. These measurements represent the conditions at the wall but from measurements and calculations reported in Chapter 6 of this work, the radial velocity profiles of the gas approaching the shock after the

six mixing lengths represented in Figure 5.14 are known. From them it is possible to predict the pressure jump across a normal shock at the centre of the flow, using the Rankine-Hugoniot equations (2.4) and (2.5). These values are superimposed on Figure 5.14 and show that the pressure ratio across the shock at the centre of the tube is a strong function of the length of the mixing tube. The fact that the two curves tend towards similar values as mixing proceeds reflects the transfer of momentum from the central fast-moving core to the initially CO_2 - rich boundary.

5.6.3. Effect of Secondary Gas Injection

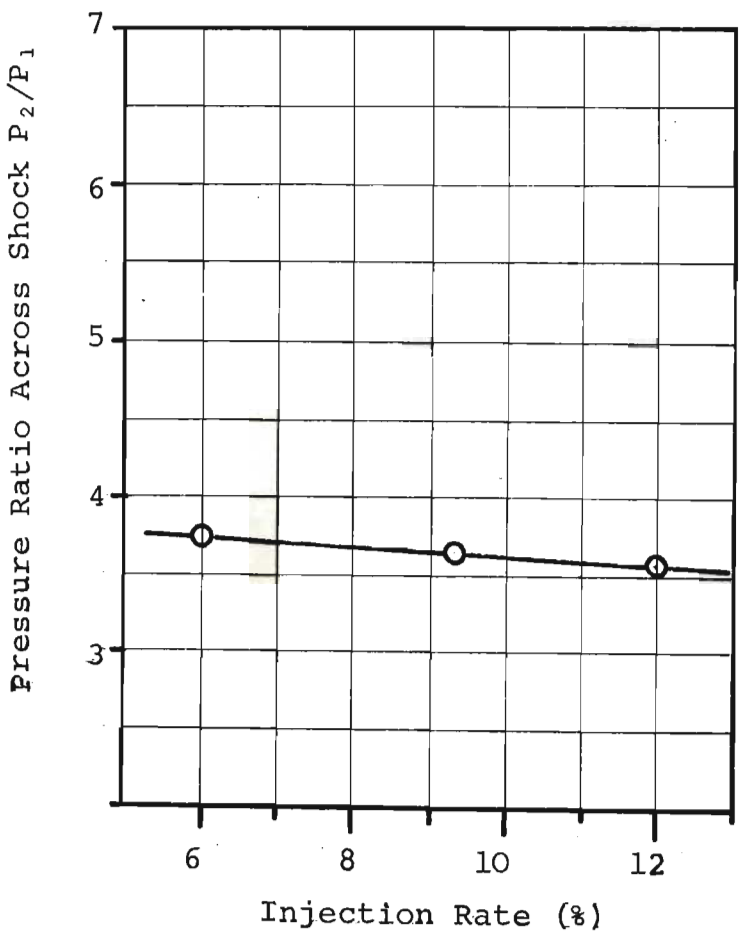

The results of the experiments where the secondary gas injection rate was varied are plotted in Figure 5.15. This demonstrates that within the variation of secondary injection rate examined, the effect is small. It should be realised that this conclusion is drawn on the basis

FIG. 5.15 EFFECT OF SECONDARY INJECTION RATE

of the pressure at the wall, where the momentum loss to the walls tends to dominate the effect of concentration variation. It will be seen in the following section that the central flow is more sensitive to concentration variation.

5.6.4. Shape of the Shock

In the absence of photographic evidence, it is difficult to be sure of the shape of the shock. Two sets of evidence are available. Firstly, from the static pressure measurements in the diffuser it can be seen that a very sharp pressure rise is measured by the tapping 3mm from the leading edge of the diffuser. Since the shock was not observed in a shadowgraph taken through the diffuser gap, it may be argued that the shock occurs wholly within the diffuser, or a very small distance (within 1mm) ahead of the plane containing the leading edge of the diffuser. Therefore, it seems that, at the wall, the position of the shock can be placed very close to the diffuser entrance.

Secondly, the position of the axial stagnation pressure profiles seem to indicate a plane shock. Figures 5.16 and 5.17 represent the results which are tabulated in Appendix 5.2. Examination of these figures shows that, in all cases, a short distance upstream of the leading edge of the diffuser the pressure shows a constant value. It is postulated that this value is that measured when the probe passed through the shock and

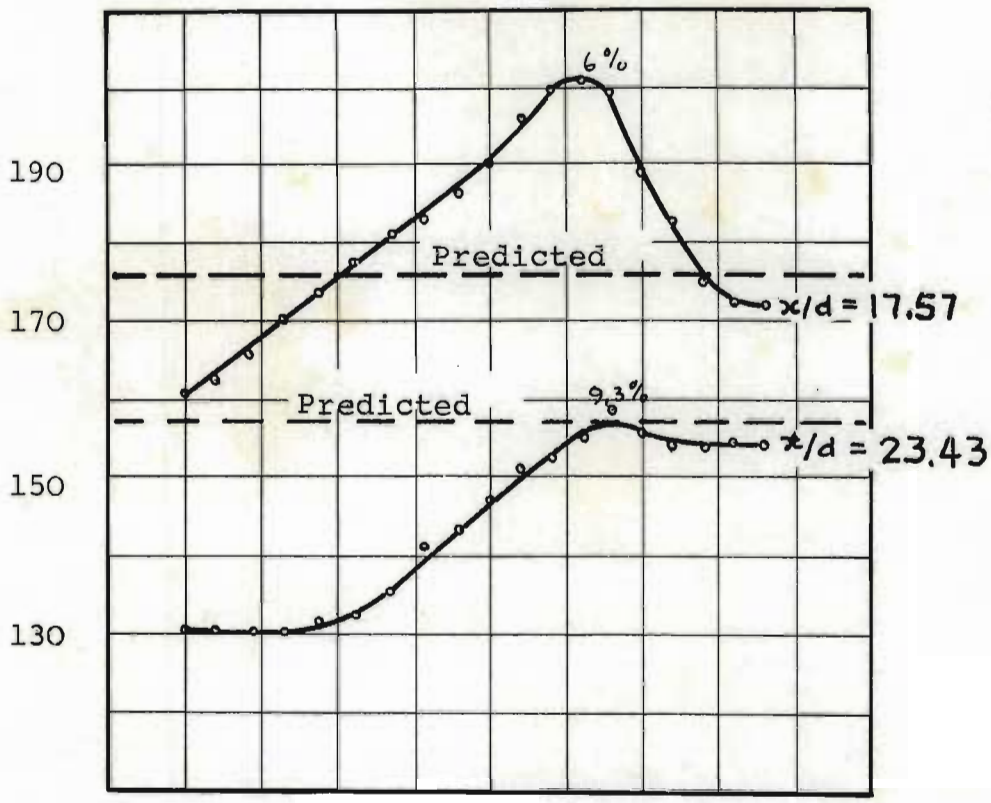

FIG. 5.16

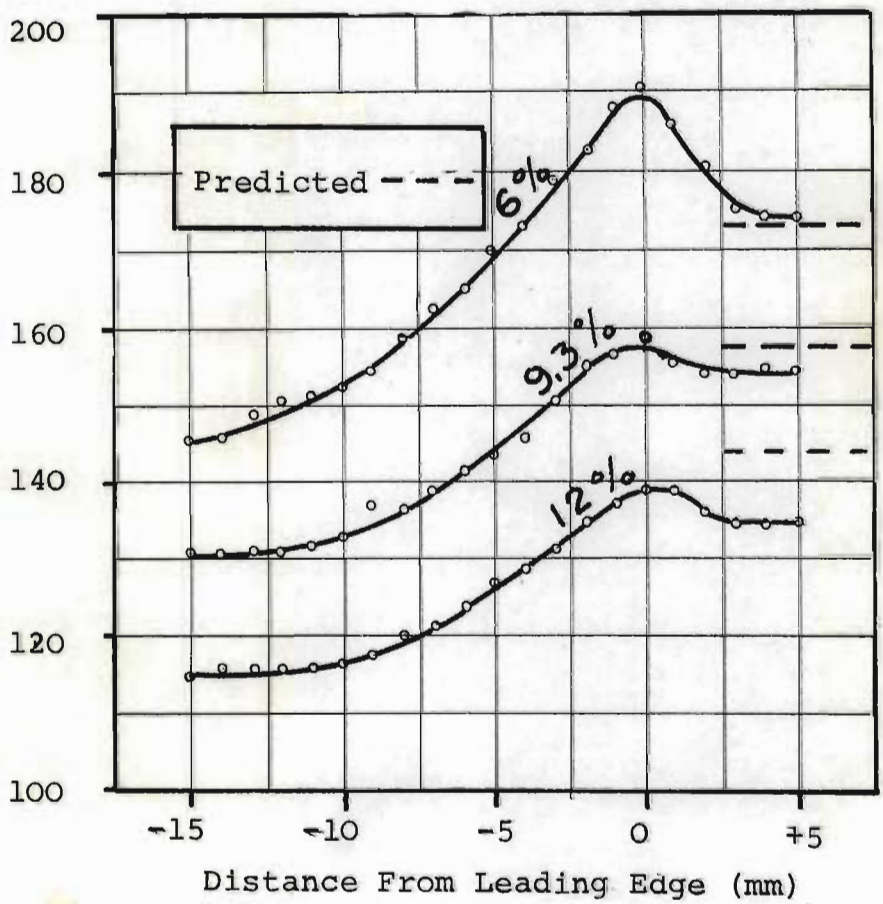

FIG. 5.17. AXIAL STAGNATION PRESSURE.

protruded into the incident supersonic flow. It then established its own bow shock and the stagnation pressure behind this shock was essentially constant for the short distance the probe could traverse.

From measurements reported in Chapter 6, where a pitot probe was traversed across a diameter just ahead of this shock, it is possible to assess the pressure which should occur

behind a normal shock. This pressure is indicated for each profile in Figures 5.16 and 5.17. For the worst case, it agrees to within 7% of the value observed for the axial profile. This could be accounted for by a slight misalignment of the probes.

The excess pressure rise just behind this constant pressure is anomalous. It does not seem that there is space available for a complex shock pattern, other than, perhaps two normal shocks very close together. No explanation can be advanced except to say that the effect might be due to the presence of the probe near the shock front. In order to elucidate this phenomenon it seems that two dimensional work would be necessary to enable photographic observation.

The decrease in pressure behind the maximum is attributed to the non-uniform incident velocity profile. For a mixing tube length of 23,4 diameters, measurements reported in Chapter 6 indicate that there is a difference in velocity between the flow at the centre of the mixing tube and that at the wall. On the basis of these velocities and the measured static pressure, it is possible (see Appendix 5.3) to predict the static pressure behind a normal shock, both at the centre and at the wall to be 118kPa and 50kPa respectively. The prediction for the wall can be regarded as an indication only because the flow between the end of the mixing tube and the entrance to the diffuser is not

known. It is not known from what radius (at the end of the mixing tube) the streamline emanates which passes next to the diffuser wall. Also, the effect of momentum transfer in this region is unknown.

Because of this discrepancy in pressure, it is expected that the static pressure at the centre and at the wall would equalise over a short distance in the subsonic flow behind the shock. This is the effect observed in Figures 5.16 and 5.17.

The pressures observed in Figure 5.16 at 17,6 diameters are higher than those at 23,4 diameters because of the decrease in supersonic velocity resulting from momentum loss to the walls.

A similar effect is observed in Figure 5.17 where smaller injection rates result in higher velocities at the centre and thus a slightly higher stagnation pressure.

5.6.5. Conclusion

After experimentally examining the formation of a standing shock at the end of a mixing duct of variable length, the following conclusions were drawn:-

(1) It is possible to establish and maintain a standing shock at the end of a mixing tube.

(2) The shock appears to be substantially normal to the incident flow.

(3) The shock could be established for a range of secondary injection rates.

(4) Because of the non-uniform velocity profile at the end of the mixing duct, the shock was not of uniform strength. The pressure jump at the centre of the flow was larger than that at the walls of the diffuser. However, the pressure equalised over a short distance in the subsonic flow behind the shock.

(5) The strength of the shock decreased with increased mixing tube length. This is a consequence of momentum loss to the walls

(6) The shock strength, as measured by wall pressure tappings, was found to depend strongly upon the diffuser gap. This was interpreted in terms of a boundary layer phenomenon. For a fixed vacuum system and nozzle size an optimum in diffuser gap spacing was discerned. However, it is thought that this optimum will depend upon vacuum system and scale

of nozzle. It is anticipated that for a larger nozzle, the boundary layer phenomenon will become less significant.

(7) Because no adequate theory was available for the prediction of the position and shape of the shock and because the conditions downstream from the shock were complex, no analysis was attempted. The flow after the shock is not irrotational as can be seen from Crocco's theorem (Shapiro (1953), p 281) when it is realised that the entropy must vary across the radius of the tube. Further, the boundary conditions in the fairly short diffuser would be difficult to specify. Therefore it was judged that an anlysis would be difficult.

CHAPTER 6

INVESTIGATION OF CONDITIONS INSIDE THE REACTOR

6.1. Control of Conditions in the Reactor

In assessing the validity of the concept of such a supersonic reactor, it was necessary to know whether the temperature during mixing could be maintained below that at which a significant chemical reaction would occur and whether the temperature jump associated with the shock was sufficient to control the product spectrum.

The injection rates used in Chapter 5 were used again because they represent approximately the conditions suggested by Roberts (1970) for the partial oxidation of methane.

Roberts indicated that high conversions to ethylene occurred at a molar methane/oxygen ratio of 11.5. He conjectured that it was possible that better conversions might be obtained for higher ratios, but 11.5 was the highest value which he considered experimentally. In this investigation a mass ratio of 10 was employed, with some tests being done at mass ratios of 7.2 and 15.7 to establish that it was possible to vary the injection rate.

6.2. Experimental Work

In order to evaluate the reactor it was necessary to know

the radial and axial profiles of static temperature, static pressure and species concentration throughout the mixing tube. It was assumed that the static pressure was constant over the radius (at any axial station). The mixing tube was parallel and so this was justifiable in the absence of shocks, to a close approximation. Species concentration could be measured by sampling the flow at points across the diameter of the tube but static temperature could not be measured directly and had to be inferred from measured stagnation temperatures.

Nitrogen was used as the primary gas and carbon dioxide as the injectant gas in the first series of runs during which radial profiles of stagnation pressure, stagnation temperature and concentration were obtained at several stations in the mixing tube. A de Laval nozzle with a throat of 5mm was used in conjunction with a mixing tube 18.1mm in diameter - as discussed above.

All measurements in this series of runs were performed under one particular set of gas dynamic conditions - those which were judged to be close to the operating conditions of a proposed prototype reactor.

The experimental program was designed to measure stagnation pressure, static pressure, stagnation temperature and species concentration at points inside the mixing tube. From these measurements it was proposed to deduce values of static

temperature and velocity at each point.

It was anticipated that, if a probe were inserted into the flow through an aperture in the wall, a system of shocks would be initiated which would interact with the boundary layer of the mixing tube and either cause an overall change to subsonic flow or, at the least, affect the flow field up-stream of the probe. For this reason, mixing tubes of varying lengths were used, the length of the tube corresponding to the axial distance downstream from the point of injection at which radial profiles were to be measured. The configuration is shown below.

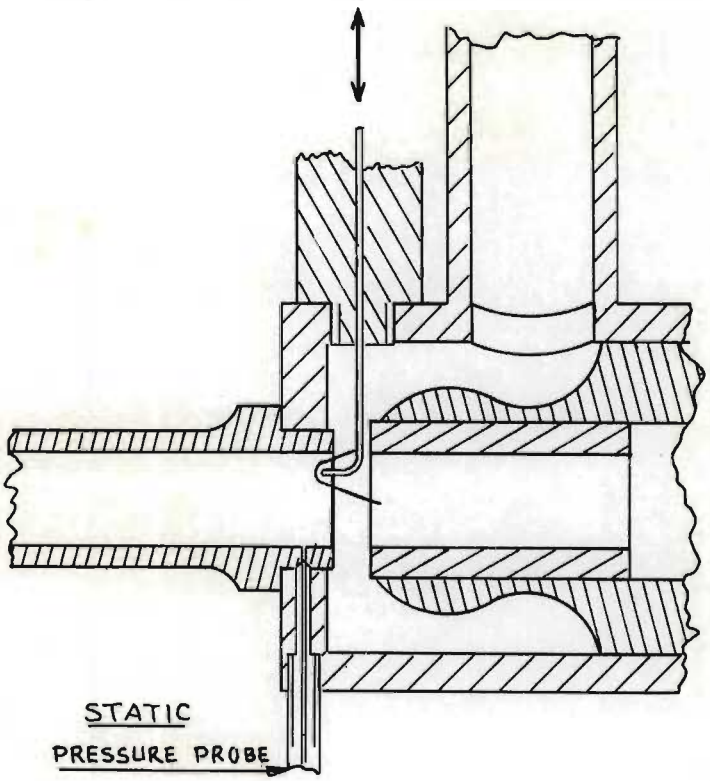

FIG. 6.1 POSITIONING OF PROBE

This enabled a probe to be used, whose shock pattern could not affect conditions upstream of the point of measurement. For the measurement of stagnation pressure, species concentration and stagnation temperature, probes, as described in Chapter 4, were used.

They were 1,5mm in diameter and of pitot shape, the hemispherical nose of the probe traversing a diameter of the mixing tube, about 3mm in from its end. Static pressure was measured by means of two wall tappings, 0.35mm in diameter, one 3mm from the end of the mixing tube and another, 10mm further upstream.

The seven stations at which profiles were measured were 5,86, 11,71, 14,64, 17,57, 20,50, 23,43 and 26,35 diameters of the mixing tube (18,1mm) downstream from the point of CO_2 injection. These covered the mixing region to the point at which the mixing was almost complete. For each radial station, a mixing tube of the required length was connected and three separate runs were performed - one each to measure profiles of stagnation temperature, stagnation pressure and species concentration. For temperature and pressure, measurements were made at thirty points, 500 microns apart across a diameter of the tube. For concentration measurements samples from fourteen points were analysed for each axial station. The first five points were 500 microns apart, starting near the wall whereafter the spacing was increased to 1mm. This implied that the spread of measured points extended past the centre-line of the tube and provided a check on the accuracy of the analyses. The closer spacing of samples near the wall enabled more analyses to be performed in that area where, because the sampling pressure was low, a greater scatter was observed.

For this experimental program, the reservoir conditions for the nitrogen were maintained at 1163kPa and 1350^{o}K. This implied a nitrogen flow rate of 23,5 g/s. Carbon dioxide was injected at a constant rate of 9,3% w/w of the nitrogen. For each run, static pressure was measured by wall tappings at the axial station and 10mm upstream from the station as well as at several points throughout the mixing tube. The extra measurements, provided confirmation that the mixing zone conditions did not change as the mixing tube length was changed and also, by extrapolation provided a check on the static pressure measurement at the axial station under consideration.

A second set of experiments was performed in order to establish what the effect was of changing the proportion of gas injected. This set of runs was performed with first 1,5 g/s and then 3,2 g/s of CO_2 injected into the primary flow of 23,5 g/s of nitrogen. This implied injection rates of 6% and 12% w/w, which could then be compared with the previous injection rate of 9,3%. Reservoir conditions were kept the same as for the previous set of runs, namely 1163kPa and 1350^{o}K. Radial profiles of concentration, stagnation pressure and stagnation temperature were measured for both injection rates at the x/d$\pm$24 station.

6.3. Results and Discussion

The results obtained from the above experimental program are presented in Appendix 6.1.

For the first set of runs, the measurements of species concentration, stagnation pressure and stagnation temperature were fitted in the radial and axial directions with cubic spline functions (Ahlberg, 1967). Using this technique, it was possible to draw a surface through the data points minimising the least square error, subject to a penalty for flexibility. By varying this penalty, it was possible to obtain a surface which followed the data more closely or less so. This provided a certain amount of smoothing of the data, but also enabled good interpolations to be made for the assessment of species concentration at intervals of 500 microns over the whole radius of the mixing tube. The curves also provided partial derivatives of the data. In Figures 6.2 to 6.7 the experimental data and smoothed curves are plotted.

At the first station, at about 6 diameters downstream from the injection point, it will be seen from Appendix 6.1 that the core of pure nitrogen at the centre of the tube has not yet been dissipated. Because the gradients of mass concentration would have been discontinuous at the edge of the potential core, the smoothing technique was not extended to

FIG. 6.2 EXPERIMENTAL CO_2 CONCENTRATION PROFILE.

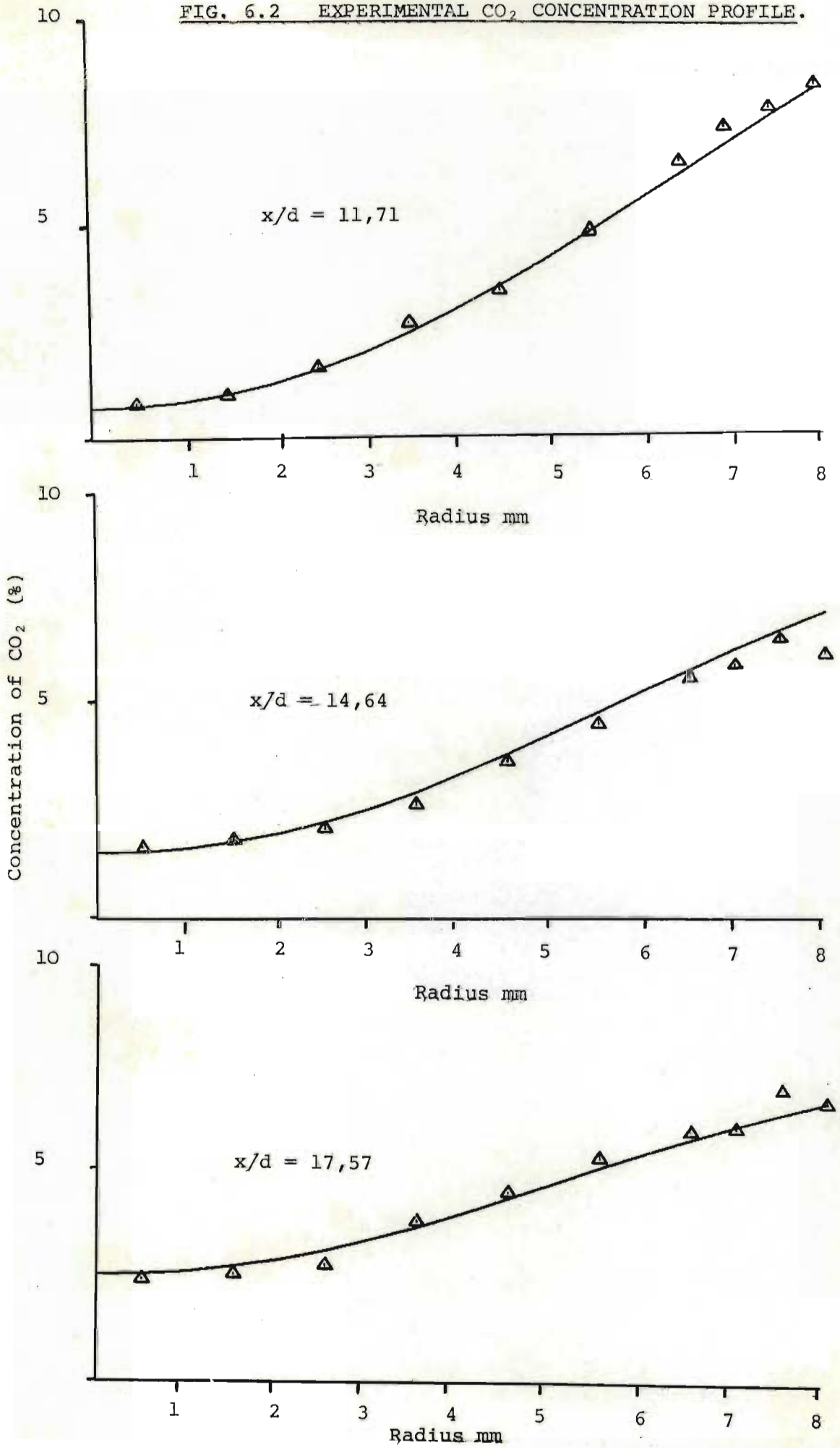

FIG. 6.3 EXPERIMENTAL CO_2 CONCENTRATION PROFILE

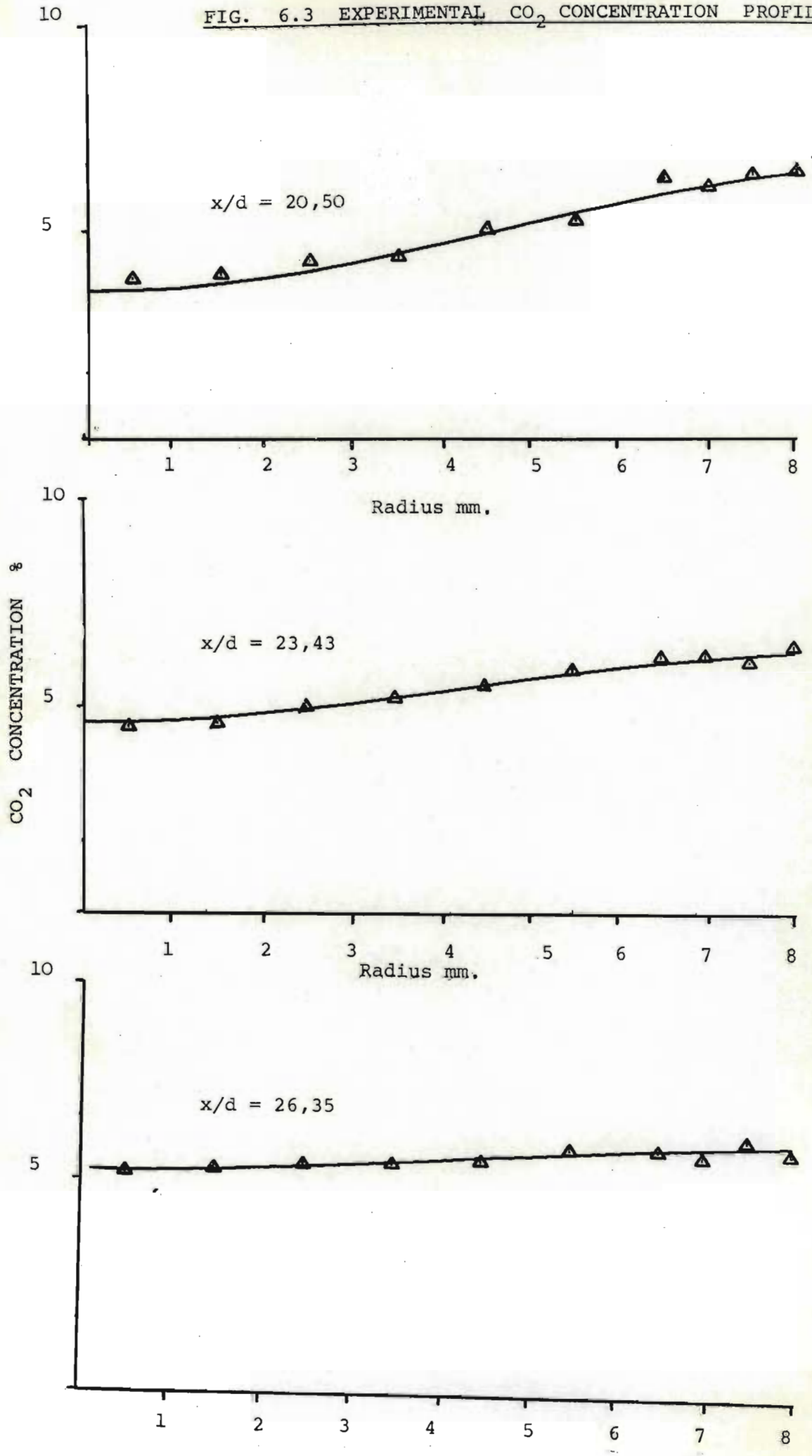

FIG 6.4 EXPERIMENTAL STAGNATION TEMPERATURE PROFILES.

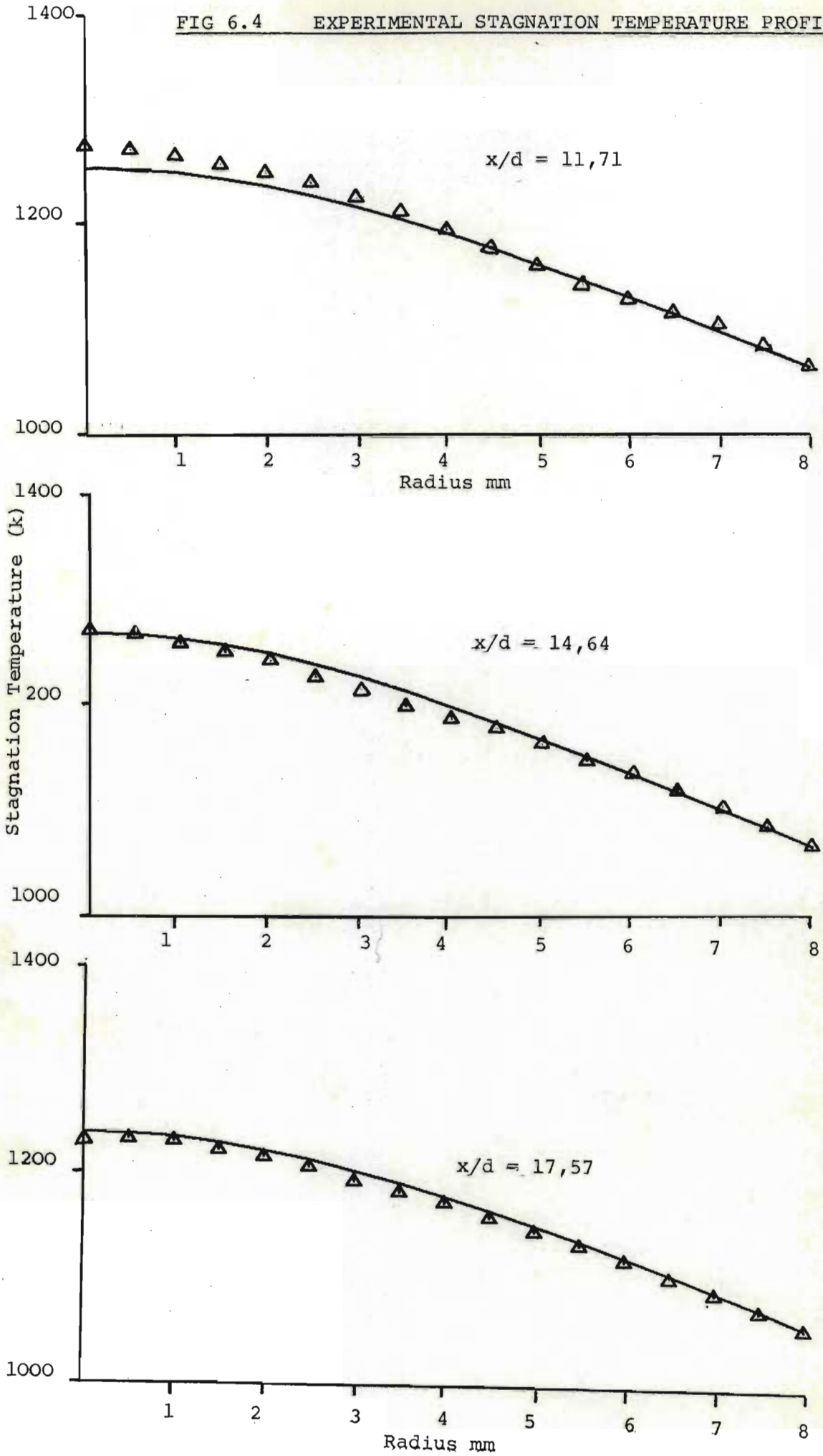

FIG. 6.5 EXPERIMENTAL STAGNATION TEMPERATURE PROFILES.

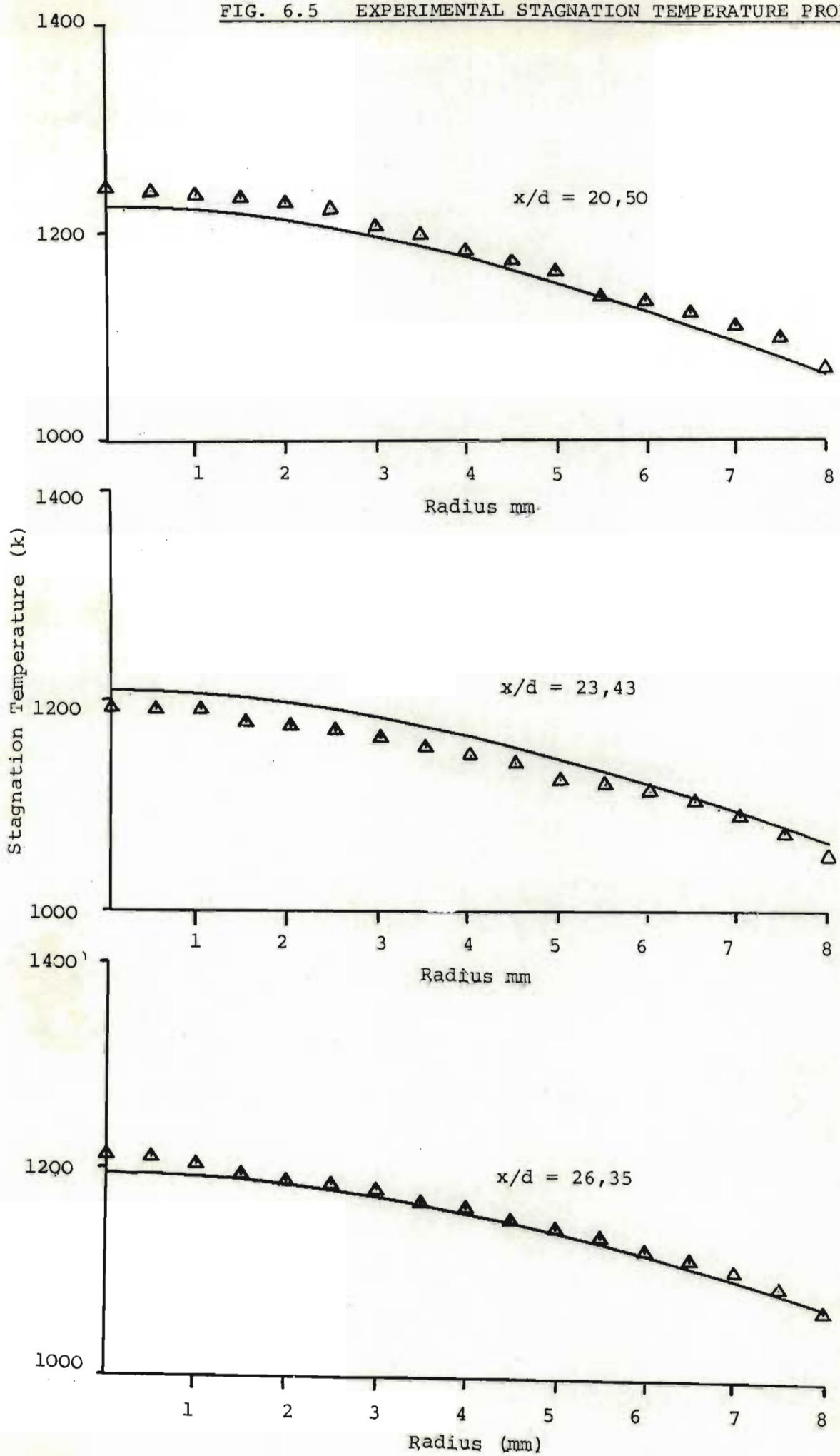

FIG. 6.6 MEASURED STAGNATION PRESSURE

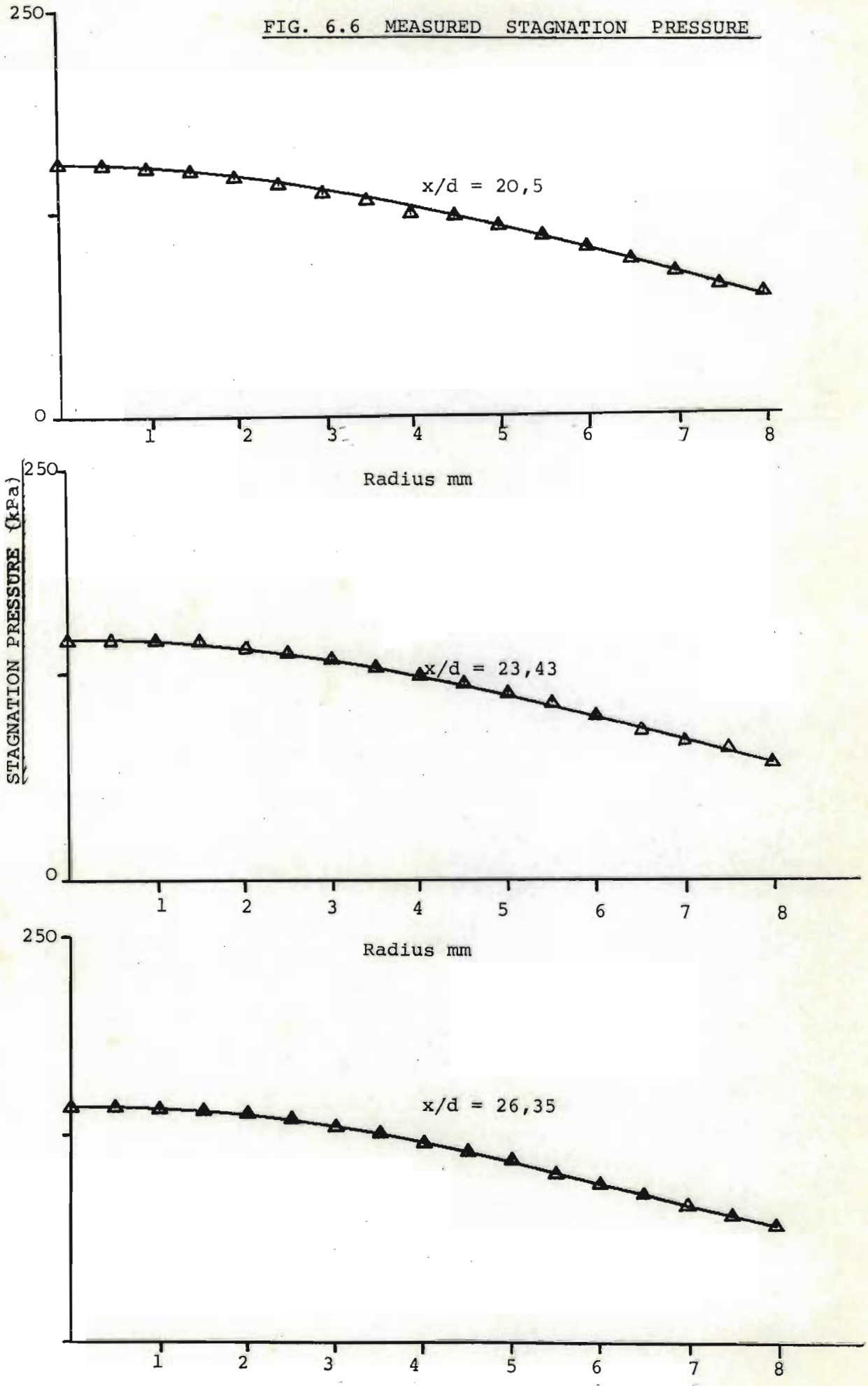

FIG. 6.7 MEASURED STAGNATION PRESSURE

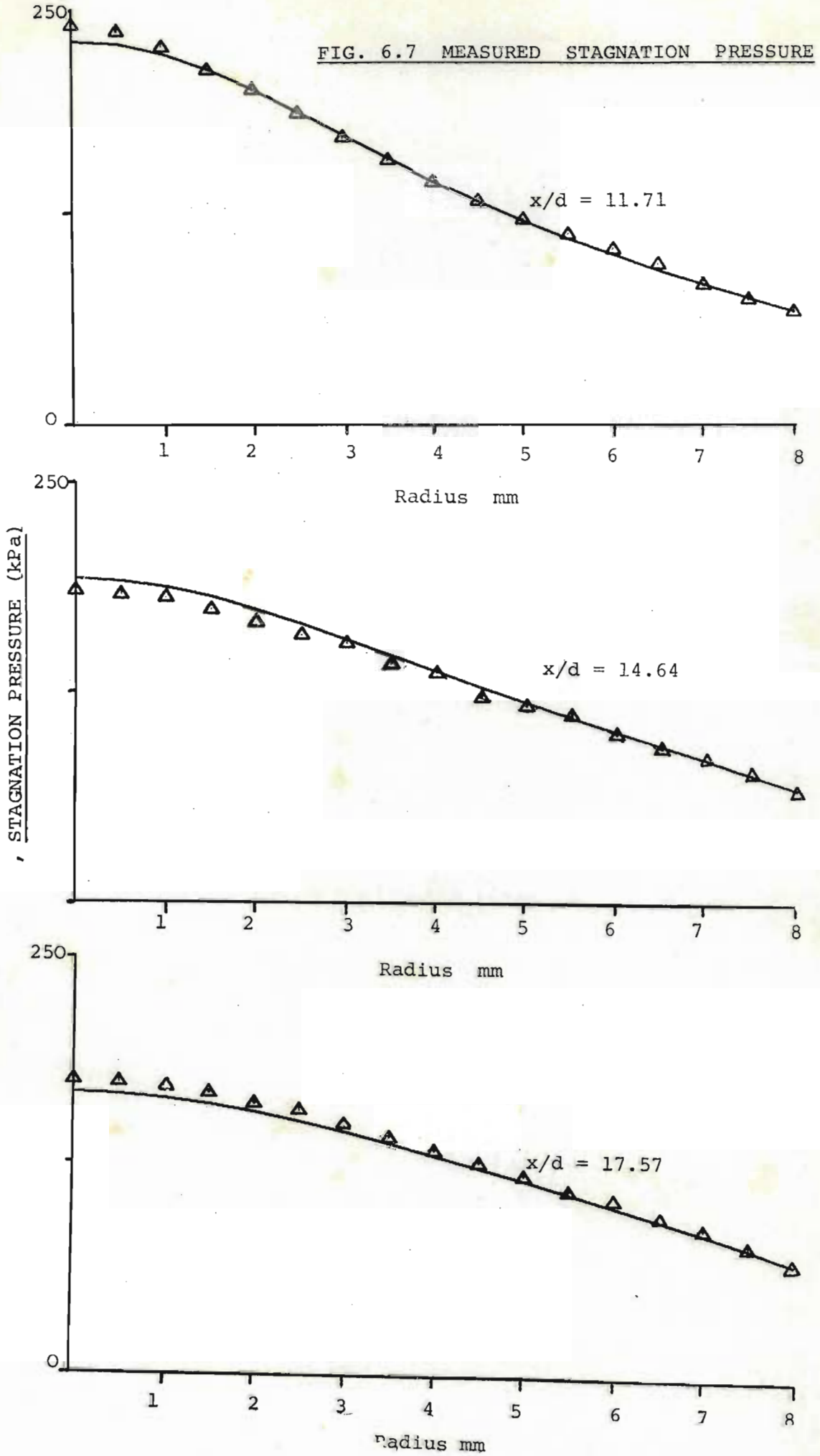

this station and profiles were not developed for mixing analysis upstream of the 12 diameter axial station.

It will be seen that the smoothed curves in some figures lie largely above or below the data points. This is a consequence of the smoothing in the axial direction and the fact that from one run to the next there was likely to be a slight variation in reservoir conditions - although they were nominally constant. A second cause of variation of observed profiles from one set of runs to the next was the positioning of the probes. The probes were slender and they had to protrude a relatively large distance from their supports. This, coupled with the rigorous operating conditions made it impossible to be sure of the position of the probe tip. Because of the scale of the equipment, it will be seen that an error of 0,2mm in the radial position of the probe tip is significant. At the centre-line of the mixing tube, a lateral error of 0,2mm also becomes significant.

Temperature measurements at the≈6, 12, 18 and 24 diameter stations used the same thermocouple which was damaged and replaced before measurements were made at the≈15, 21 and 27 diameter stations. Although the instruments were nominally identical, one of them apparently gave slightly higher readings than the other by up to about 2%.

Measurements are shown up to a maximum radius of 8mm although

the mixing tube diameter was 18mm. This discrepancy is explained by the fact that the probe diameter was 1,5mm, so that when its centre line was 8mm from the mixing tube centre line, this implied a gap of 250 microns between the probe and the wall. It was undesirable for the probe to touch the wall.

The data from the second set of runs, where injection rate was varied, are plotted in Figure 6.8 together with smoothed curves. For these runs, it was clearly impossible to smooth in two directions as with the previous set.

6.4. Data Reduction

With values obtained from the smoothed data at radial intervals of 500 microns, together with static pressure measurements at each axial station, it was possible to infer radial profiles for static temperature and velocity. The calculations discussed below were performed at each of 17 points ranging on a radius from the centre-line of the mixing tube to a radius of 8mm. The calculations were repeated at each of six axial stations.

It was necessary to know, at each point, the specific heat ratio $\gamma = C_p/C_v$ of the mixture as well as its density. Accordingly, from an assumed average temperature, an estimate was made of C_p for both nitrogen and carbon dioxide using

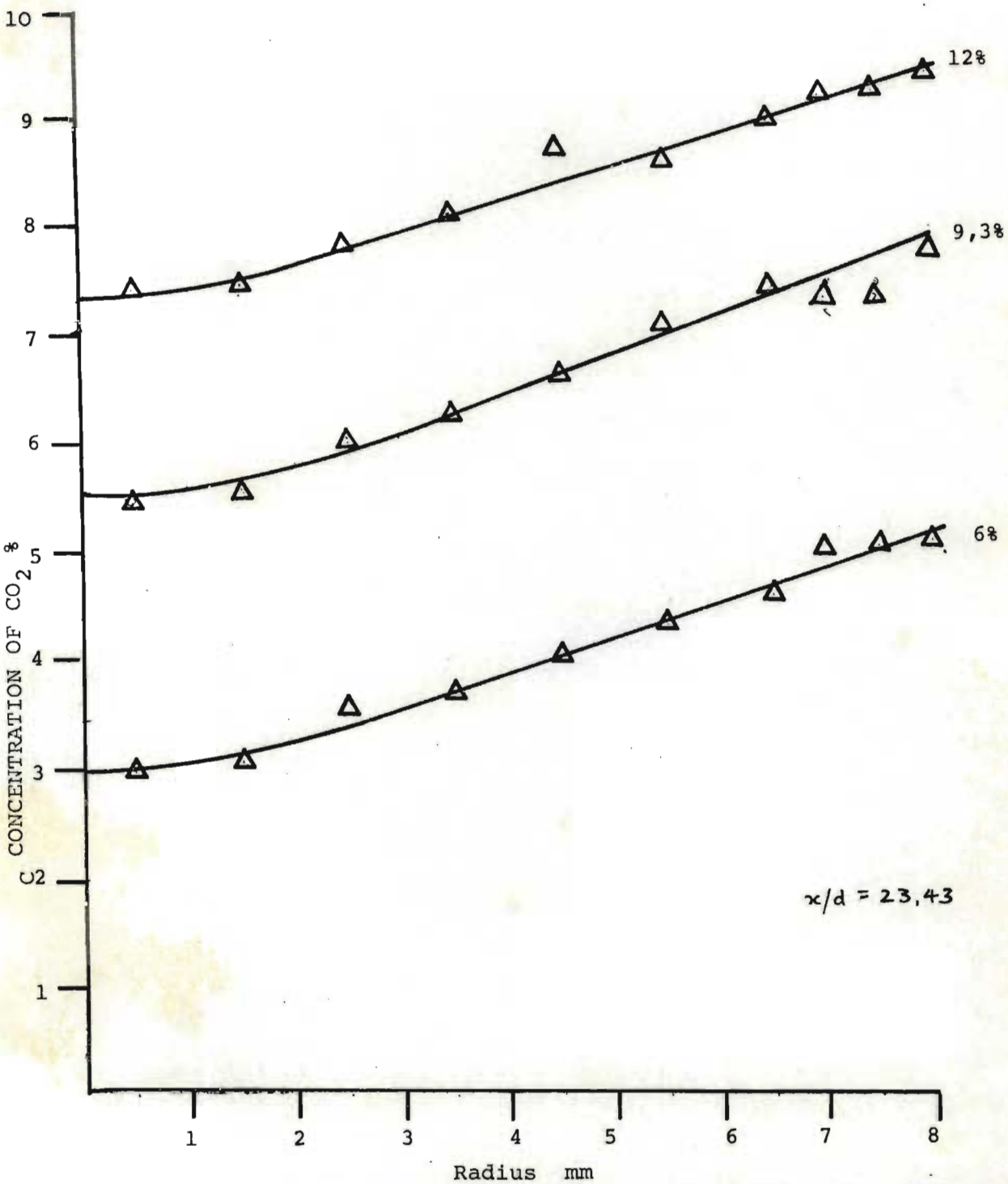

FIG 6.8 EXPERIMENTAL CO_2 CONCENTRATION PROFILES AT 3 INJECTION RATES.

a relation quoted by van Wylen (1959), p 551. The relation

$$R = C_p - C_v$$

where R is the gas constant, was then used to obtain C_v for pure nitrogen and pure carbon dioxide at that temperature. From a knowledge of the species concentration at each point, it was then possible to calculate

$$C_{v_{mixture}} = C_{v_{CO_2}} \times \text{mass fraction}_{CO_2} + C_{v_{N_2}} \times \text{mass fraction}_{N_2}$$

and C_p for the mixture by a similar relation. The quotient of C_p upon C_v then provided a value of γ for the mixture at the point under consideration - for an assumed temperature. In the temperature range considered, it was found that γ was not a strong function of temperature.

The gas constant for the mixture, R_m, was obtained from the relation

$$R_m = R_{CO_2} \times \text{mass fraction of } CO_2 + R_{N_2} \times \text{mass fraction of } N_2$$

When using a pitot tube in supersonic flow, a bow shock forms across the nose of the tube. The difference between the static pressure in front of the shock and stagnation pressure measured behind the shock may be considered as arising firstly

from a non-isentropic supersonic to subsonic compression through a normal shock, followed by isentropic stagnation. The Raleigh-Pitot equation (6.1) (Liepman and Roshko, 1957)

$$\frac{P_{static}}{P_{stagnation}} = \left[\frac{\frac{2\gamma}{\gamma+1} M_1^2 - \frac{\gamma-1}{\gamma+1}}{\left[\frac{\gamma+1}{2} M_1^2\right]^{\gamma/\gamma-1}}\right]^{1/\gamma-1} \qquad (6.1)$$

provides a relation between the static pressure, measured by wall tappings, and the stagnation pressure, as measured by the pitot tube, in terms of γ and the incident Mach number M_1. From a knowledge of P_{static}, $P_{stagnation}$ and the local γ (at an assumed temperature intermediate between the static temperature and the stagnation temperature), it was possible to solve the Rayleigh-Pitot equation numerically for M_1, using a Newton-Raphson technique. A convergence accuracy of 0,01% was obtained.

From a knowledge of the stagnation temperature of the gas after passing through the bow shock, ahead of the temperature probe, and the ratio of pressures across the shock P_2/P_1, it is possible to use the Rankine-Hugoniot relation (equation 2.4)

$$\frac{T_{stagnation}}{T_{static}} = \frac{P_2}{P_1}\left[\frac{\frac{\gamma+1}{\gamma-1} + \frac{P_2}{P_1}}{1 + \frac{\gamma+1}{\gamma-1}\frac{P_2}{P_1}}\right] \qquad (2.4)$$

to assess the static temperature before the bow shock.

In order to assess the value of P_2, the static pressure just after the shock, we may use the relation (6.2) (van Wylen, 1959)

$$M_2^2 = \frac{M_1^2 + \frac{2}{\gamma-1}}{\frac{2}{\gamma-1} M_1^2 - 1} \tag{6.2}$$

to evaluate M_2, the Mach number of just after the shock, from M_1 the known Mach number just before the shock. Knowing M_2, we can use the relation for an isentropic stagnation (2.2)

$$\frac{P_0}{p} = 1 + \left(\frac{\gamma-1}{2} M^2 \right)^{\gamma/\gamma-1} \tag{2.2}$$

where p is the static pressure at a Mach number M and P_0 is the stagnation pressure.

Thus, we obtain

$$P_2 = P_0 \left(1 + \frac{\frac{\gamma-1}{2} M_1^2 + 1}{\frac{2\gamma}{\gamma-1} M_1^2 - 1} \right)^{\gamma-1/\gamma} \tag{6.3}$$

The static temperature was then used to calculate the velocity as

$$v = M_1 \times a$$

where a, the local speed of sound may be calculated from

$$a = \sqrt{\gamma_{mixture} \; R_{mixture} \; T_{static}}$$

The local density was calculated from the perfect gas law. The justification for assuming perfect gas behaviour was that the static pressures were relatively low and the temperature high.

The results of these calculations are presented in Tables 6.8 to 6.13 and are plotted in Figures 6.9 to 6.14.

A scatter was observed in the measurement of the static pressure by wall tappings. On closer examination, it became clear that the assumption of uniform static pressure across a diameter of the mixing tube was not strictly valid. It was found that, at small distances downstream from the injection point, the pressure measured at the wall was sensitive to small variations in the injection rate. Because these small variations could not have had the influence on the speed of flow at the centre of the duct, which would have been implied

TABLE 6.8.

CALCULATED PROPERTIES AT x/d = 11,71.

Radius mm	T_1	T_2	V_1	V_2
.0	428.	1277.	1388.	328.
.5	430.	1276.	1386.	329.
1.0	437.	1272.	1377.	329.
1.5	449.	1266.	1364.	331.
2.0	464.	1258.	1346.	333.
2.5	483.	1247.	1323.	336.
3.0	504.	1234.	1296.	339.
3.5	527.	1219.	1265.	343.
4.0	550.	1202.	1231.	347.
4.5	572.	1183.	1195.	351.
5.0	594.	1162.	1158.	356.
5.5	614.	1139.	1119.	361.
6.0	633.	1114.	1078.	366.
6.5	650.	1088.	1036.	372.
7.0	666.	1059.	992.	378.
7.5	681.	1029.	944.	386.
8.0	693.	995.	895.	395.

TABLE 6.9.

CALCULATED PROPERTIES AT x/d = 14,64

Radius mm	T_1	T_2	V_1	V_2
.0	509.	1256.	1310.	342.
.5	511.	1255.	1308.	342.
1.0	516.	1251.	1301.	343.
1.5	524.	1246.	1290.	344.
2.0	535.	1238.	1275.	346.
2.5	548.	1228.	1256.	348.
3.0	562.	1216.	1234.	351.
3.5	578.	1202.	1209.	354.
4.0	594.	1186.	1181.	357.
4.5	610.	1168.	1151.	361.
5.0	625.	1148.	1119.	365.
5.5	640.	1127.	1085.	369.
6.0	654.	1104.	1049.	374.
6.5	669.	1078.	1010.	380.
7.0	683.	1051.	967.	387.
7.5	698.	1021.	920.	396.
8.0	713.	988.	867.	408.

TABLE 6.10.

CALCULATED PROPERTIES AT x/d = 17,57

Radius mm	T_1	T_2	V_1	V_2
.0	573.	1235.	1242.	354.
.5	575.	1234.	1240.	355.
1.0	578.	1231.	1235.	355.
1.5	583.	1226.	1226.	356.
2.0	590.	1219.	1214.	358.
2.5	598.	1209.	1199.	359.
3.0	608.	1198.	1181.	361.
3.5	618.	1186.	1160.	364.
4.0	629.	1171.	1137.	366.
4.5	640.	1154.	1112.	369.
5.0	651.	1136.	1084.	373.
5.5	663.	1116.	1054.	377.
6.0	674.	1094.	1021.	382.
6.5	686.	1071.	985.	387.
7.0	699.	1045.	946.	395.
7.5	713.	1016.	901.	405.
8.0	728.	984.	850.	418.

TABLE 6.11.

CALCULATED PROPERTIES AT x/d = 20,50

Radius mm	T_1	T_2	V_1	V_2
.0	622.	1214.	1183.	365.
.5	623.	1213.	1181.	365.
1.0	625.	1210.	1177.	366.
1.5	628.	1206.	1170.	367.
2.0	633.	1199.	1160.	368.
2.5	639.	1191.	1148.	369.
3.0	646.	1181.	1133.	371.
3.5	653.	1169.	1115.	373.
4.0	661.	1156.	1095.	376.
4.5	670.	1141.	1073.	379.
5.0	679.	1124.	1048.	382.
5.5	689.	1106.	1020.	386.
6.0	699.	1086.	989.	392.
6.5	710.	1063.	956.	398.
7.0	722.	1039.	918.	406.
7.5	734.	1013.	877.	417.
8.0	747.	983.	829.	430.

TABLE 6.12.

CALCULATED PROPERTIES AT x/d = 23,43.

Radius mm	T_1	T_2	V_1	V_2
.0	656.	1194.	1136.	373.
.5	656.	1193.	1134.	373.
1.0	658.	1190.	1131.	374.
1.5	660.	1186.	1125.	375.
2.0	664.	1181.	1116.	376.
2.5	669.	1173.	1105.	377.
3.0	674.	1164.	1092.	379.
3.5	681.	1154.	1076.	381.
4.0	688.	1142.	1057.	384.
4.5	696.	1128.	1036.	388.
5.0	705.	1113.	1012.	392.
5.5	715.	1096.	986.	397.
6.0	725.	1078.	957.	403.
6.5	736.	1057.	925.	411.
7.0	747.	1035.	890.	419.
7.5	758.	1010.	852.	430.
8.0	768.	983.	809.	443.

TABLE 6.13.

CALCULATED PROPERTIES AT x/d = 26,35.

Radius mm	T_1	T_2	V_1	V_2
.0	680.	1173.	1095.	380.
.5	680.	1173.	1094.	380.
1.0	682.	1171.	1091.	381.
1.5	684.	1167.	1086.	381.
2.0	687.	1162.	1078.	383.
2.5	692.	1156.	1068.	384.
3.0	697.	1148.	1055.	387.
3.5	705.	1139.	1039.	390.
4.0	713.	1128.	1021.	394.
4.5	723.	1116.	999.	398.
5.0	733.	1102.	976.	404.
5.5	744.	1087.	949.	411.
6.0	755.	1070.	921.	418.
6.5	766.	1052.	890.	427.
7.0	777.	1032.	857.	437.
7.5	787.	1010.	823.	448.
8.0	795.	986.	787.	461.

FIG. 6.9 CALCULATED STATIC TEMPERATURES

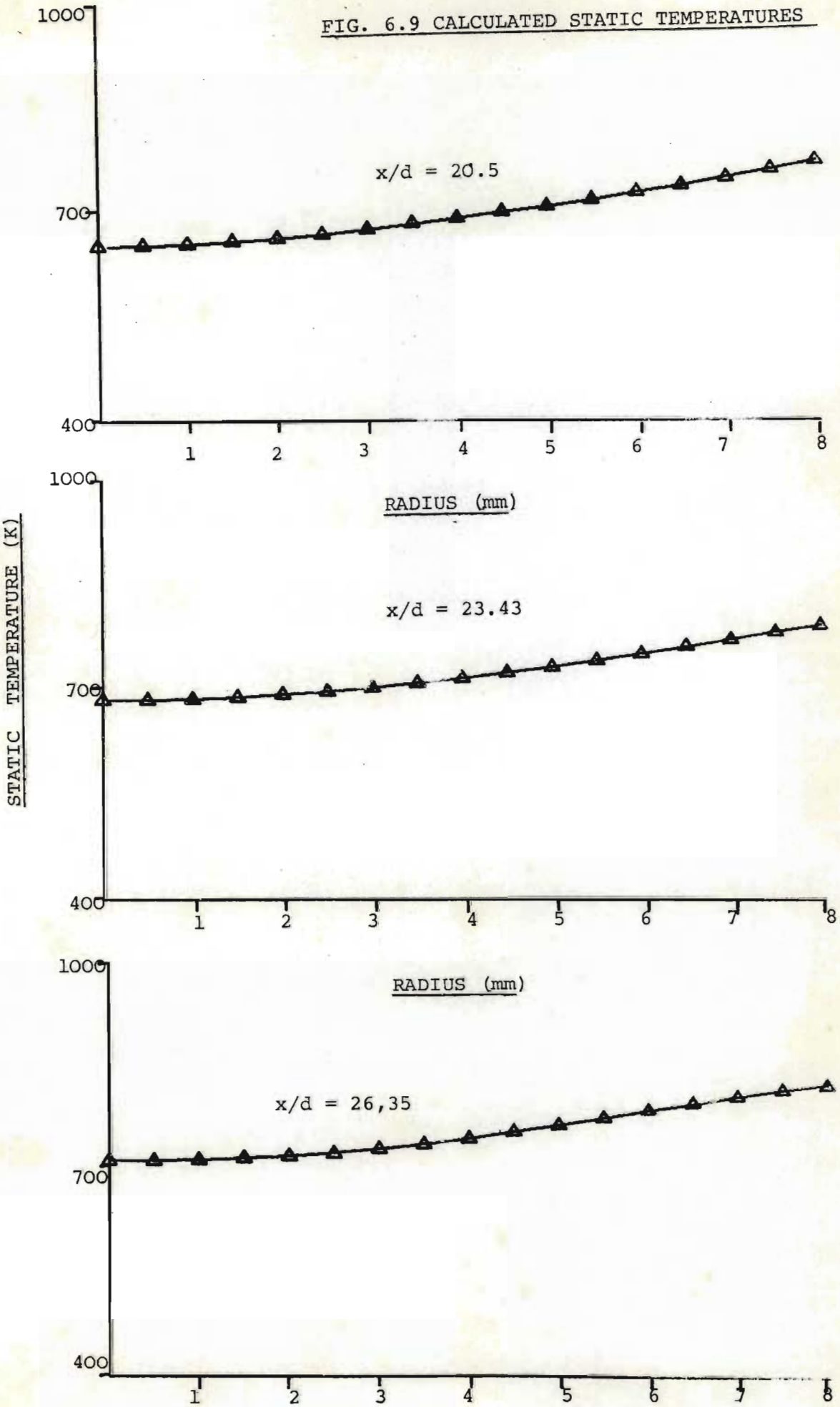

FIG. 6.10 CALCULATED STATIC TEMPERATURES

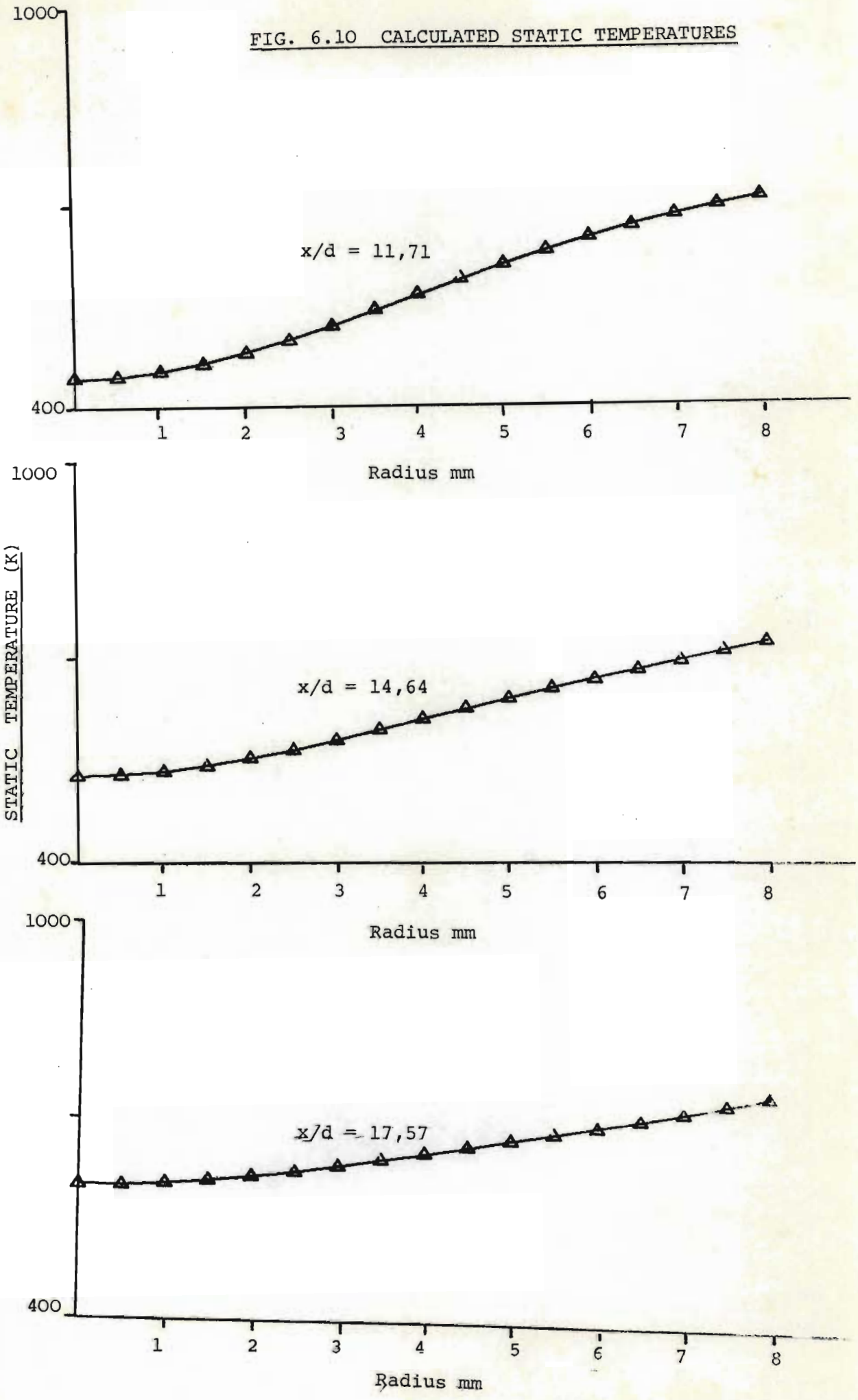

FIG. 6.11 CALCULATED VELOCITY PROFILES

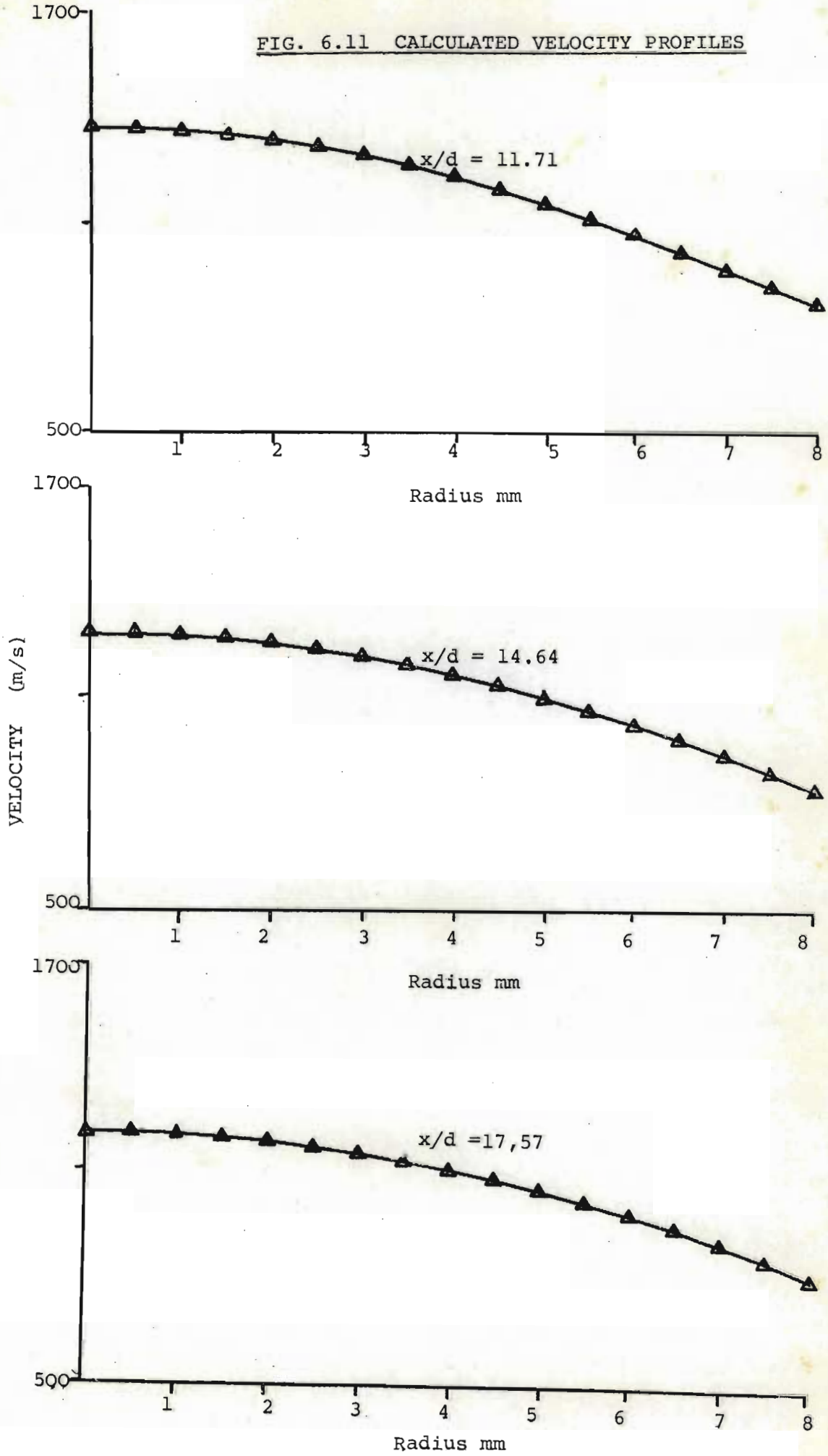

FIG. 6.12 CALCULATED VELOCITY PROFILES

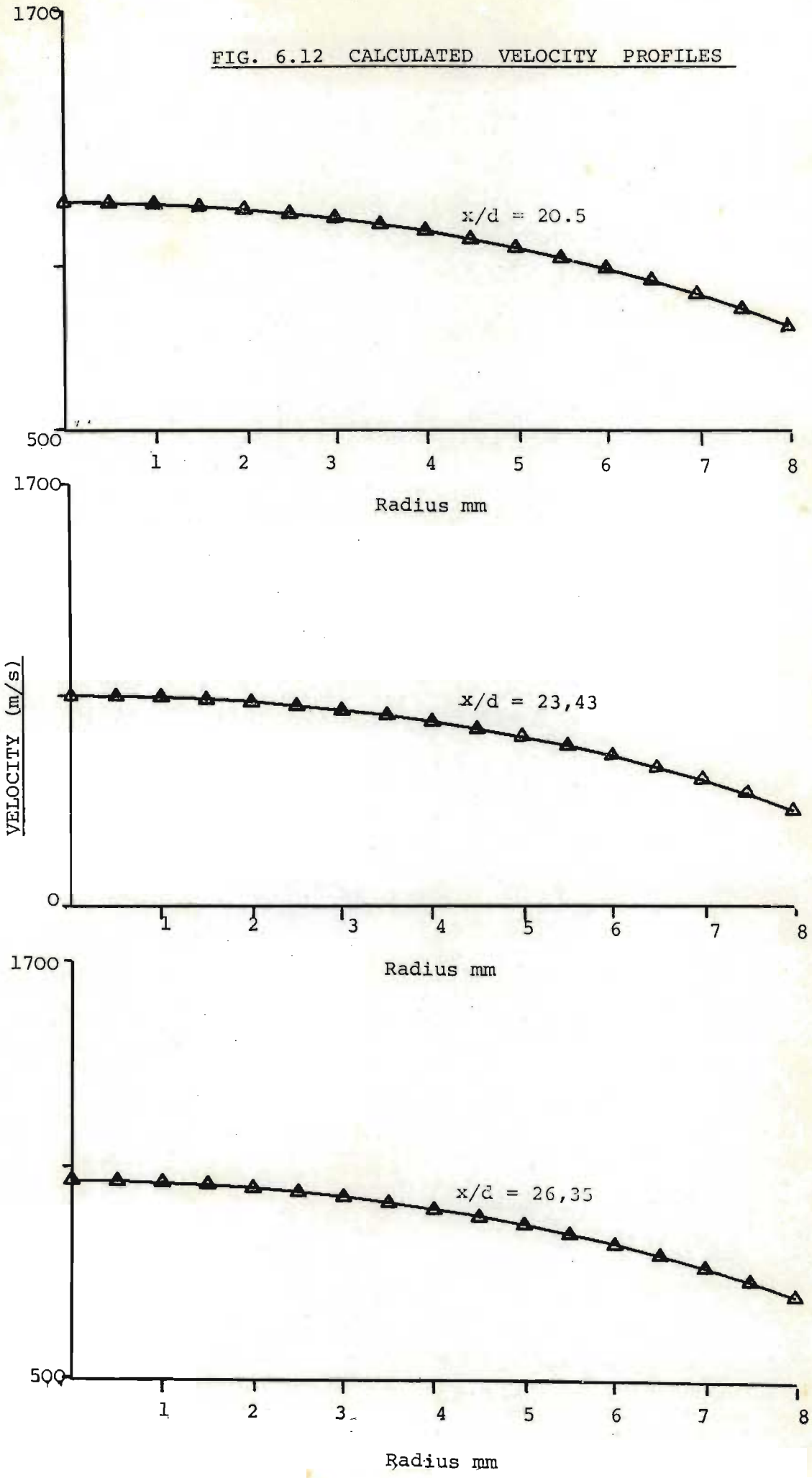

FIG. 6.13 CALCULATED DENSITY

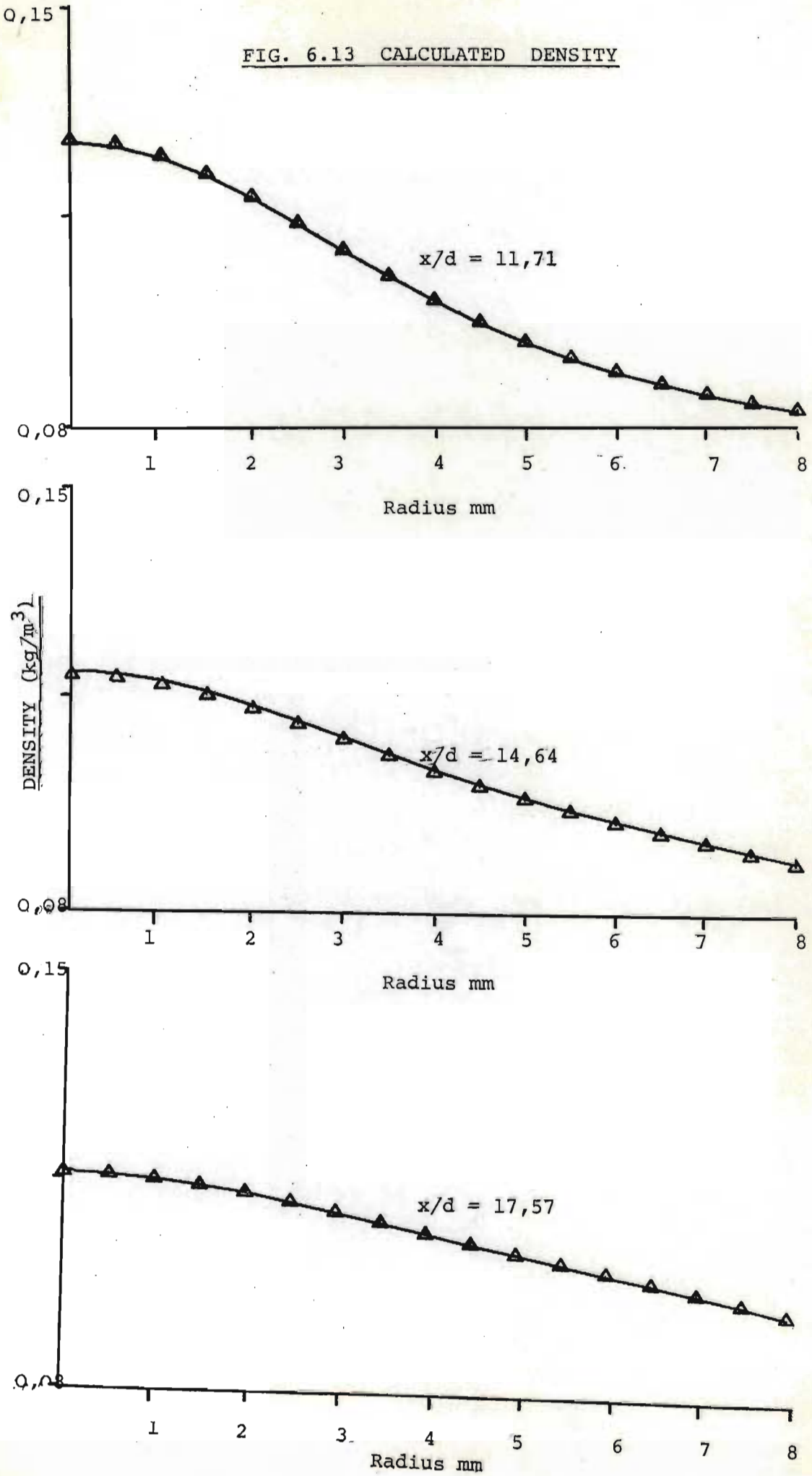

FIG. 6.14 CALCULATED DENSITY

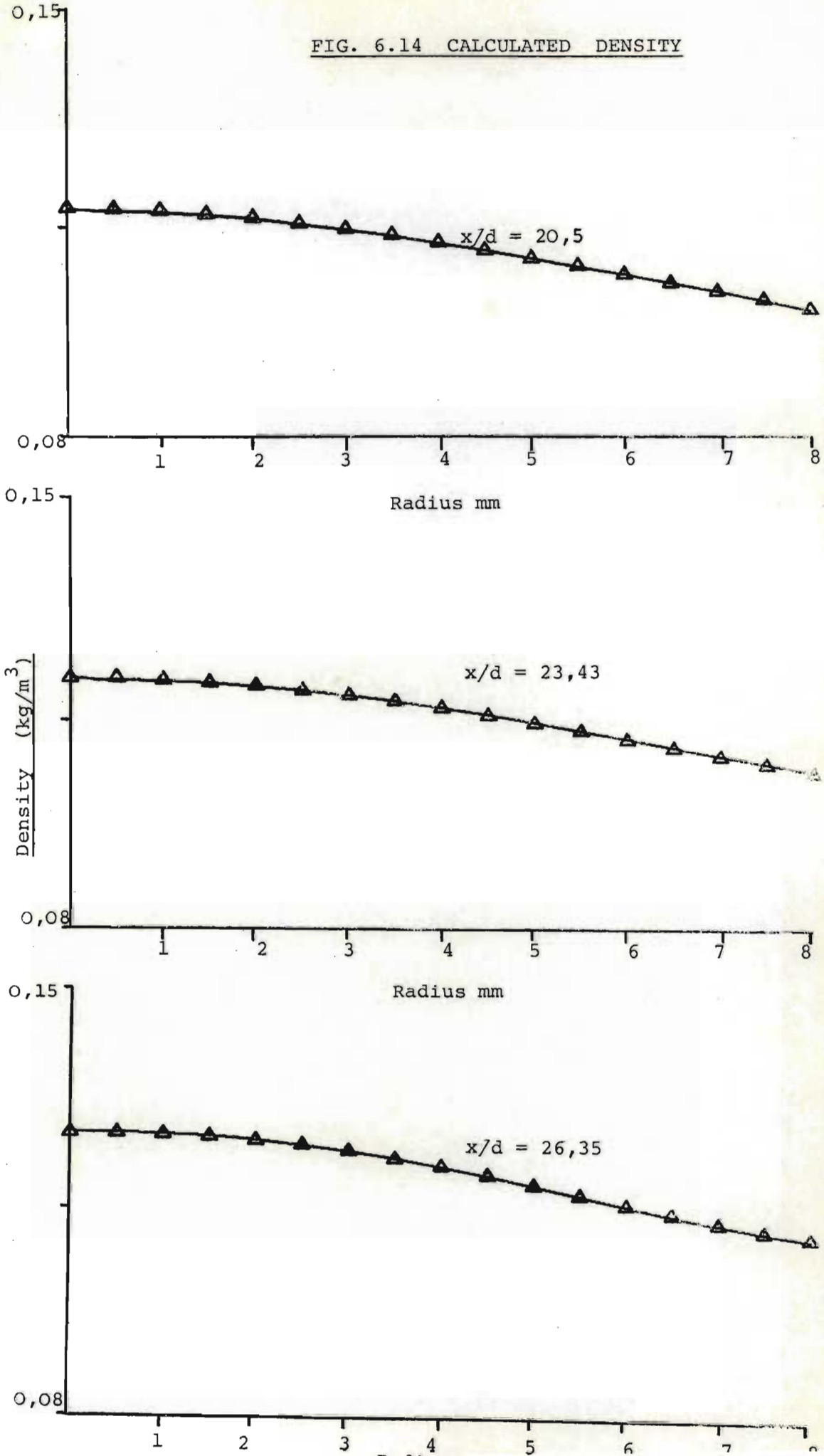

by equation (6.1), it follows that the static pressure was not uniform across the duct and that oblique shocks must have been present. At greater distances down the duct, this effect became less severe. In order to assess the static pressure for use in equation (6.2), a line was drawn through the data to produce the least square error. The scatter was of the order of $\pm$ 5%.

The static pressure used are listed below.

x/d	Static Pressure (kPa)
11,77	15,9
14,64	17,4
17,57	19,9
20,50	20,5
23,43	22,0
26,35	23,7

6.5. Mass Balance

A mass balance was performed at the last six axial stations. Owing to the thickness of the probe, measurements could only be taken up to a maximum radius of 8mm - i.e. 1mm from the wall and, for this reason, it was necessary to extrapolate the measured and computed flow properties into the region adjacent to the wall. The cubic spline functions developed earlier were used for this extrapolation. It was realised that the properties were likely to change sharply near the wall, but it was felt that a mass balance would still be informative. The balance was performed separately for each species by summing the flow of each species through each of 18 annular segments 500 microns wide. Values of measured and computed flow properties were obtained at the midpoint of each annulus by interpolation, again using the cubic spline functions developed earlier. The results of the mass balance are presented in Tables 6.14 and 6.15 and are plotted in Figure 6.17.

On the basis of reservoir conditions, the discharge of the nozzle was determined to be 23,5 g/s of nitrogen. (see Appendix 6.3). The rate of CO_2 injection was measured to be 2,40 g/s for the first set of tests. The results of the mass balance indicate that in the first set of tests, the flow of nitrogen inferred from measurements taken across a diameter of the mixing tube agrees with the known flow rate

TABLE 6.14 Mass Balance for Constant Injection Rate

Non-dimensional distance from Injection point x/d	Measured CO_2 Injection rate	Mass Flow Rate of CO_2 g/s	Measured N_2 Injection rate	Mass Flow Rate of N_2 g/s
11,8	2,4	1,54	23,5	23,3
14,7	2,4	1,52	23,5	23,3
17,7	2,4	1,58	23,5	23,4
20,6	2,4	1,67	23,5	23,7
23,4	2,4	1,77	23,5	23,7
26,5	2,4	1,83	23,5	23,7

TABLE 6.15 Mass Balance at x/d = 23,4 for three Different Injection Rates

Measured CO_2 Injection rate g/s	Measured Mass Flow of Nitrogen g/s	CO_2 Balance	N_2 Balance
1,5	23,5	1,13	24,3
2,4	23,5	1,77	23,7
3,2	23,5	2,07	21,7

to within 1%. The known injection rate for CO_2 of 2,4 g/s is considerably greater than the value inferred from measurements across the mixing tube. Because of this discrepancy, all the relevant measurements were checked. This implied checking the concentration measurement technique, the measurement of all the pressures and temperatures and the calibration of the orifice used for flow measurement. When it became fairly certain that the measurements were correct, it was postulated that there exists along the wall of the mixing tube a CO_2 rich boundary layer, less than 1mm thick which cannot be measured because of the limitation of the probe diameter and the fact that there is likely to be a shockwave-boundary layer interaction if the wall is approached too closely.

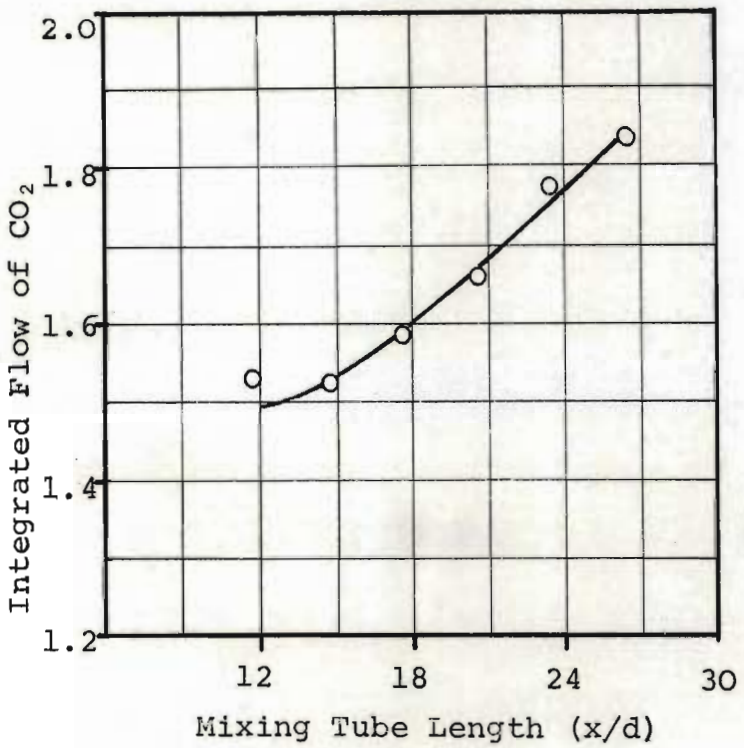

FIG. 6.17 RESULT OF MASS BALANCE

Evidence which supports this theory is that the mass balance for nitrogen was remarkably accurate and the fact that the mass flow obtained for CO_2 from the balance shows an increase at stations where the mixing is more advanced. This is consistent with the idea of a CO_2 - rich boundary layer being progressively diluted. The concentration profiles were then extrapolated by eye into the wall region on the basis of there being such a boundary layer and it was seen that, with quite credible profiles, the balance could be satisfied.

The concentration profiles thus obtained were not correct because they did not take into account boundary layer effect on the velocity profiles, but they showed that the overall CO_2 balance was sensitive to a thin anulus of moderately high concentration at the wall.

In view of this phenomenon, momentum and energy balances were not attempted. The excellent balance obtained for the nitrogen flow vindicates the way in which the data were smoothed using cubic spline functions.

For the second set of runs, with varying injection rates, the nitrogen mass balance was not accurate. It is assumed that this is because it was not possible to smooth the data in two dimensions as was done for the first set.

The carbon dioxide balance indicated the same phenomenon as

that observed for the first set of runs and, again, a carbon dioxide-rich boundary layer is postulated to explain the phenomenon.

6.6. Assessment of the Performance of the Reactor

6.6.1. Choice of Mixing Tube Length

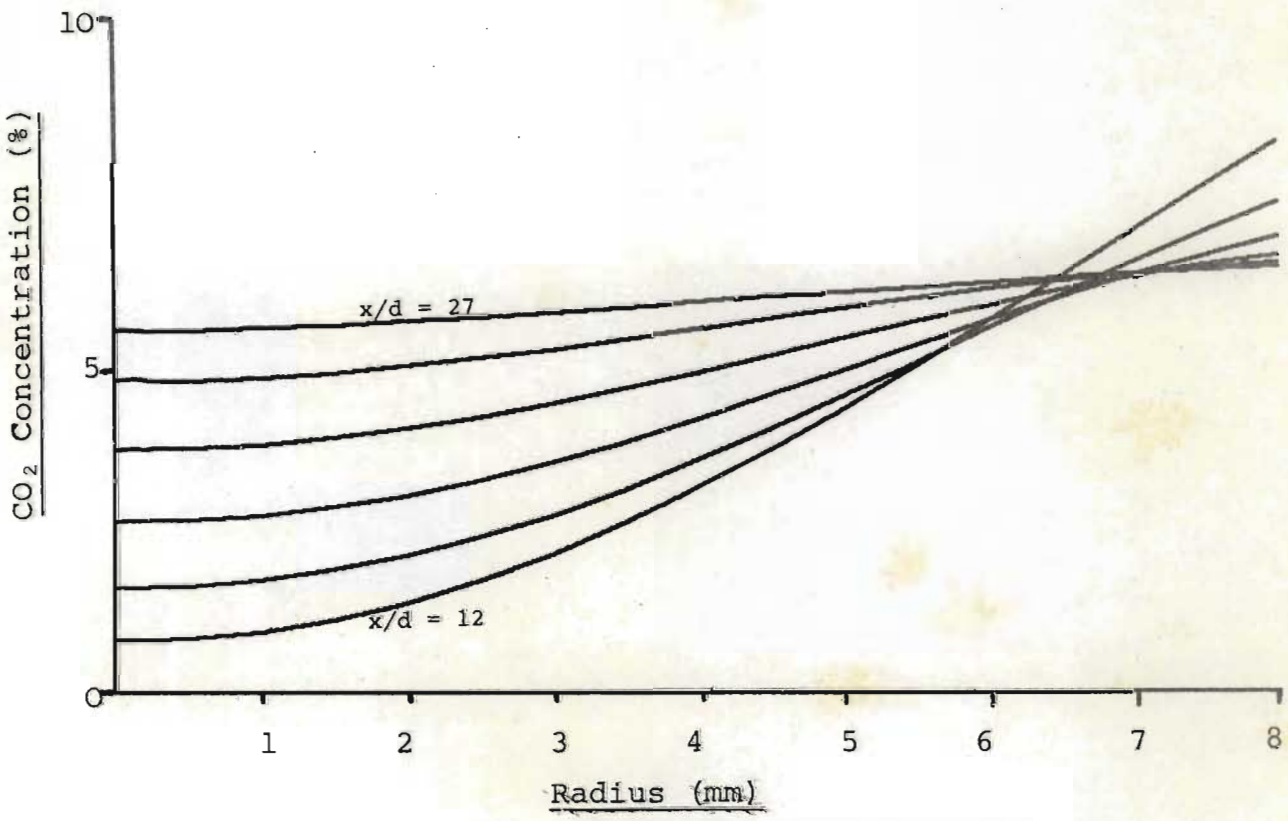

FIG. 6.18

Figure 6.18 shows a family of mass concentration profiles with the length of mixing tube as a parameter. These curves are the same as those represented in Figures 6.2 and 6.3. After 27 diameters, the mixing is well advanced. If the difference between centre-line concentration c_{ℓ}, and the

concentration which would occur after complete mixing, c_∞, is plotted against length of mixing, suitably non-dimensionalised, Figure 6.19 is obtained. The CO_2 - rich boundary layer was considered to be out of the mixing region, and the CO_2 flow obtained from Figure 6.17 at 30 diameters was used, to obtain c_∞ = 7,48%.

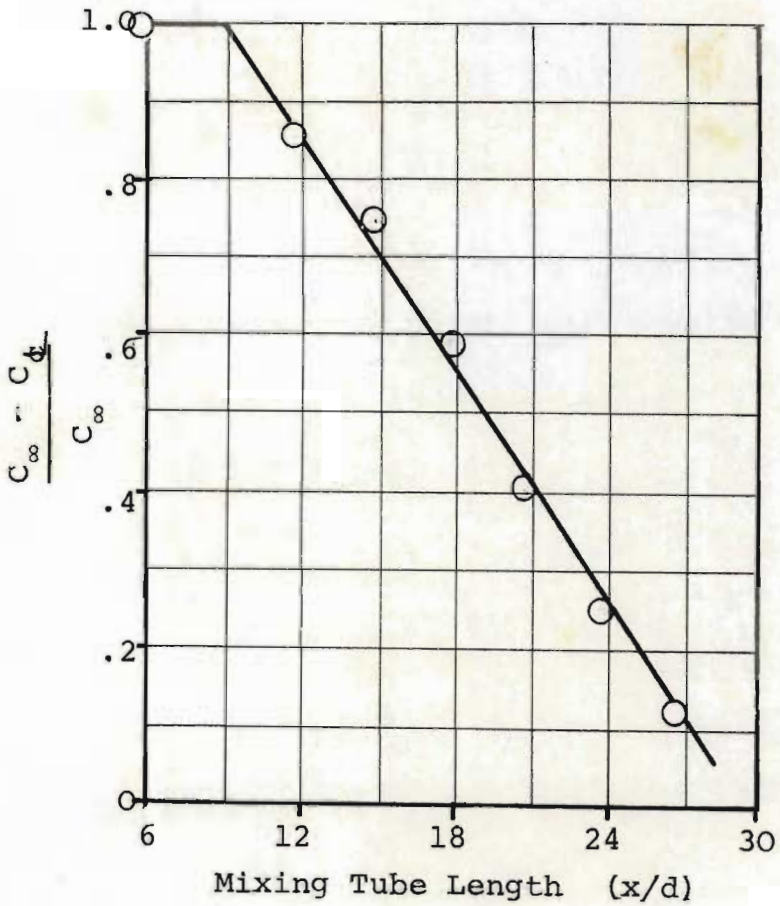

FIG. 6.19

Although the choice of the figure for c_∞ influences the slope of the curve, it does not change the nature of the plot - which indicates an almost linear relation.

If substantially complete mixing is required, it therefore seems that a mixing length of 30 diameters is sufficient.

Figure 6.20 shows the variation of static temperature with distance down the mixing tube and the temperature which would result if a normal shock occurred at that point. These

curves are identical with those obtained in section 6.4. It will be seen that although the profiles for both pre-shock and post shock temperatures become flatter with more

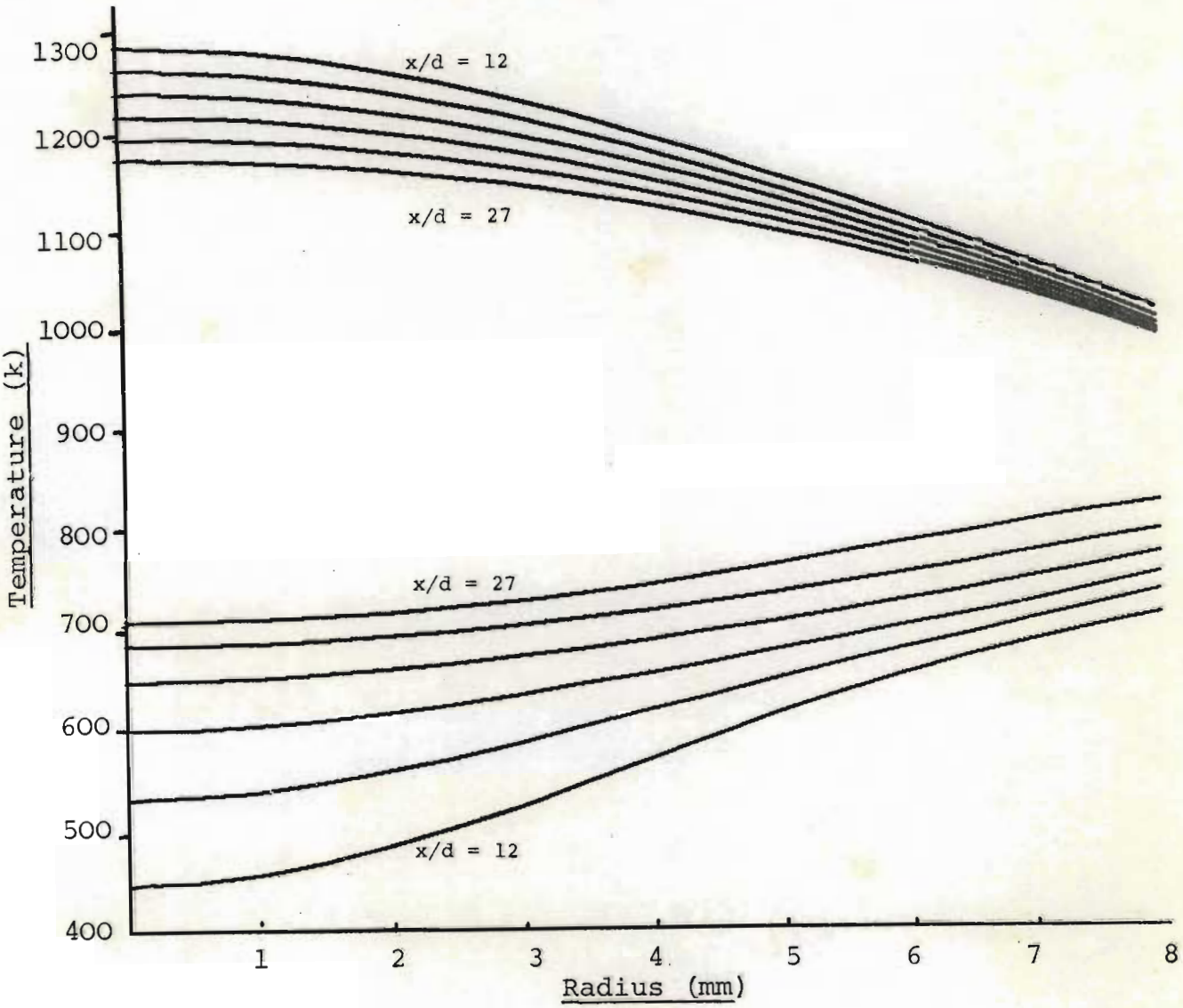

FIG. 6.20

advanced mixing, the temperature jump across the shock becomes smaller. This is a consequence of the fact that momentum is being lost to the walls by friction and that with reduced velocity, the static temperature increases.

There is also the secondary effect of heat loss to the walls. Consequently, one cannot use the concept of either a final static temperature at the end of a very long mixting tube or a final velocity.

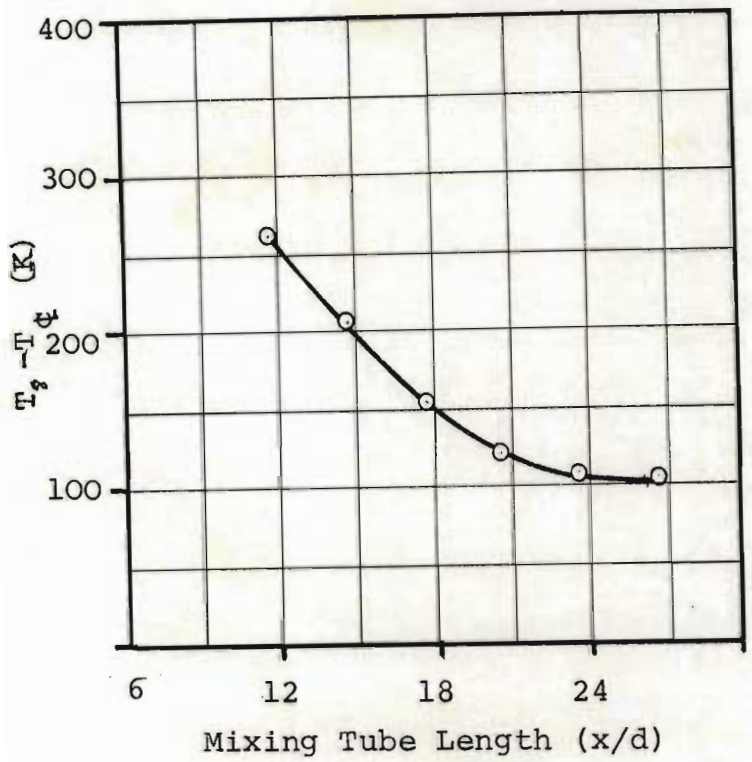

FIG. 6.21

Figure 6.21 provides an indication of the flattening of the static temperature profile with increased length of mixing tube. The difference between the static temperature at the centre line, T_{ℓ}, and the static temperature at a radius of 8mm, T_8, is plotted against mixing tube length. The plot shows that the rate of improvement in the profile becomes very small after 30 diameters.

Figure 6.22 provides a similar measure of the uniformity of the temperature jump associated with a shock at each mixing tube length. In this figure the difference between the

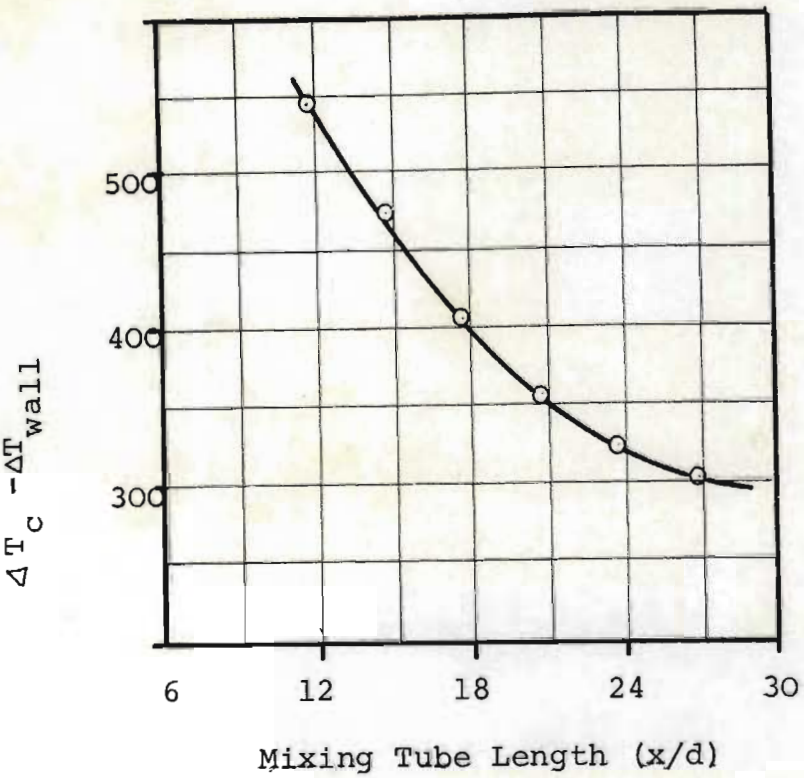

FIG. 6.22

static temperature jump at the centre line Δt_c and the static temperature jump at the edge of the mixing zone, Δt_8, is plotted against mixing tube length. Again the plot shows that the rate of improvement after about 30 diameters is small.

On the basis of Figures 6.19, 6.21 and 6.22, it seems that a mixing tube length of 30 diameters is desirable. It also seems likely that this figure will hold for reactors of different size because the determination largely excludes boundary layer effects.

It is also necessary to answer the question of whether the mixing information obtained from a nitrogen-carbon dioxide system can be applied to a methane-carbon dioxide or methane-oxygen system. It seems probable that it can. Although no other information appears in the literature on the subject

of confined mixing of this nature, information is available on mixing in free jets. Studies have been conducted where different substances have been mixed under conditions of supersonic flow. (Zakkay, Kraus and Woo, (1964) Alpinieri, 1964). The mixing profiles obtained were independent of the molecular weight of the gas injected.

6.6.2. Temperatures Occurring in the Reactor

In considering the results of the experimental investigation, it is necessary to establish whether the static temperature in the mixing zone is sufficiently low and whether the temperature after the shock is sufficiently high and sufficiently uniform. Examination of Figure 6.17 shows that the static temperature tends to increase after greater mixing lengths. This is a consequence of momentum loss to the tube walls. Extrapolation of the data indicates that the temperature at 30 diameters, the probable length of mixing tube in a reactor, varies by $55^{o}K$ about a median temperature of $792^{o}K$.

The temperature after the shock shows the opposite tendency in that it decreases with increased mixing length. This is the result of both heat and momentum loss to the walls of the mixing tube. Extrapolation to 30 diameters suggests a variation of $108^{o}K$ about a median of $979^{o}K$.

The minimum temperature jump at 30 diameters was 132°K and the maximum was 320°K.

In assessing these figures, however, the measurements of pressure inside the diffuser should be borne in mind (see Figures 5.16 and 5.17). These showed that there was a large radial pressure gradient behind the shock but that this gradient decreased rapidly with axial distance as the pressure equalised in the subsonic region. This implies that the temperature would also have equalised very rapidly. Extrapolation from Tables 6.8 to 6.13 shows that the mean velocity behind a shock at 30 diameters is about 450 metres per second. This implies that it would take the gas about 0,03 m secs to traverse the 15mm before the pressure and temperature were substantially uniform. Thus the effective temperature jump over the whole diameter of the flow (bearing in mind the non-linearity of the Rankine-Hugeniot equations) will be of the order of 250°K.

It is possible to raise or lower the temperatures throughout the reactor by changing the reservoir temperatures of the reactant gases. Also, recent investigations * into the partial oxidation of methane in a batch shock tube indicate that a temperature jump of about 200°K is sufficient to provide the desired product spectrum.

*Woodburn, private communication.

Thus, with subsonic injection of a cold secondary gas, it is possible to control both the temperature during mixing and the temperature jump so that the desired product spectrum is obtained. If, however, the secondary gas is injected supersonically at high stagnation temperature, it is anticipated that, with the same overall pressure ratios, the temperature jump would be more uniform. A greater temperature jump can be attained by simply increasing the speed of the flow, but this implies a greater pressure loss across the reactor.

6.6.3 Effect of Changing the Injection Rate

Figure 6.23 shows the profiles of temperature before and after a shock occurring at $x/d = 24$. It may be seen that the effect of varying the injection rate is small. The effect is masked by the limits of experimental accuracy.

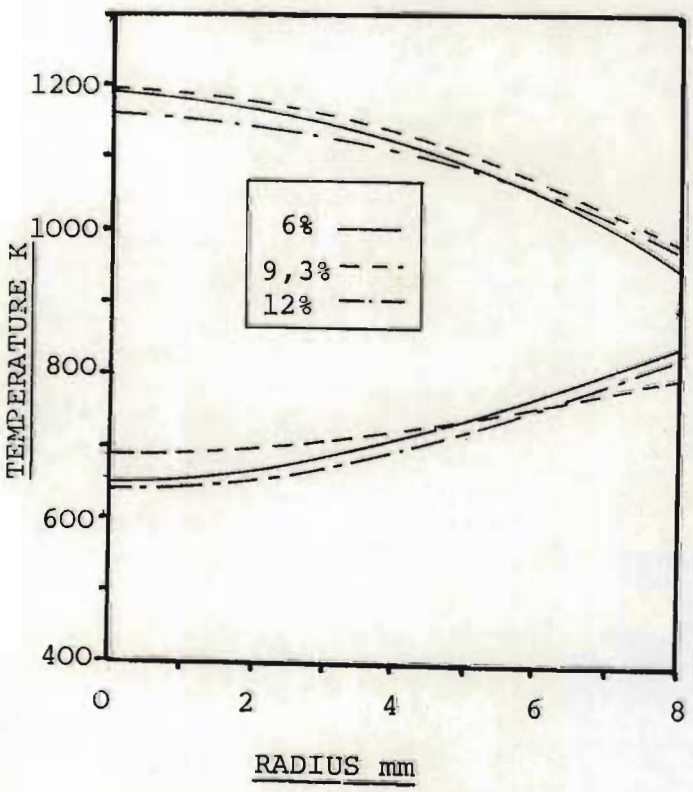

FIG.6.23 VARIATION OF PRE- AND POST-SHOCK TEMPERATURES WITH INJECTION RATE

6.7. Conclusion

It was concluded that:-

(1) It is possible to inject a secondary gas and still maintain supersonic flow.

(2) Complete mixing occurs within a fairly short distance, namely 30 diameters.

(3) The temperature before the shock is fairly uniform and can be controlled by choosing the reservoir conditions correctly.

(4) The temperature immediately after the shock is moderately uniform and becomes completely uniform after a very short time - of the order of 0,03 milli-seconds.

(5) The temperature jump obtained is sufficiently large to control the product spectrum in the partial oxidation of methane but this temperature jump can readily be increased by increasing the Mach number at the shock.

(6) The injection rate of carbon dioxide can be varied and with cold, subsonic injection it is seen that better temperature profiles are obtained at lower injection rates. If large secondary injection rates are required, it is desirable to heat the secondary gas and perhaps inject it supersonically.

(7) It is observed that the effect of momentum loss to the walls of the tube is severe in that this, more than the effect of secondary injection, decreases the Mach number

during mixing. This necessitates the high initial Mach number for the primary stream in order to keep the temperature during mixing to a tolerable level and this implies a large penalty in running costs. Therefore it would be desirable to effect mixing in a shorter distance, by an improved injection scheme.

CHAPTER SEVEN

ANALYSIS OF SUPERSONIC MIXING IN A LONG DUCT

7.1. Introduction

As discussed in Chapter 3, no technique exists for the prediction of supersonic mixing in a long duct. An obvious line of approach to the problem is to formulate conservation equations as specified below in cylindrical coordinates (Libby, 1962).

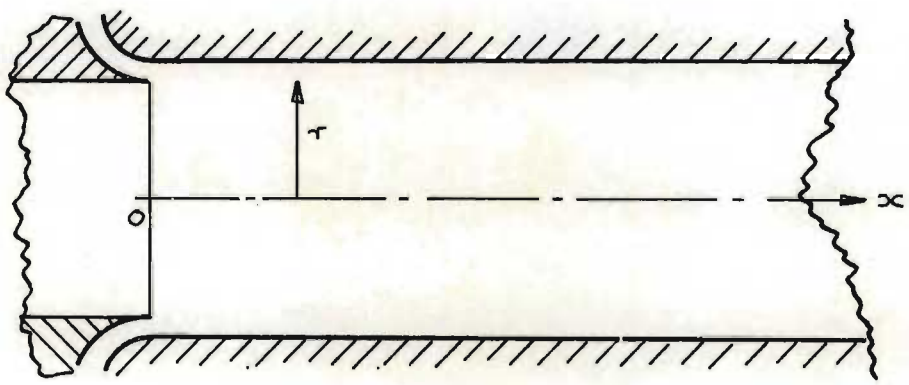

Global Conservation of Mass

$$\frac{\partial}{\partial x}(\rho u) + \frac{1}{r}\frac{\partial}{\partial r}(\rho v r) = 0 \qquad (7.1)$$

Conservation of Momentum

$$\rho u \frac{\partial u}{\partial x} + \rho v \frac{\partial u}{\partial r} = \frac{1}{r}\frac{\partial}{\partial r}\left(\varepsilon \rho r \frac{\partial u}{\partial r}\right) \qquad (7.2)$$

Conservation of Energy

$$\rho u \frac{\partial H}{\partial x} + \rho v \frac{\partial H}{\partial r} = \frac{1}{r} \frac{\partial}{\partial r} (\varepsilon_H \rho r \frac{\partial H}{\partial r}) \tag{7.3}$$

Conservation of Species

$$\rho u \frac{\partial C_i}{\partial x} + \rho v \frac{\partial C_i}{\partial r} = \frac{1}{r} \frac{\partial}{\partial r} (\varepsilon_m \rho r \frac{\partial C_i}{\partial r}) + w_i \tag{7.4}$$

where C_i is the mass fraction of the i^{th} species and w_i is the rate of production of the i^{th} species by chemical reaction. In this case $w_i \equiv 0$.

$\varepsilon_\tau, \varepsilon_H, \varepsilon_m$ are the turbulent transfer coefficients of momentum, energy and mass respectively.

The next step would be to assume

$$\varepsilon_\tau = \varepsilon_m = \varepsilon_H = \varepsilon$$

and postulate a variation of ε with u and r. Here, the assumptions made for supersonic free mixing can be considered.

The Prandtl mixing length hypothesis

$$\varepsilon = kb(u_{max} - u_{min}) \tag{7.5}$$

where b is a measure of the width of the jet, was used by Libby (1961). Since b is assumed to increase linearly with x, this is equivalent to saying that ε increases linearly with x. This formulation predicts that free streams at equal velocities would remain segregated. This has been demonstrated to be false by Alpinieri (1964).

He investigated the use of different forms for equation (7.5). For the velocity difference in (7.5), he substituted the difference in momentum fluxes and mass fluxes. When experimental conditions were set such that these differences became zero, no tendency towards segregation was observed, thus demonstrating the inadequacy of the Prandtl model.

Despite this limitation, this has been the model used in subsequent analyses (Schetz,(1968), Shivamoggi (1976)).

For the case of a ducted flow, clearly the concept of a jet-spread parameter is inapplicable and equation (7.5) cannot be used directly. Therefore, as a contribution towards dealing with the problem of supersonic mixing in a duct, it was proposed to use the data of the present investigation to describe the variation of ε.

7.2. Analysis for Diffusion of Mass

Consider the annular element described in Figure 7.2. A shell balance was performed for the mass of injectant gas and equation (7.6) was obtained (see Appendix 7.1).

$$\rho u \frac{\partial c}{\partial x} + \rho c \frac{\partial u}{\partial x} + uc \frac{\partial \rho}{\partial x} = \varepsilon \left(\frac{1}{r} \frac{\partial c}{\partial r} + \frac{\partial^2 c}{\partial r^2}\right) \qquad (7.6)$$

Although, the specification of ρ, u, $\frac{\partial u}{\partial x}$ and $\frac{\partial \rho}{\partial x}$ by analytical means is difficult the treatment of equation (7.6) becomes easier if these quantities can be determined by experiment.

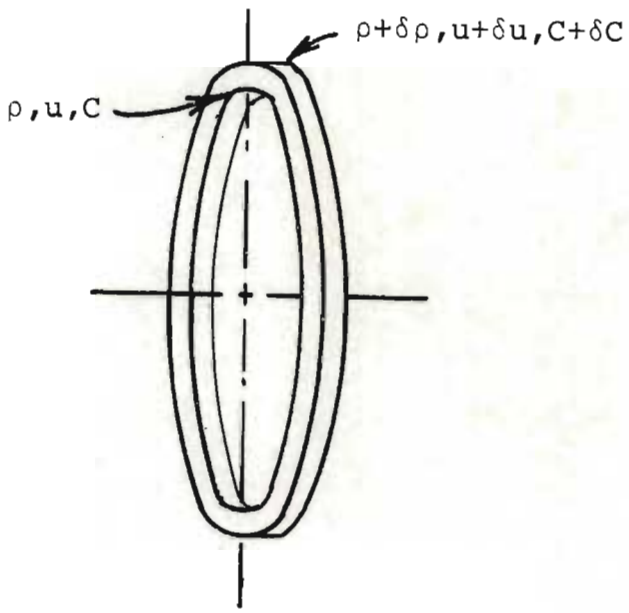

FIG. 7.2 MASS BALANCE ELEMENT

Accordingly, the approach employed was to work from a measured concentration profile and, using an assumed form of the variation of ε, together with measured values of ρ, u, $\frac{\partial u}{\partial x}$ and $\frac{\partial \rho}{\partial x}$, to use equation (7.6) to predict the development of the concentration

profile at later stations. These could then be compared with experimentally determined values.

The known initial concentration profile was taken to be that measured at x/d = 11.7 because this was the first station which could be considered as not being in the near field.

As has been discussed in Chapter 6, it was observed that a CO_2-rich boundary layer persisted throughout the length of the mixing zone and this boundary layer was progressively diluted. This analysis was limited to the flow outside this boundary layer and the boundary condition was handled by the use of an imaginary, frictionless porous wall, through which a known amount of CO_2 diffused. The mixing duct was taken to be only 16mm in diameter and the spline functions developed in Chapter 6 were used to integrate the CO_2 flow in a cross-section of this diameter, at each of the six axial stations where measurements had been taken. The results are plotted in Figure 7.3. A least square error straight line was put through these points and it was possible to calculate that a mass flux of 0,0141 kg/m^2s was necessary through the porous wall in order to make it equivalent to the effect of the CO_2-rich boundary layer.

For the numerical solution of equation (7.6) a grid having 19 nodes in the radial direction and a mesh of 1mm in the

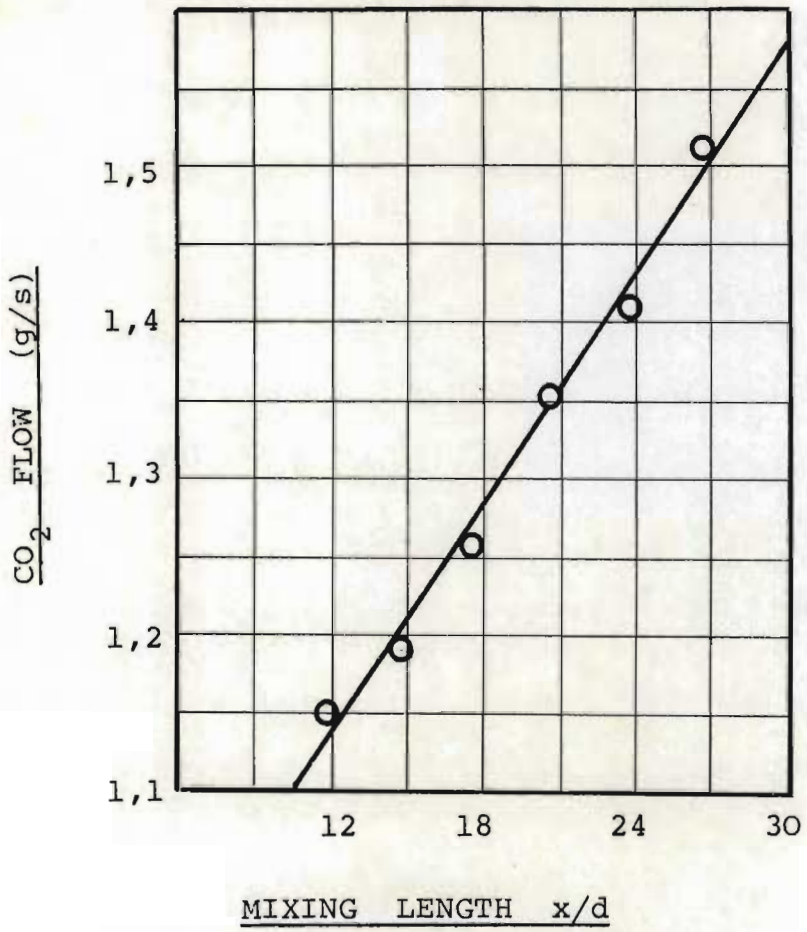

FIG. 7.3 MASS BALANCE TO DETERMINE FLOW THROUGH POROUS WALL

axial direction was laid down. Node number 2 was on the centre-line of the duct and node number 18 corresponded to the position of the imaginary porous wall. The boundary conditions could then be handled by a reflection about the centre-line and a hypothetical concentration at node number 19. This concentration was assessed by using the value of the turbulent diffusivity, ε, at that point to compute what concentration would be necessary at node number 19 to provide the mass flux necessary through the porous wall.

The method of Crank and Nicholson (see Mitchell, 1969) was used to solve equation (7.6) - with x replacing time as the independant variable. The method demands that equation (7.6) be cast into the form:

$$\frac{\partial c}{\partial x} = -\frac{c}{u}\frac{\partial u}{\partial x} - \frac{c}{\rho}\frac{\partial \rho}{\partial x} + \frac{\varepsilon}{\rho u r}\frac{\partial c}{\partial r} + \frac{\varepsilon}{\rho u}\frac{\partial^2 c}{\partial r^2} \qquad (7.7)$$

Then, working from a known axial station, where j=j, say, and seeking to determine the conditions at the next station, j=j+1, for any node, i, we can write the value of $\frac{\partial c}{\partial x}$ at mid-mesh as

$$\left(\frac{\partial c}{\partial x}\right)_{i,j+\frac{1}{2}} = (c_{i,j+1} - c_{i,j}) / G$$

where $c_{i,j}$ is the mass fraction of carbon dioxide at the node i, and at the axial station, j. G is the axial mesh

width - 1mm in this analysis.

We can then use the trapezoidal rule to say that

$$\left(\frac{\partial c}{\partial x}\right)_{i,j+\frac{1}{2}} = \tfrac{1}{2}(RHS_{i,j} + RHS_{i,j+1}) \qquad (7.8)$$

where $RHS_{i,j}$ represents the right hand side of equation (7.7), written at the mesh point, (i,j).

If, then, the right hand side of equation (7.8) is expressed in finite difference form, with a central difference expression for the second derivative, there results at each point an equation in terms of the properties at the points (i,j), (i+1,j)(i-1,j), (i,j+1), (i+1,j+1)(i-1,j+1).

The properties at the j^{th} station are known. Thus, writing equation (7.8) at the 17 mesh points (2,j) through (18,j) and incorporating the boundary conditions already discussed for (1,j) and (19,j) results in a 17 x 17 tri-diagonal matrix in the 17 unknown concentrations at the points (2,j+1) through (18,j+1).

In this way, working from an initial, measured, concentration profile and assuming some $\varepsilon(r,x)$ it is possible to predict concentration profiles at subsequent stations and then compare these with measured data.

This technique was written into a computer program which read estimates for the parameters of the proposed diffusivity function at a teletype and displayed the predicted concentration profiles for later stations on a storage oscilloscope. Measured profiles were also displayed and the cumulative square error was computed. In this way it was possible to obtain an intuitive understanding of the effect of the formulation of the diffusivity function and to vary the form and constants of the function in order to obtain the minimum cumulative square error.

7.2.2. Results and Discussion

It was found that the best form for the diffusivity function was

$$\varepsilon = (x - x_0) \times (R - r) \times A$$

where R was the radius of the duct i.e. 9mm.

The values of x_0 and A which gave the best fit to the experimental data were

$$x_0 = 0{,}155$$
$$A = 5{,}07$$

The experimental data end fitted curves are shown in FIgure 7.4.

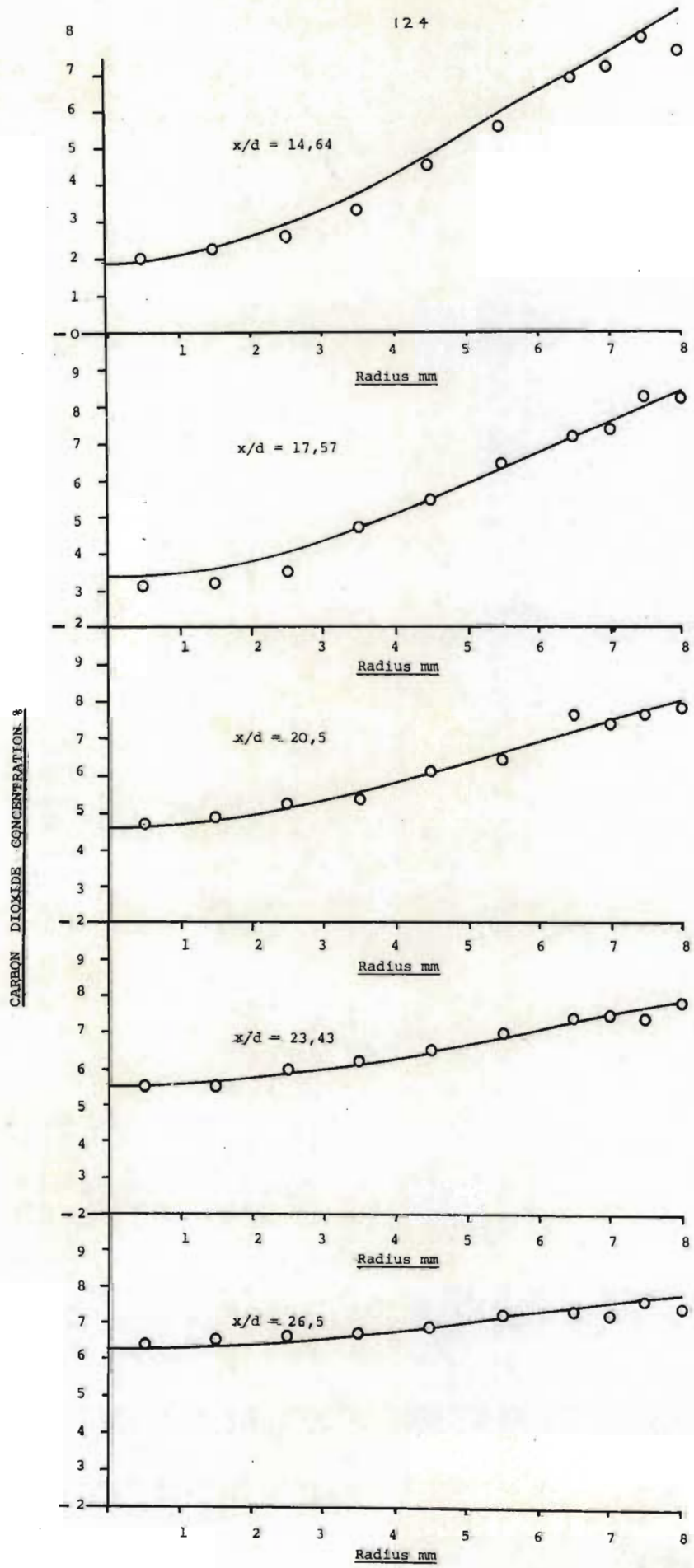

FIG. 7.3 COMPARISON BETWEEN PREDICTED (SOLID LINE)

The term x_0 reflects the distance of a hypothetical origin from the plane of injection. The diffusivity on the axis increases linearly from a value of zero at $x = x_0$. The physical significance of this origin is that it marks the end of the potential core of pure nitrogen - as may be seen from Figure 6.19. The value of x_0 was derived solely by fitting the best function to the data and it lends credence to the model that x_0 should correspond to the end of the nitrogen core.

The term $(R - r)$ represents the distance from the actual wall of the duct (not the hypothetical porous wall). This term implies that the diffusivity increases linearly with distance from the wall - from a value of zero at the wall.

The fact that the centre-line diffusivity increases with distance as does that for the Prandtl model customarily employed for free jets invites the conjecture that the increase in diffusivity for free jets is not physically related to the spread of the jet. The same form is observed in this case where the width of the mixing zone is constant.

7.3. Analysis for Momentum Transport

A similar analysis was performed for momentum transport. A shell momentum balance yielded:

$$2\rho u \frac{\partial u}{\partial x} + u^2 \frac{\partial \rho}{\partial x} = \varepsilon \left| \frac{\partial^2 u}{\partial r^2} + \frac{1}{r} \frac{\partial u}{\partial r} \right| \qquad (7.10)$$

It will be seen that this equation is non-linear in u. The Crank-Nicholson technique was never-the-less applied and experimental values for ρ and $\frac{\partial \rho}{\partial x}$ were used. The non-linearity was dealt with iteratively and convergence to 0,01% was obtained.

Subsequent velocity profiles were predicted from a measured initial velocity profile using equation (7.10) and an assumed diffusivity function. It was found that the prediction was bad and this is ascribed to the inaccuracy of experimental data for ρ and $\frac{\partial \rho}{\partial x}$.

As mentioned in Chapter 6, it was found that the assumption of constant pressure across the mixing duct was not strictly valid, particularly at stations close to the plane of injection. This implies that the properties inferred from the ratio of the static pressure at the wall to the measured stagnation pressure in the flow will not be accurate. In particular, it was found that, along the axis of the duct, the density gradient, $\frac{\partial \rho}{\partial x}$, was negative in the intial region. Because this gradient was determined from a variation of only 5% in the density, it was concluded that the inferred values of density were not sensitive enough to permit a meaningful assessment of momentum diffusivity. Also the initial velocity profile from which subsequent profiles were derived is probably not reliable.

CHAPTER EIGHT

CONCLUSION

Several aspects related to the development of a supersonic chemical reactor were examined.

A method of producing a standing normal shock in a duct at high Mach number was devised. It was established that a shock could be produced even for a non-uniform incident stream as is the case after flow in a duct.

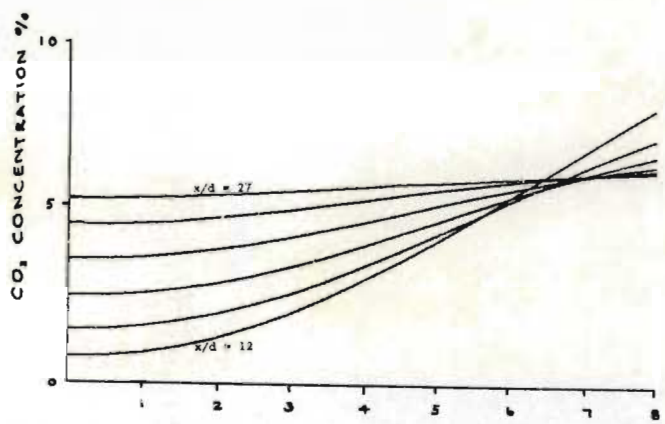

FIG. 8.1(a) CO_2 ONCENTRATION

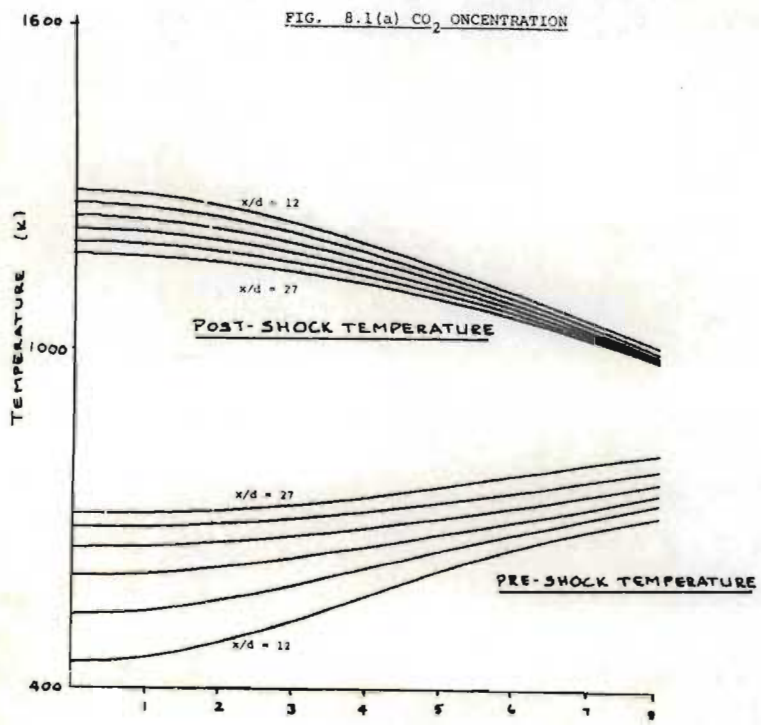

FIG. 8.1 (b) TEMPERATURE PROFILES

A secondary gas was injected into the supersonic flow and the conditions in the mixing section were examined. It was found that temperature and injectant concentration, the most significant factors for the reactor,

varied as shown in Figure 8.1. Figure 8.1(a) shows the variation of CO_2 concentration with radius for six mixing lengths. Figure 8.1(b) shows static temperature and post-shock temperature variation with radius for six mixing lengths.

From Figure 8.1, it may be seen that, within a reasonable distance, an acceptable concentration profile may be obtained It may also be seen that a temperature jump is obtained at the shock and it is judged that this jump is suitable for the partial oxidation of methane to ethylene.

APPENDIX 2.1

CALCULATION OF NITROGEN MACH NUMBER AT INJECTION POINT

It is required that the speed of the nitrogen flow before the carbon dioxide injection be such that after mixing, the static temperature of the mixture will be approximately $400^{\circ}K$.

There will also be two opposite effects. The momentum deficit of the carbon dioxide will cause the nitrogen to be retarded in the mixing process, thus causing its static temperature to rise. On the other hand, the lower stagnation temperature of the carbon dioxide will tend to cool that of the nitrogen. A third effect, namely the momentum loss to the walls of the mixing tube will not be considered - nor the heat loss to the walls.

The injected carbon dioxide will be considered to have ambient stagnation temperature and a high subsonic velocity at injection, say Mach 0,95.

$$\text{Injectant velocity of } CO_2 = 0{,}95 \times a$$

$$= 0{,}95 \times \sqrt{\gamma RT}$$

from equation (2.1)

$$\frac{300}{T} = 1 + \frac{\gamma-1}{2}(0{,}95)^2$$

$$T = 1 + \frac{1-1{,}285}{2} \times 0{,}95^2$$

$$\doteq 265{,}81\ K$$

Stagnation temperature after mixing

$$= \frac{\text{mass}_{CO_2} \times C_{p_{CO_2}} \times T_{CO_2} + \text{mass}_{N_2} \times C_{p_{N_2}} \times T_{N_2}}{\text{mass}_{CO_2} \times C_{p_{CO_2}} + \text{mass}_{N_2} \times C_{p_{N_2}}}$$

$$= \frac{91\% \times 936,8 \times 300 + 90,9\% \times 1039 \times 1350}{9,1\% \times 936,8 + 90,9\% \times 1039}$$

$$= 1263 \text{ K}$$

Gas constant after mixing = 287,01 J/kg mole K

Specific heat ratio after mixing = 1,384

The method of calculating these is discussed in Chapter 6.

Required Mach number after mixing is derived from equation 2.1.

$$\frac{1263}{400} = 1 + \frac{1-1,384}{2} * M^2$$

and $M = 3,35$

Thus, velocity of mixing $= 3,35 \sqrt{\gamma RT}$

$$= 3,35 \sqrt{1,384 * 287 * 400}$$

$$= 1335 \text{ m/s}$$

But velocity after mixing

$$= \frac{\text{Initial Momentum of } CO_2 + \text{Initial Momentum of } N_2}{\text{Total Mass}}$$

i.e. $1335 = \frac{9,1\% \times 241 + 90,9\% \times V \text{ initial}}{100}$

and initial velocity of nitrogen = 1445 m/s

1445 = Mach number of nitrogen x local speed of sound

$$= M_{N_2} \times \sqrt{\gamma RT}$$

but, using equation (2.1), $T = \frac{T_o}{1+\frac{\gamma-1}{2} M^2}$

i.e. $1445 = M_{N_2} \times \sqrt{\frac{\gamma R T_o}{\left(1+\frac{\gamma-1}{2} M_{N_2}^2\right)}}$

and Mach number of nitrogen flow at injection point = 3,74

APPENDIX 2.2.

Calculation of Experimental Conditions

Given that the nitrogen Mach number is 3,74 it is necessary to calculate the reservoir pressure upstream of the nozzle, assuming that the mixed flow is compressed through a normal shock back to ambient pressure, taken as 101 kPa.

From Appendix 2.1,

Mach number just before shock = 3,35

From equation (2.5), taking a mean value of γ between that at 400 K and that at 1300 K, i.e. γ = 1,34, we have

$$\text{Pressure ratio across shock} = \frac{2 \times 1{,}34 * 3{,}35^2 - 1{,}34 + 1}{1{,}34 + 1}$$

and Pressure before shock = 7,95 kPa

Assuming that there is no pressure difference across the mixing tube, equation (2.2) may be used to predict the nitrogen reservoir pressure. Taking a value for γ at an intermediate temperature i.e. γ = 1,375

$$\frac{P_o}{7{,}95} = 1 + \frac{\gamma-1}{2} M^2)^{\gamma/\gamma-1}$$

and $$P_o = 892 \text{ kPa}$$

This value will probably be too low because allowance has not been made for frictional losses in the mixing tube.

APPENDIX 2.3.

Calculation of Specific Nitrogen Flow

For a reservoir pressure of 892 kPa and γ = 1,32 (at 1250 K) the specific mass flow of a de Laval nozzle is calculated

Mass flow/unit area = density at throat x sonic velocity at throat.

from equation (2,1),

$$T^* = 1350/(1+ \frac{\gamma-1}{2} \times 1^2)$$

$$= 1164 \text{ K}$$

from equation (2.2.),

$$p^* = 482 \text{ kPa}$$

and from Gas Tables by Canjar and Manning (1967)

$$\rho^* = 1{,}262 \text{ kg/m}^3$$

Velocity at throat $= \sqrt{\gamma RT}$

$$= \sqrt{1{,}32 \times \frac{8312}{28} \times 1164}$$

$$= 675{,}4 \text{ m/s}$$

Thus specific mass flow = 675,4 x 1,262 = 852,3 kg/m^{2}s

Calculation of Specific Heating Load

For a specific mass flow of 852,3 kg/m^{2}s the power is calculated which would heat this gas from ambient temperature to 1350 K.

From Gas tables by Canjar and Manning (1967) the enthalpy increase per kilogram, at constant pressure, between the limits of 300 K and 1350 K is found to be 1,21 MJ/kg.

Thus the specific heating load is 1031 MW/m^2

APPENDIX 4.1

Design of Heater and Power Supply

Heater Design

Of the three basic types of heater available viz. pebble bed, arc and electric resistance, it seemed that the electric resistance heater offered the easiest way to meet the requirements of the nozzle. The pebble bed heater was ruled out because it does not allow controlled variation of the gas temperature and is not essentially a continuous heater.

Of the remaining two types, the resistance scheme was chosen in preference to the arc heater on the grounds that it was technically less complex and that ionisation of the gas was undesirable. A further consideration was that, if the work were extended to using methane as the experimental gas, the resistance heating scheme could be used whereas the arc heating scheme could not.

Graphite heating elements were selected and the publication of Allegre et. al. (1966) was used as a guide in the initial heater design. Allegre describes a heater developed to provide continuous operation at gas temperatures of 1800^{o}K and a flow rate of 18 g/s of nitrogen. Although the flow

rate required for the present investigation was considerably higher than that of Allegre, their design provided a useful guide.

Considerable modification and development was required before the heater finally performed satisfactorily but it is proposed to describe only the final configuration. The heater consisted of three graphite elements contained in a cylindrical stainless steel pressure vessel approximately 300mm diameter by 700mm long. A detailed drawing is shown in Figure A4.1. Each element was formed from graphite and consisted of a core and a sleeve passing over it - see Figure A4.2.

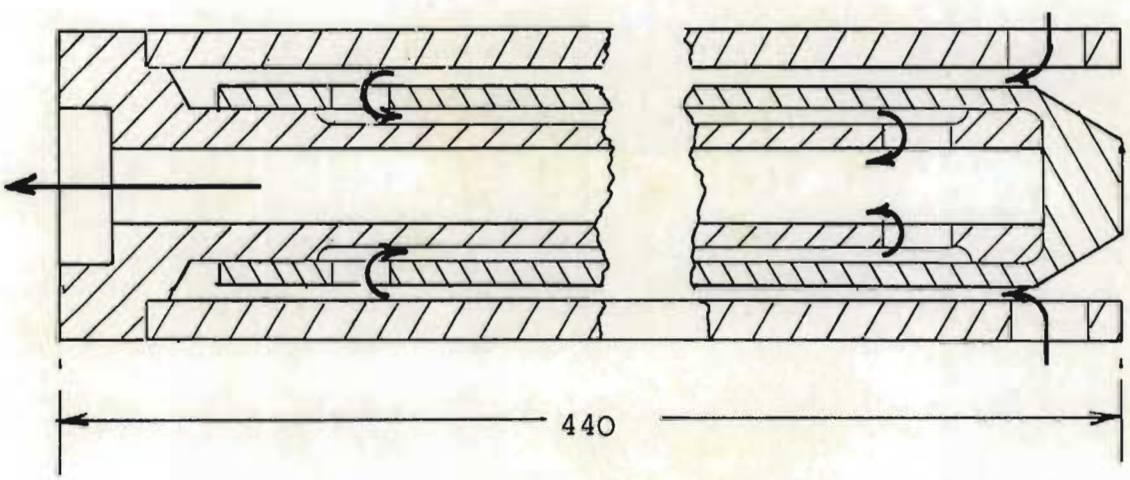

FIG. A4.2 GRAPHITE RESISTANCE ELEMENT

and the compound element was contained within another cylindrical carbon sleeve which was not electrically heated. The object was that gas was forced to pass through the anulus formed between the outer sleeve and the resistor sleeve. It then entered the anulus between the resistor core and sleeve and from there is passed into a passage down the centre of the core. It thus traversed the resistor three times.

The bundle of three resistors and sleeves was contained within two stainless steel shells between which there was a radial clearance of 3mm. The gas inlet to the heater was positioned such that the cold gas passed over the outer stainless steel sleeve, back through the anulus between the two layers, then over the outer resistor sleeve and so into the resistors i.e. it travelled up and down the heater six times before being discharged.

This rather complex arrangement proved necessary to provide efficient insulation of the resistors. The heater of Allegre et. al. relied extensively on water cooling but, because the present heater was four times as large and had three resistors instead of one, the cooling required would have been excessive. The use of incoming gas as an insulating medium had the further advantage of preheating it before it reached the resistors, thus allowing them to

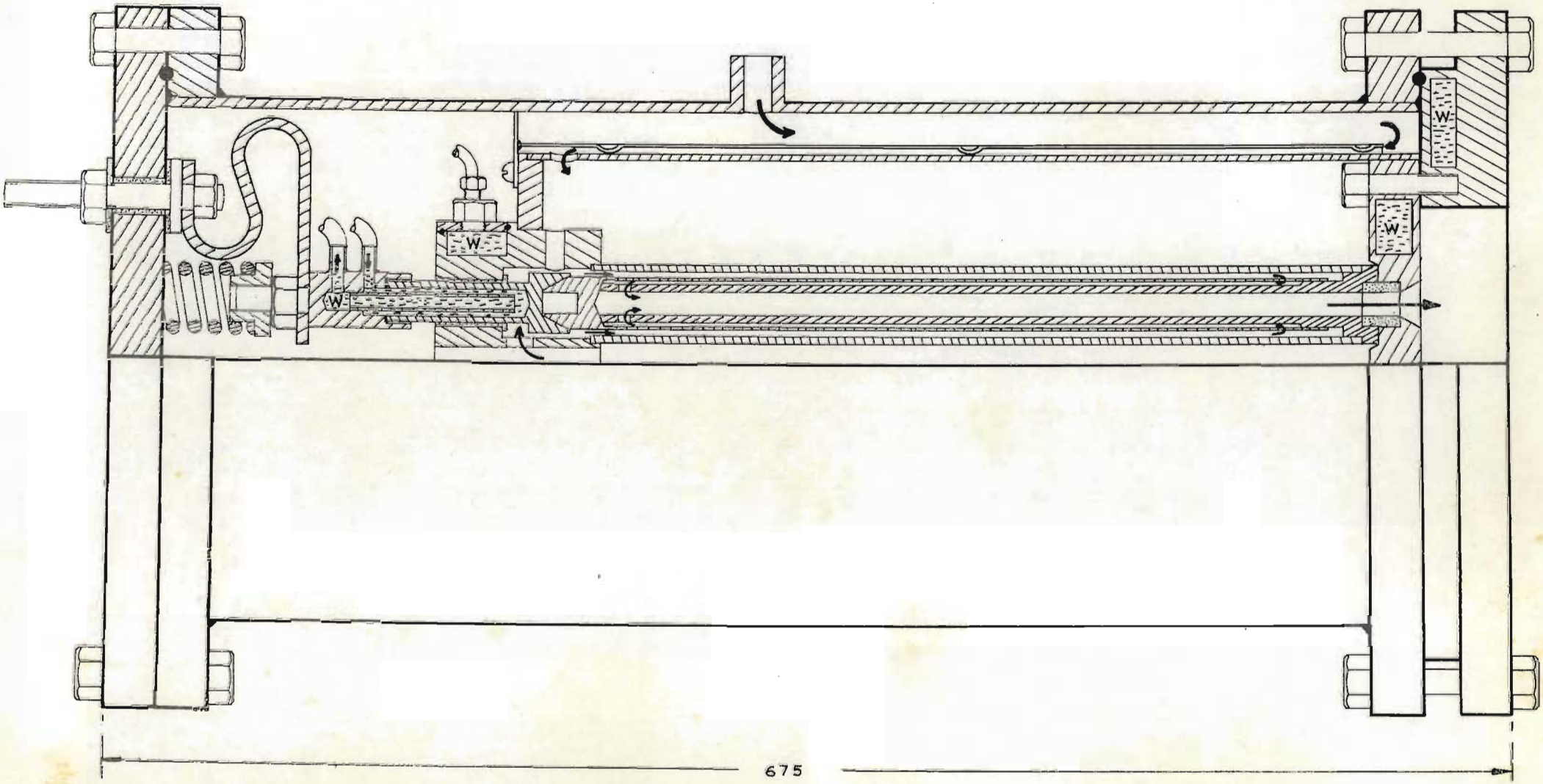

ELECTRIC RESISTANCE HEATER

run cooler.

The electrical terminals at the ends of the resistors were made from brass and were water cooled and the contact surfaces of the resistors were electrolytically copper plated to reduce contact resistance.

All three resistors made contact with a common terminal block at the one end but had separate electrically insulated, terminals at the other end. This electrical circuit was made possible by running the heater from a three phase supply in a "star" configuration. The water-cooled common terminal acted as a manifold to collect the gas streams from the three resistors into a common settling chamber. The passages through which the gas traversed the manifold were lined with graphite inserts in order to minimise heat transfer.

It was found that impurities in the nitrogen resulted in the oxidation of the resistors into carbon monoxide. Consequently, over the course of many test runs the resistance of the elements would gradually increase and this would limit the heating power available. As discussed in the following section, the power supply was limited to a maximum line voltage of 34,64 volts (phase voltage 60) and a maximum line current (equal to phase current) of 2500 amps. In order to maximise the life of resistors it was decided to design

them with too much material and too little electrical resistance at the outset so that, with oxidation, their resistances would gradually increase to the point of peak power transmission and thereafter the power transmission would begin to decline again. Figure A4.3 shows the maximum power as limited by maximum current and voltage.

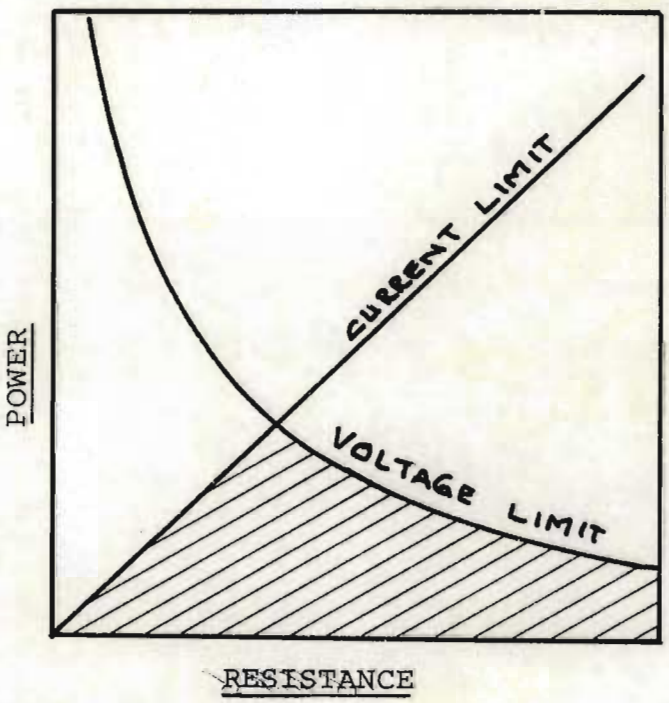

FIG. A4.3

Because of the difficulties associated with computing a heat transfer coefficient for the resistors, it was decided to simply use the Nusselt number of the flow for the heater of Allegre et. al.

The final result was a heater capable of running at a pressure of 2 MPa and providing a gas temperature variable up to about 2000^{o}K. The insulation scheme was so efficient that the surface of the heater, which was not water-cooled, ran

at a temperature below the ambient as a result of Joule-Thompson cooling of the gas in expanding from the high pressure supply system. The heater was designed to handle 120 grams of nitrogen per second.

Power Supply

The heater was designed to provide a flow rate of 120 grams of nitrogen per second, at a temperature of 1450°K. This was slightly above the stagnation temperature at which it was anticipated to run the nozzle (1350°K), but it was felt desirable to over-design the system. Clearly for a limited power supply, experiments at a higher temperature would have necessitated a decrease in mass flow rate.

In view of the low electrical resistance of graphite (0,012Ωmm) the power supply had to provide a high amperage at fairly low potential. The supply system designed comprised a three phase transformer, transforming a phase voltage of 380 volts to 60 volts, and a saturable reactor. The principle of the saturable reactor is that the high voltage circuit passes through a choke whose back emf is sufficient to limit the current flow to a very small value. Around the core of the choke is a winding which can be excited by a direct current. The result, on full excitation of the d.c. winding is that the magnetic flux of the core can be saturated. Since the

back emf,

$$E \propto \frac{d\phi}{dt}$$

when $\frac{d\phi}{dt}$ is forced equal to zero by saturation, no back emf can be generated and the full current can be passed into the transformer.

This stratagem allows the control of very large secondary currents, simply by varying a small d.c. injection current.

The injection current was obtained from a thyristor rectification network. Its maximum value was 70 amps and it could be varied by operating a motor driven variable resistance. The output current was closely proportional to the injectant current. Clearly the output voltage of transformer was not sinusoidal except at full power and the power factor was poor at low power levels.

The transformer used was rated at a maximum current of 2500 amps per phase. This implied a maximum power output of 260k watts. Tables of thermodynamic properties for nitrogen (Canjar and Manning, 1967) indicate that in order to heat 120 g/s of nitrogen from room temperature to 1450^{o}K a power input of 160kW is necessary.

APPENDIX 4.2.

Gas Analysis

It was necessary to develop a system which allowed on-line sampling and analysis of mixtures of carbon dioxide in nitrogen. The pressure at which the sample was taken would vary from sample to sample. The required accuracy of the technique was at least 0,25% and the sampling and analysis had to take not longer than 15 seconds per sample.

After extensive development, the scheme shown in the figure below was adopted.

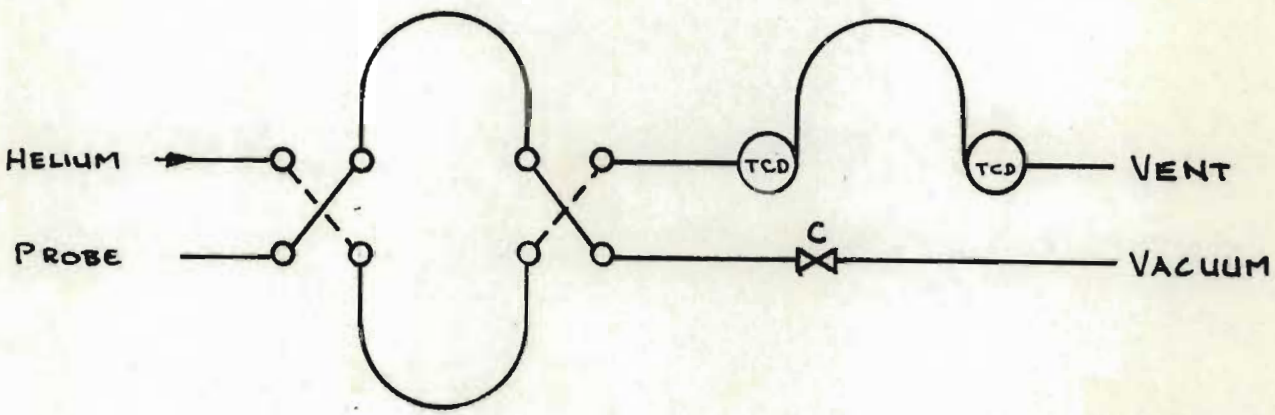

There were essentially two gas circuits involved. A vacuum pump, regulated by a needle valve, C, continuously drew gas through one of the sampling loops connected to a double pole double throw pneumatically operated valve. The valve was developed specifically for use in gas chromatograph circuits and have very small dead volumes on all the switched lines. It was operated pneumatically and provided almost instantaneous changes from one set of connections to another.

The other end of the sampling loop communicated with the sampling probe. This arrangement provided a continually changing sample of gas in the sampling loop.

At the same time, the other circuit was in operation. This provided for a regulated helium supply which, for this position of the valve, purged the other sampling loop and then passed into an analysis circuit. This was formed from a GOW-MAC gas chromatograph whose gas circuitry had been modified. The incoming gas passed over a thermal conductivity detector and then into a column packed with "POROPAK, Q". The column was approximately 80 mm long. At the other end of the column was the second thermal conductivity detector and, after passing over this detector, the gas was vented.

When the sampling switch was operated, it transposed the sampling loops so that helium now made up the pressure deficit in the tube which had been filled with the gas mixtures to be analysed and thereafter drove the mixture into the analysis circuit. When it passed over the first detector, a strong signal was recorded but when the slug had passed into the column, both detectors were immersed in a helium stream, at the pressures which had occurred before the sampling valve was actuated. The signal produced by the GOW-MAC measuring bridge was therefore equal to the baseline value for pure helium. The packed column then separated the nitrogen and carbon dioxide components so that the helium carrier gas carried out first a quantity of nitrogen followed by the carbon dioxide which had been contained in the mixture to be analysed.

The passage of these two components over the second thermal conductivity detector produced two peaks in the bridge output. The first thermal conductivity detector had all the while been immersed in a helium stream at constant pressure.

Meanwhile the other sampling tube had been connected into the sampling line and so had been purged of helium and refilled with the current concentration of mixture to be sampled. In this way, the system was made double-acting and, by choosing the correct length of column and the correct length for the sampling tubes, it was possible to sample and analyse samples consecutively at intervals of 10 seconds. The scheme had the further advantage that the pressure at which the sample was taken did not affect the analysis. This pressure was measured by a pressure transducer and the signal was recorded by the computer.

Unfortunately extremely high accuracy was required for the analysis because it was desirable to be confident of analysis to within 0,25%. An analysis to 0,25% corresponded to only 10% accuracy when dealing with a sample of 2,5% CO_2 in nitrogen, which was the sort of cencentration which needed to be analysed. In fact, it was found that generally, analyses were correct to approximately 0,1%.

In order to process the electrical signal from the GOW-MAC, a technique had to be developed to provide automatic attenuation. It was found that peak height was not an accurate enough representation of the proportions of gas present in the sample and it was necessary to integrate the area under the curve. For a concentration of 1% carbon dioxide in nitrogen the heights of the peaks were in the ratio of the order of 100:1

at high pressure would have peaks ten times as high as a sample taken near the wall where the pressure was lower. Consequently, it was necessary to be able to attenuate the signal so that both the very large nitrogen peak and the diminutive carbon dioxide peak could be adjusted to fit comfortably into the upper range of the Analogue to Digital Converter of the computer.

Accordingly a computer program was developed which, sampling at a frequency of 10Hz, could predict the probable magnitude of the next reading, on the basis of the foregoing reading, and choose a suitable attenuation factor so that the next reading would fall in the upper half of the A to D's range. This reading was then multiplied by a suitable factor to take account of the attenuation which applied when it was taken and it was then stored on magnetic disc. The result was that for each sample , a curve was obtained, represented by about 100 points.

After the run, this data was displayed, one analysis at a time on an oscilliscope and the limits of the peaks were decided by visual appraisal. These were transmitted to an integration program in the computer which integrated the area under the peaks between the limits provided. The ratio of the peak area to the total area could then be calibrated against samples of known concentration. The results of analyses of known gas samples at varying sampling pressures are plotted. Examination of the figure shows that, above a sampling pressure of 60 kPa, the readings are accurately constant. If the analysis was then plotted against this constant value, it is seen that a straight line results. For analyses at pressures below 60 kPa, it was necessary to interpolate.

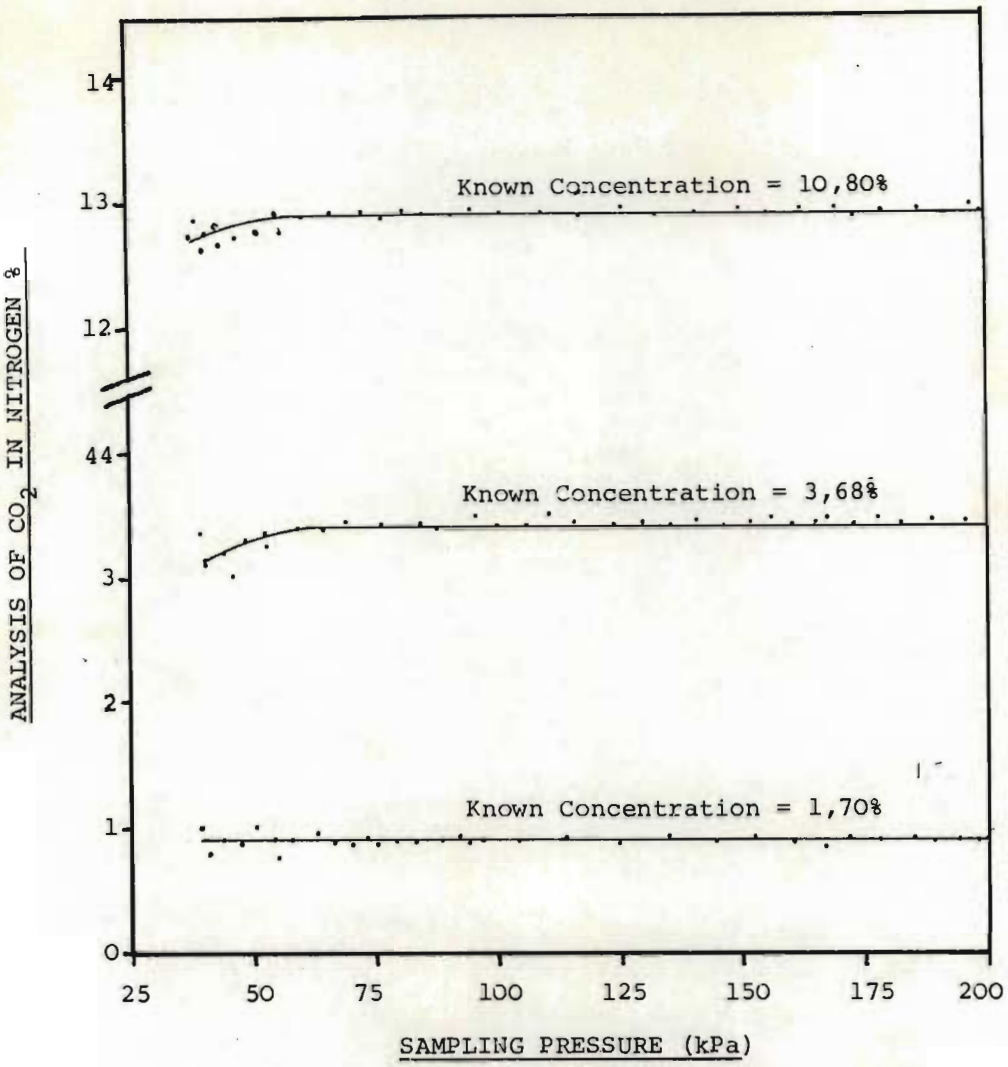

VARIATION OF CO_2 ANALYSIS WITH SAMPLING PRESSURE

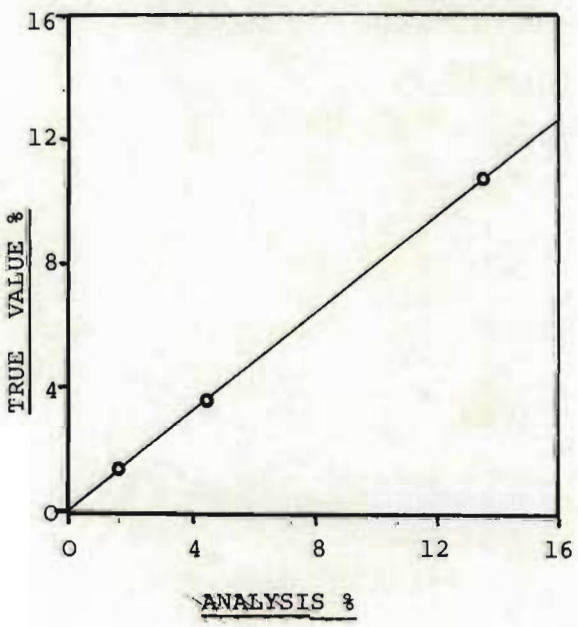

CALIBRATION CURVE FOR CO_2 ANALYSIS

APPENDIX 5.1.

CALIBRATION OF SECONDARY GAS METERING ORIFICE

For the measurement of the secondary gas injection, a 1 mm ϕ sharp edged orifice was used at a "choked" or super-critical pressure ratio

$$\text{Critical Pressure Ratio} = \left(\frac{2}{\gamma+1}\right)^{\frac{\gamma}{\gamma-1}}$$ (Coulson & Richardson, 1970)

For Carbon dioxide, $\gamma = 1{,}285$ (Perry, 1963)

Thus Critical pressure ratio $P_c = 0{,}55$

The absoblute pressure in the outer torus of the injection manifold was maintained below 40 kPa so that the orifice remained super-critical at all times, provided that the orifice press exceeded 75 kPa (abs). In view of the difficulty with the CO_2 mass balance discussed in chapter 6, the orifice was calibrated in three separate ways.

Two different air rotameters were connected separately to the down-stream side of the orifice plate and exhausted to atmosphere. The upstream pressure was varied through a range which ensured that the orifice remained super-critical. The reading of the rotameters was then modified to take account of the difference in density between air and carbon dioxide. The results are plotted in the accompanying figure.

The third measurement of orifice flow relied upon an evacuated vessel of known dimensions connected downstream of the orifice.

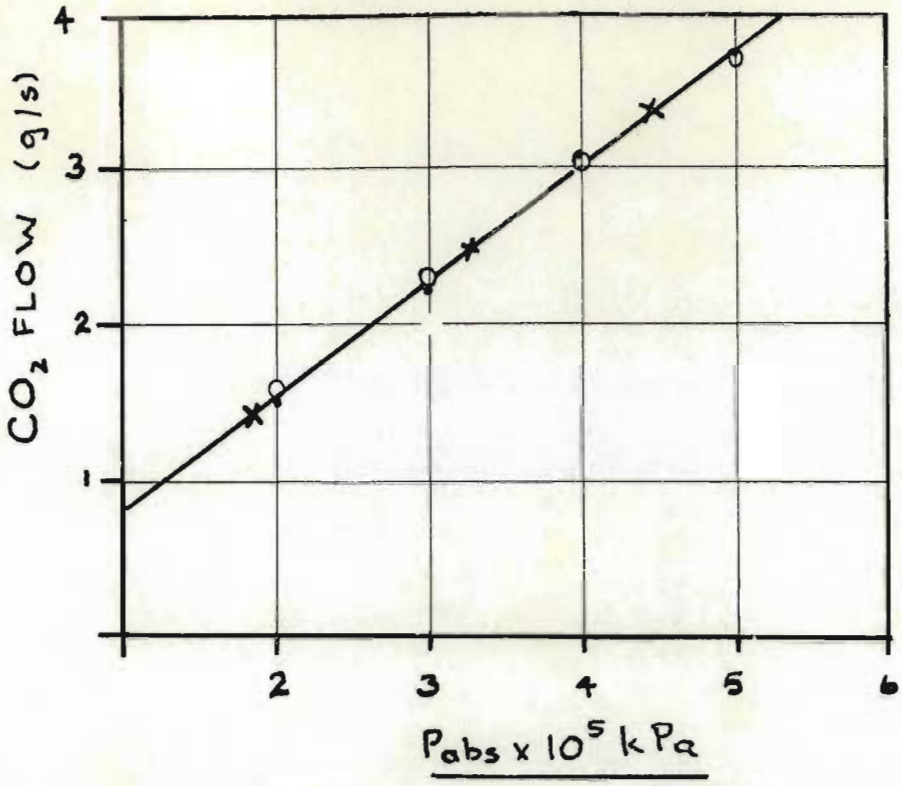

CALIBRATION CURVE FOR ORIFICE

Pressure at any time in the vessel was measured by transducers and logged by a computer to provide a record of pressure versus time. Three determinations were then performed with the orifice pressure being set in turn to that corresponding to the three secondary injection rates which were studied in the mixing analyses. It was found that the pressure in the vessel increased linearly with time, indicating a constant flow rate. The slope of this line was used to calculate the flow rate from the perfect gas law. The three calibration points so obtained are also plotted on the accompanying figure.

It was found incidentally, that published values for orifice discharge coefficients at high Reynolds numbers are lower than observed coefficients under super-critical conditions - by about 30%.

APPENDIX 5.2 EFFECT OF DIFFUSER GAP ON SHOCK STRENGTH

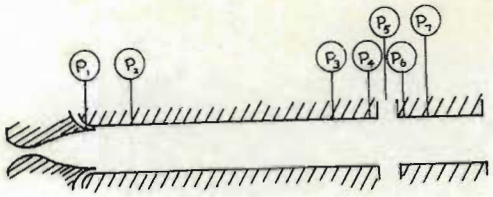

P_0	P_1	P_2	P_3	P_4	P_5	P_6	P_7
		Diffuser Gap = 5,5 mm					
1061	9	17	85	84	75	100	100
1138	9	12	32	50	48	89	90
1163	9	11	29	45	45	88	89
1215	10	12	27	40	41	90	91
1279	10	13	27	28	36	90	91
1317	11	13	28	29	36	91	92
1368	12	13	29	30	36	92	93
		Diffuser Gap = 6,5mm					
946	14	63	87	87	80	99	100
1010	8	11	84	83	78	99	100
1035	8	11	84	84	78	99	100
1163	9	11	25	30	39	88	89
1253	10	12	26	29	36	90	91
1355	11	13	29	30	33	93	94
		Diffuser Gap = 8mm					
959	15	66	88	88	81	99	101
1048	9	12	84	85	79	100	101
1061	9	11	84	85	79	100	101
1163	10	11	24	48	44	89	90
1189	10	11	25	47	43	89	91
1253	11	12	24	38	38	87	88
1317	12	13	26	35	36	87	90
1368	12	13	28	31	35	90	91
		Diffuser Gap = 9,5 mm					
1176	10	11	25	58	49	91	92
1202	10	12	26	54	47	90	91
1266	11	13	27	50	43	88	88
1304	11	14	27	50	43	88	88

APPENDIX 5.2 (continued)

DISTANCE OF PROBE	TEST			
FROM LEADING EDGE	6%	9,3%	12%	9,3%
mm	x/d=24	x/d=24	x/d=24	x/d=17,56
-15	147	131	115	161
-14	147	131	115	163
-13	149	131	115	166
-12	151	131	116	170
-11	152	132	116	174
-10	153	133	117	177
-9	155	137	118	181
-8	159	137	120	183
-7	163	139	122	186
-6	166	142	124	187
-5	170	144	127	190
-4	173	147	129	196
-3	179	152	132	200
-2	183	155	136	201
-1	188	157	138	200
0	190	159	139	189
+1	187	156	139	183
+2	181	154	138	175
+3	176	154	137	173
+4	175	155	137	173
+5	174	155	137	173

APPENDIX 5.3

PREDICTION OF STATIC PRESSURE AFTER A NORMAL SHOCK

The information reported in Chapter 6, regarding the conditions of the gas flow as it approached the diffuser is used in this appendix to predict the static pressure after a normal shock, both both at the centre of the diffuser and at the wall.

From a knowledge of the velocity of the flow, its composition and its static temperature, the Mach number of the flow can be calculated. This may be used in the Rankine-Huganot equations which apply for a normal shock to provide an estimate of the pressure ratio across the shock. From a knowledge of the static pressure before the shock, it is then possible to predict the static pressure after the shock.

APPENDIX 6.1.

MEASURED MASS CONCENTRATION PROFILES.

Radius (mm)	Concentration %							x/d
	6	12	15	18	21	24	27	
.5	0.	.98	2.04	2.91	4.68	5.42	6.42	
1.5	0.	1.24	2.25	3.07	4.81	5.53	6.57	
2.5	0.	2.01	2.57	3.34	5.19	6.01	6.72	
3.5	0.	3.24	3.24	4.60	5.29	6.24	6.79	
4.5	.21	4.11	4.44	5.41	6.08	6.63	6.88	
5.5	2.42	5.79	5.48	6.40	6.33	7.05	7.25	
6.5	5.18	7.65	6.78	7.17	7.56	7.43	7.27	
7.0	8.60	8.62	7.06	7.26	7.29	7.44	7.08	
7.5	16.17	9.14	7.84	8.34	7.63	7.26	7.58	
8.0	16.39	9.79	7.41	7.99	7.71	7.72	7.20	

APPENDIX 6.1 (continued).

MEASURED STAGNATION TEMPERATURE PROFILE.

Radius mm	Stagnation Temperature. 12	15	18	21	24	27	x/d
.0	1340.	1345.	1293.	1305.	1243.	1265.	
.5	1336.	1340.	1292.	1300.	1240.	1262.	
1.0	1325.	1332.	1290.	1295.	1240.	1255.	
1.5	1315.	1323.	1280.	1291.	1225.	1242.	
2.0	1305.	1313.	1272.	1285.	1220.	1235.	
2.5	1285.	1300.	1261.	1278.	1215.	1231.	
3.0	1270.	1282.	1245.	1256.	1206.	1225.	
3.5	1250.	1265.	1233.	1245.	1195.	1210.	
4.0	1236.	1242.	1220.	1225.	1185.	1205.	
4.5	1225.	1220.	1203.	1210.	1176.	1190.	
5.0	1206.	1200.	1186.	1200.	1156.	1180.	
5.5	1186.	1178.	1170.	1170.	1150.	1170.	
6.0	1170.	1160.	1152.	1165.	1142.	1155.	
6.5	1150.	1145.	1133.	1150.	1130.	1145.	
7.0	1130.	1130.	1115.	1135.	1112.	1130.	
7.5	1108.	1105.	1095.	1120.	1091.	1113.	
8.0	1085.	1080.	1075.	1085.	1065.	1085.	

APPENDIX 6.1 (continued).

MEASURED STAGNATION PRESSURE PROFILES.

Radius (mm)	Stagnation Pressure (kPa) 12	15	18	21	24	27	x/d
.0	240.	185.	176.	155.	147.	144.	
.5	236.	183.	175.	154.	147.	144.	
1.0	227.	181.	173.	152.	147.	143.	
1.5	213.	174.	169.	150.	146.	142.	
2.0	201.	167.	163.	146.	143.	140.	
2.5	187.	159.	159.	142.	139.	137.	
3.0	172.	154.	150.	136.	135.	132.	
3.5	158.	142.	143.	131.	130.	128.	
4.0	145.	136.	135.	123.	125.	122.	
4.5	133.	122.	128.	121.	120.	116.	
5.0	122.	117.	120.	115.	114.	111.	
5.5	113.	111.	111.	109.	108.	103.	
6.0	104.	100.	106.	102.	100.	97.	
6.5	95.	92.	96.	94.	91.	90.	
7.0	83.	85.	89.	86.	84.	84.	
7.5	74.	77.	79.	78.	80.	78.	
8.0	67.	66.	69.	73.	71.	72.	

APPENDIX 6.2

CALCULATION OF NOZZLE DISCHARGE

$T_0 = 1350^{\circ}K$

$P_0 = 1163kPa$

Then applying equation 2.1 for $M = 1$ yields

$T^* = 1125^{\circ}K$

and equation 2.2 yields

$P^* = 614,4kPa$

For these conditions, Conjar and Manning (1967) provide a density of $\rho^* = 1,742\ Kg/m^3$.

Mass flow rate $= a \times A^* \times \rho^*$

$= \sqrt{1.4 \times 296,9 \times 1125} \times \pi \times 0,0025^2$

$= 23,4g/s$

APPENDIX 7.1

Derivation of Conservation of Mass Equation

Consider an anulus of the flow of thickness ∂r, at a radius of r and of length ∂x, as shown below .

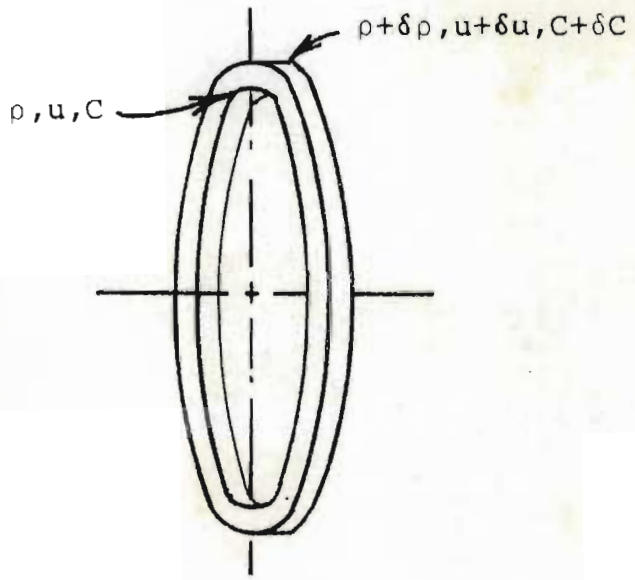

At (x,r), the flow properties are u, c, T and ρ and at ($x+\partial x$, $r+\partial r$) they are $u+\partial u$, $c+\partial c$, $T+\partial T$ and $\rho+\partial\rho$. Then, Mass flow of CO_2 into the shell

$$= 2\pi r\partial r\rho uc - 2\pi r\partial x\varepsilon_m \frac{\partial c}{\partial r}$$

and Mass flow of CO_2 out of the shell

$$= 2\pi r\partial r(\rho+\partial\rho)(u+\partial u)(c+\partial c) - 2\pi(r+\partial r)\partial x\varepsilon_m\left(\frac{\partial c}{\partial r} + \frac{\partial}{\partial r}\left(\frac{\partial c}{\partial r}\right)\partial r\right)$$

Because the flow has reached a steady state the mass accumulation is zero:-

$$r\partial r\left[\rho u\partial c + \rho c\partial u + uc\partial\rho\right] - \varepsilon_m\partial x\left[r\frac{\partial^2 c}{\partial r^2}\partial r + \frac{\partial c}{\partial r}\partial r\right] = 0$$

Deviding by $r\partial r\partial x$ and taking the limit as ∂r and ∂x tend to

zero yields

$$\rho u \frac{\partial c}{\partial x} + \rho c \frac{\partial \rho}{\partial x} + uc \frac{\partial \rho}{\partial x} - \varepsilon_m \left| \frac{\partial^2 c}{\partial r^2} + \frac{1}{r} \frac{\partial c}{\partial r} \right| = 0$$

REFERENCES.

Abramovitch, G.N. "The theory of turbulent jets", M.I.T. Press, Cambridge,Massachusetts, 1963.

Allegre,J., Bisch,C. & Faulmann, D. "La soufflerie hypersonique SH3 du laboratoire d'Aerothermique du C.N.R.S." C.N.R.S. publication no. 272, 1966.

Ahlberg, J.H., Nilson,E.N. & Walsh, J.L. "The theory of splines and their applications", Academic Press, New York. 1967.

Alpinieri, L.J. "Turbulent mixing of co-axial jets", AIAA Journal, 1964, p1560.

Aungier, R.H. "A computational method for exact, direct and unified solutions for axisymmetric flow over blunt bodies of arbitary shape", AFWL-TR-70 Air force weapons laboratory, Kirtland, New Mexico, U.S.A., 1970.

Baddour, R.F. and Timmins, R.S. "The application of plasmas to Chemical Engineering". Pergammon Press, London, 1967.

Bauer, R.C. "An analysis of two-dimensional laminar and turbulent compressible mixing", AIAA Journal, 1966, p392.

Berman, R.J. "Bow shock shape about a spherical nose", AIAA Journal, 1965, p778.

Bershader, D. & Griffith, W. "Recent developments in shock tube research", 9th International Shock tube Symposium, Stanford University, 1973.

Bluston, H.S. "An experimental study of jet turbulent mixing at subsonic-supersonic speeds", AIAA Journal. 1966, p1137.

Canjar, L.N. & Manning, F.S. "Thermodynamic properties and reduced correlations for gases", Gulf Publishing Co., Houston, Texas, 1967.

Channapragada, R.S. "Compressible jet spread parameter for mixing zone analysis", AIAA Journal, 1963, p 2188.

Channapragada, R.S. & Woolley, J.P. "Turbulent mixing of parallel compressible free jets", AIAA Journal, 1965, Preprint no 65-606.

Conlan, & Trytten, "A high speed computer technique to determine nozzle contours for supersonic wind tunnels", Naval Ordinance Laboratory, White Oak, Maryland, TR64-81, 1964.

Corrsin, S. & Uberoi, M.S. "Further experiments on the flow and heat transfer in a heated turbulent air jet", NACA Report, 998 of 1952.

Cookson, R.A., Flanagan, P. & Penny, G.S. "A study of free-jet and enclosed supersonic diffusion flames", 12th Symposium (International) on Combustion, Poitiers, France, 1968.

Crane, L.J. "The laminar and turbulent mixing of jets of compressible fluid", Journal of Fluid Mechanics, vol 3, part 1, 1957.

Curle, S.N. & Davis, H.J. "Modern Fluid Dynamics", vol 2, von Nostrand, London, 1971.

Diesner, H.J. & Schugerl, K. "Investigation of a novel nozzle reactor", Advances in Chemistry Series, N133, p 46, 1974.

Donaldson, C. du P. & Gray, K.E. "Theoretical and experimental investigation of the compressible free mixing of two dissimilar gases", AIAA Journal, 1966, p 2017.

Dumitrescu, L.Z. "Minimum length axisymmetric laval nozzles" , AIAA Journal, 1975, p 520.

Ferri, A. & Fox,H. "Analysis of fluid dynamics of supersonic combustion process controlled by mixing", 12th Symposium (International) on Combustion, Poitiers, France, 1968.

Foelsch, K. "The analytical design of an axially symmetric Laval nozzle for a parallel and uniform jet", Journal of the Royal Aerenautical Society, p 161, 1949.

Forstall, W. & Shapiro, A.H. "Momentum and mass transfer in co-axial gas jets", ASME, Journal of Applied Mechanics, 1949, p 399.

Freedman, S.I., Radbill, J.R. & Kaye, J. "Theoretical investigations of a supersonic laminar boundary layer with foreign gas injection", AIAA Journal, 1963, p 149.

Glowaki, W.J. "Program for the design of contoured axi-symmetric nozzles for high temperature air", Naval Ordinance Laboratory, White Oak, Maryland. AD 465605. 1965

Grabitz, G. "Approximate analytical solution of steady axisymmetric supersonic free jet of a reacting gas", Archives of Mechanics, vol 28, 1976, p 923.

Green, J.E. "Interactions between shock waves and turbulent boundary layers", Pergammon Press, Progress in Aerospace Sciences, Vol II, Ed. D Kucheman et al., 1970.

Hawk, N.E. & Amick, J.L. "Two dimensional secondary jet interaction with a supersonic stream", AIAA Journal, 1967, p 655.

Hill, C.R. & Peterson, P.G. "Mechanics and thermodynamics of propulsion", Addison-Wessley, New York, 1967.

Houghton, E.L. & Boswell, R.P. "Further aerodynamics for Engineering students", Edward Arnold, London, 1969

Hsia, H.T.S. "Equivalence of secondary injection to a blunt body in supersonic flow", AIAA Journal, 1966, p 1832.

Ibberson, V.J. & Sen, M. "Plasma jet reactor design for hydrocarbon processing", Trans. INSTN. Chem. Engrs. Vol 54, 1976, p 265.

Kleinstein, G. "On the mixing of laminar and turbulent axially symmetric compressible flows", PIBAL Report, Polytechnic Institue of Brooklyn, 1963, p 756.

Korkhan, K.D. "Comments on bow shock shape about a spherical nose", AIAA Journal, 1966, p 381.

Korkhan, K.D. & Gregorek, G.M. "Shock-wave profiles about hemispherical noses at low supersonic Mach numbers", AIAA Journal, 1977, p 740.

Libby, P.A. "Theoretical analysis of turbulent mixing of re-active gases with application to supersonic combustion of hydrogen", Journal of the

Libby, P.A. & Schetz, J.A. "Approximate analysis of the slot injection of a gas in laminar flow", AIAA Journal 1963, p 1056.

Liepman, H.W. & Roshko, A. "Elements of gasdynamics", John Wiley and Sons, New York, 1957.

Lorber, A.K. & Schetz, J.A. "Turbulent mixing of multiple co-axial gaseous fuel jets in a supersonic air-stream", AIAA Journal, 1975, p 973.

Maczynski, J.F.J. "A round jet in an ambient co-axial stream", Journal of Fluid Mechanics, 1962, p 597.

Maydew, R.C. & Reed, J.F. "Turbulent mixing of compressible free jets", Research Report, Sandia Corporation, 1963, p 4764.

Mitchell, A.R. "Computational methods in partial differential equations", John Wiley and Sons, London, 1969.

Morganthaler, J.H. "Supersonic mixing of hydrogen and air", John Hopkins University, Phd. thesis, Applied Physics Laboratory, 1965.

Newton, J.F. & Dowdy, M.W. "Investigation of liquid and gaseous secondary injection phenomena on a flat plate with M=2,01 to M=4,54", Jet Propulsion Laboratory, Pasadena, California, 1963, Report TR 32-542.

Osgerby, I.T. "An investigation of supersonic combustion and heterogeneous turbulent mixing related to the design/operation of scramjets", University of Sheffield, Phd. thesis, Dept. of Fuel Technology and Chemical Engineering, 1965.

Reynold, A.J. "Variation of turbulent Prandtl and Schmidt numbers in wakes and jets", International Journal of Heat and Mass Transfer, 1976, p 757.

Roberts, H.L. "The selective partial oxidation of methane in a chemical shock tube", University of Natal, Phd. thesis, Dept. of Chemical Engineering, 1970.

Ragsdale, R.G. & Edwards, O.J. "Data comparison and photographic observations of co-axial mixing of dissimilar gases at nearly equal stream velocities", NASA TN 1965, p 3131.

Schetz, J.A. & Favin, S. "The ignition of slot injected gaseous hydrogen in a supersonic airstream", AIAA Journal, 1966, p 644.

Schetz, J.A. & Gilreath, H.E. "Subsonic injection into a M2,1 stream of air two-dimensionally", AIAA Journal, 1967, p 2149.

Schetz, Gilreath + Hubard, 12th International Symposium on Combustion 1969, 1141

Schetz, J.A. "Turbulent mixing of a jet in a coflowing stream" AIAA Journal, 1968, p 2006.

Schligting, H. "Boundary-Layer Theory", McGraw-Hill, New York, 1968.

Schulte, H.E. "A comparison of approximate methods of predicting shock detachment distance for supersonic 2D inlets", Airforce Institute of Technology, Wright Patterson Air Force Base, M.S. thesis, School of Engineering, Ohio, 1974.

Seddon, J. "The flow pattern produced by interaction of a turbulent boundary layer with a normal shock wave of strength sufficient to cause

Shapiro, A.H. "The dynamics and thermodynamics of compressible fluid flow", Ronald Press Co., New York, 1953.

Shivamoggi, B.K. "Theoretical analysis of the effect of compressibility and free-stream turbulence on free-mixing turbulent gas flows", ASME Journal of Applied Mechanics, 1976, p 217.

Squire, H.B. & Trouncer, J. "Round jets in a general stream", Aeronautical Research Council TRR&M, 1944.

Switchenbank, J.E. & Chigier, N.E. "Vortex mixing for supersonic combustion", 12th Symposium (International) on Combustion, Poitiers, France, 1968, p 1153.

Thayer, W.J. & Corlett, R.C. "Gas dynamic and transport phenomena in the two-dimensional jet interaction flow field", AIAA Journal, 1972, p 488.

Ting, L. & Libby, P.A. "Remarks on the eddy viscosity in compressible mixing flows", Journal of Aerospace Science, 1960, p 797.

Tucker, M. "Approximate calculation of turbulent boundary-layer development in compressible flow", NACA TN 2337, 1951.

van Wylen, G.J. "Thermodynamics", John Wiley and Sons, New York, 1959.

Visich, M. & Libby, P.A. "Experimental investigation of mixing of Mach number 3,95 stream in presence of wall", NASA TN, 1960, D247.

Zakkay, V. & Krause, E. "Mixing problems with chemical reactions", 21st Meeting, AGARD Combustion and Propulsion Panel, London, 1963.

Zakkay, V., Krause, E. & Woo, S.D. "Turbulent transport properties for axisymmetric heterogeneous mixing", AIAA Journal, 1964, p 1939.

Zukoski, E.E. & Spaid, F.W. "Secondary injection of gases into a supersonic flow", AIAA Journal, 1964, p1689.